Forschungszentrum Karlsruhe

Technik und Umwelt

Wissenschaftliche Berichte

FZKA 6199

IFMIF
International Fusion Materials Irradiation Facility
Conceptual Design Evaluation Report

A Supplement to the CDA
by the IFMIF TEAM

Edited by A. Möslang
Institut für Materialforschung
Projekt Kernfusion

An Activity of:
The International Energy Agency (IEA)
Implementing Agreement for a Program of Research and Development
on Fusion Materials

Forschungszentrum Karlsruhe GmbH, Karlsruhe
1998

Forschungszentrum Karlsruhe GmbH
Postfach 3640, 76021 Karlsruhe

ISSN 0947-8620

Abstract

This report documents the main results of the Conceptual Design Evaluation (CDE) on the International Fusion Materials Irradiation Facility (IFMIF), conducted during 1997 and 1998. Following the recommendations of the FPCC in January 1997, the activities proposed by the IEA/IFMIF Subcommittee for the CDE phase were, according to the limited funding, to concentrate mainly on a critical evaluation of the design developed during the preceding Conceptual Design Activity (CDA) phase and on improvements of key devices and instrumentation tools. The IFMIF activities continues to be coordinated by the international leadership team already used for the CDA. This CDE report follows basically the work breakdown structure of the project and therefore has the four major sections Test Facilities, Target Facilities, Accelerator Facilities and Design Integration. A major outcome of the CDE was, that in all areas the conceptual design was confirmed and extended, with no substantial changes.

Test Facilities: Special emphasis was put on the validation and improvement of the high-flux test module (HFTM) for structural materials irradiation and the medium-flux test module (MFTM) for tritium release experiments. The HFTM design has been extended mainly to implement additional requirements of the users' community and to take into account more recent flux/volume and heat deposition calculations from the neutronics. Without neutron reflector approximately 15% burn up and 7.5 dpa can be achieved annually in the medium flux position in a typical breeder ceramic. Significant progress has been achieved in the neutronics with respect to the source term of the D-Li reaction, the 20-50 MeV data evaluation and the assessment of on-line neutron/gamma monitors. An IFMIF simulation experiment was performed with 40 MeV deuterons for measuring the neutron yield as well as the Be-7 and tritium production yield in lithium. User specific tasks have been added because of their relevance for the overall IFMIF performance. These tasks included an evaluation of the Li-target backwall, small-specimen test technology development and a very detailed re-evaluation of irradiation parameters. This re-evaluation is based on extended MCNP transport code calculation and has shown that all relevant irradiation parameters of the IFMIF HFTM matches very well with the related ITER and DEMO values.

Target Facilities: During the CDE phase significant improvements of the conceptual design have been made that include (i) an optimization of the overall system design, (ii) extended thermo-hydraulic calculations to assess the Li jet stability under different conditions, (iii) a probabilistic evaluation of accident sequences showing very low values for potential accident probabilities, and (iv) a detailed outline of lithium purification and on-line monitor systems. As a major result, a notable cost reduction has been achieved by decreasing the total volume of the lithium cells by 37%. A hydraulics analysis for the stability of the target lithium jet has shown in accordance with a water simulation experiment, that the convection flows on both sides of the beam footprint and therefore does not influence the jet stability.

Accelerator Facilities: During the CDE, the three major task areas were (i) RF system development and test, (ii) injector system development and test and (iii) all other conceptual design activity-With respect to high current cw accelerator experience, the IFMIF project presently gains from relevant results in other accelerator projects. E.g. at the University of Frankfurt a 200 mA cw 94% proton beam (corresponds by scaling to 140 mA deuterons) was extracted in July 1998 through a 8 mm aperture, and also at CEA-Sacley a 126 mA cw proton beam was transported recently through a 10 mm aperture for a long operation time with 96% availability. Finally, within a US program, a 100 mA cw proton linac prototype to about 10 MeV is under construction. Relevant activities came

also from JAERI, Japan. For the IFMIF project these results and improvements are highly significant, because the experimental data strongly validate the predictions from the codes, greatly increasing confidence that the reference IFMIF design objectives are realistic and can be met largely with available technology.

Design Integration: In the task area “safety assessment” probabilistic risk assessment calculations were performed taking into account the entire IFMIF plant and its subsystems. Within the framework of the task “reliability, availability and maintainability”; the IFMIF team conceived and developed the accelerator system model (ASM), and used it to guide conceptual design choices and to establish a credible RAM model. Finally, within the task area “central control system” two instruments have been evaluated for the interface between the accelerator, target and test cell: An infrared camera device to measure the beam position and temperature distribution on the Li-target, and a multi-channel based neutron monitor for on-line measurements of the special neutron distribution inside the test cell.

MAJOR CONTRIBUTORS

Test Facility Group

Möslang, A.; Leader
Class M.
Daum E.
Esposito B.
Fischer U.
Haines J.
Jitsukawa S.
Mercurio G.
von Möllendorff, U.
Schmitz G.
Shiba K.
Turroni P.
Wilson P.
Zinkle S.

Accelerator Group

Jameson R.; Leader
Teplyakov V, Deputy
Chernogubovsky M
Eriksson M
Ferdinand R
Hojo Y
Hollinger R
Kinsho M
Klein H
Lagniel J-M
Piaszczyk C
Pozimski J
Rennich M
Sugimoto M
Tanabe Y
Volk K

Li-Target Team

Kato Y.; Leader
Cevolani S.,
Tirelli D.
Stefanelli R.
Giusti D.
Bianchi F.
Burgazzi L.
Katsuta H.
Takeuchi H.
Nakamura H.
Ida M.
Kakui H.
Hua T
Green L.

Design Integration Group

Shannon T.; Leader
Takeuchi H.
Kita Y.
Rennich M.
Martone M.
Burgazzi L.
Piaszczyk C.
Yutani T.

CONTENTS

1 EXECUTIVE SUMMARY

1.1 Introduction

Following the recommendations of the FPCC in January, 1997, the IEA/IFMIF Subcommittee at their meeting in Brussels on January 30-31 proposed a new plan for the activities in 1997-98. The objective of the plan was to maintain the viability of the project in 1997-98 and to be in a position to begin engineering design and development work in the near future. This phase of work was called Conceptual Design Evaluation (CDE). The design leaders met in Paris on February 3 to redefine the tasks to focus on evaluation of technical issues resulting from the conceptual design activity. A three year Engineering Validation Phase (EVP) was defined during the CDA as the first step in the IFMIF project. This is a necessary step to prepare for engineering design and construction. However, tasks that were related to engineering and construction planning and development were dropped from the CDE. This engineering work will be considered later, after the decision to proceed with a construction project.

In order to address technical issues requiring development work, the plan relied heavily on activities already underway and largely funded by programs other than IFMIF. The limited IFMIF funds were used to start a few new CDE activities and to sustain the key members of the international design team to track the development work and to maintain and update the design, cost estimate and documentation. The specific tasks for the CDE are documented in a detailed plan for 1997-98 [1].

The IFMIF work continues to be coordinated by the international leadership team used for the CDA. In 1997-98, the progress was reviewed and checked with international conference calls and by meetings of each of the three main facility groups (Accelerator, Target and Test Facilities). Meetings of the Subcommittee and design leaders were held in October and November 1997 to review the results of the work and to plan for the work in 1998. Two general group meetings were held in 1998. Following is a summary of the international meetings and discussions held during the two-year CDE period.

Group Meetings and Discussions

1997

IEA/IFMIF Subcommittee	30-31 January	EC/Brussels, Belgium
Design Leaders Meeting	3 February	IEA/Paris, France
Accelerator Facilities Workshop	26-30 May	Saclay/Paris, France
Test Facilities Workshop	7-9 July	FzK/Karlsruhe, Germany
Design Leaders Discussion	31 July	International Conference Call
Design Leaders Meeting	30 October	Sendai, Japan
Users Group Workshop	1 November	Sendai, Japan
Target Facilities Workshop	3-7 November	ENEA/Bologna, Italy
IEA/IFMIF Subcommittee	5 November	JAERI/Tokyo, Japan
Design Leaders Discussion	14 November	International Conference Call

1998

Design Leaders Meeting	23-26 March	ORNL/Oak Ridge, TN, USA
Design Team Meeting	23-26 September	Knoxville, TN, USA

At the final CDE meeting of the design team on September 23-25, the results of the CDE tasks were reviewed and approved. The team concluded that the basic concept defined in the CDA report is credible and no major changes are recommended. Although the detailed design

and analysis has confirmed that the main system choices are valid, a number of changes have been identified to improve the design at the component level. A summary of the major findings shall be presented below.

Proposed Strategy

A three-year Engineering Validation Phase (EVP) [2] was defined during the IFMIF project. The EVP includes the design, development and testing of the prototype components necessary to prepare for engineering design and construction. Due to the delays and funding cuts in the international fusion program, the IFMIF team has defined interim steps such as the two year CDE.

We now suggest a new phase, the Key Element Technology Phase (KEP). The purpose of KEP is to prepare for the EVP. Key technology issues will be addressed by in-depth analysis design studies and the evaluation and design of the test apparatus needed to begin the EVP. The schedule showing this shown in Fig. 1.

[1] T. E. Shannon, *International Fusion Materials Irradiation Facility, A Proposed Plan for Conceptual Design Evaluation (CDE),* Memo, February 26, 1997.

[2] *Proposed Task for IFMIF-EVP (International Fusion Materials Irradiation Facility - Engineering Validation Phase), JAERI – Memo 08-173, (August, 1996*

1.2 Test Facilities

During the CDE phase the activities were mainly concentrated on design improvements of key devices, on an evaluation of instrumentation tools, as well as on detailed neutronics calculations of relevant nuclear responses. User specific tasks have been added and discussed during a related Users meeting at Sendai on November 1 1997.

Component design and development

The Test Facilities CDA design concept was basically confirmed. Special emphasis was put on the validation and improvement of the high flux test module (HFTM) and the medium flux test module (MFTM) for tritium release experiments.

The HFTM design has been extended and improved mainly to implement additional requirements of the users' community and to take into account more recent flux/volume and heat deposition calculations from the neutronics. In order to test the fabricability, thermohydraulics and structural integrity after thermal cycling tests, a detailed design for a sub-sized test apparatus was done. Presently, the first version of such an instrumented test module is fabricated at FZK.

The CDA design of the T-release test module has been completely revised and extended. Based on existing layouts from JAERI and FZK, ENEA has provided a harmonized design that is optimized with thermohydraulic calculations and that allows a relatively high specimen package density. In order to account for the growing demands of the solid breeder blanket community regarding the qualification of suitable ceramics, JAERI has improved greatly the related sub-test module design for pebble beds. Based on the present neutron spectrum approximately 15% burn up and 7.5 dpa can be achieved annually in the medium flux position in a typical breeder ceramic enriched to 50% 6Li.

Neutronics

Source term of D-Li-reaction. A complete reassessment of the various components of the nuclear model was carried out at FZK, resulting in a physically sounder model for the neutron source term. The evaluated neutron yield of 5.5%- 7.3% causes an average HFTM volume (collided) of 455 cm^3 with an uncertainty of ±180 cm^3. That is, the need for a complete measurement of the Li(d,xn) cross-section is ever-present. An IFMIF simulation experiment was performed at FZK with 40 MeV deuterons for measuring the neutron yield as well as the Be-7 and tritium production cross sections in lithium.

20-50 MeV data evaluation: Complete transport and activation files from the FZK/INPE Obninsk evaluation work are available for various selected isotopes. In addition to these efforts

and to the related activities at JAERI, complete transport files for many isotopes were released independently by LANL in 1997. For the first time detailed specific activity and decay heat calculations have been carried out for iron in the HFTM.

Neutron/gamma monitors. Very recently, new technology sub-miniature fission chambers have been developed by CEA having an external diameter of only 1.5 mm and a length of 12 mm. The possibility of using a similar detector for IFMIF was evaluated by ENEA and looks very promising. Further development activities are suggested to select appropriate fissile materials.

Users

Although the user tasks are basically not related to design requirements, they represent important activities in the present phase because of their relevance for the overall IFMIF performance.

Re-evaluation of irradiation parameters: In order to demonstrate the suitability of IFMIF for irradiation experiments, a comprehensive characterization of the neutronics of the high flux test region and for Fe as the major constituent of ferritic/martensitic steels was carried out at FZK. Also a parametric study (shape variation of beam foot print, code and neutron yield variations) of the high flux test volume was performed. Detailed 3D models were developed for use with MCNP calculation to obtain a good understanding of how different material loadings and alloy variations change the neutronic response inside the test modules.

The displacement damage qualification shows that with respect to the fraction of damage energy produced by PKA´s as a function of their kinetic energy, IFMIF matches very well with the related ITER and DEMO values. Also with respect to the gas/dpa ratios IFMIF represents the typical values of ITER/DEMO first walls. This makes IFMIF a very valuable and powerful tool for the development of structural materials. In order to achieve also favorable irradiation conditions for ceramic breeders, it is necessary to adapt the lower energy tail of the IFMIF neutron spectrum closely to DEMO typical values. Related design studies for a suitable neutron moderator/reflector should therefore become a first priority task

Evaluation of the Li-Target backwall. A first collection of materials data is available. It is based on reduced activation ferritic/martensitic steels (mainly F82H) and includes swelling behavior, fracture toughness, Charpy impact and tensile properties up to 32 dpa.

Small specimen test technology. Minor progress has been achieved during the CDE. Activities towards a full qualification of these specimens are essential in order to fully utilize the available irradiation volume and to account for the IFMIF flux gradients. It is proposed that in the future the SSTT activities will be supported more strongly within respective materials programs.

1.3 Target Facilities

Four subtasks were discussed . They were basically agreed to be carried out in CDE phase by co-operation of EU, JP and US at the DI Meeting at Frascati in Oct. 1996. The content of these subtasks was as follows:

Optimization of System Design:

The optimization of the target system layout was performed to reduce the lithium cell volume, to match the two target assembly systems, and to add the access/utility spaces. As a result, the total volume of lithium cells was reduced by 37 %. This result will contribute to reduce the costs of the Ar gas circulating system. The thermal stress analysis in the normal operation conditions was made for all the components. The maximum thermal stress was about 1/2 of the maximum allowable value.

From the practical point of view, an improved target assembly was proposed by JP and EU. In the Japan proposal, lip welding technique using YAG laser and remote handling machines were adopted.

Hydraulics Performance:

An analysis for the stability of the target lithium jet and a water simulation experiment were done. The analysis shows that the convection flows on both sides of the beam footprint do not

influence the stability. The characteristics of the small ripples of the jet flow were clarified by water experiments in JAERI. The amplitude of the ripple and the flow velocity in the boundary layer were measured. These results suggest that the relation between the ripple patterns on the jet and the flow in the boundary layer on the nozzle could be significant.

With a modified code, transient response of lithium temperature due to the loss of one/ two beams was shown under the condition of constant temperature of the secondary coolant.

Lithium Safety

A probabilistic evaluation of the accident sequences was made.

The methods of the fault trees and event trees are introduced to perform a probabilistic evaluation of the accident in the target facility. The frequencies/probabilities of occurrence of the most dangerous accident sequences, i.e. involving the backwall rupture, are evaluated in a preliminary manner. The results show very low values for the probabilities of accident sequences.

Lithium Purification and on-line Monitor

An analysis of a cold trap swamping method for tritium trapping was carried out. This method is the backup for the yttrium getter hot trap. By this method, the tritium inventory of about 3 grams can be achieved by a hydrogen injection rate into the lithium of about 3 appm/day (4.5 g/day). Evaluations and improvements of the target system conceptual design have been made in these CDE-Tasks. On these bases, the development of the following key elements is planned and will be performed in the next phase:

- More practical target assembly with remote handling machine
- Impurity purification and on-line monitoring system
- Analysis of the lithium loop transient state

Anyway, the design of a lithium test loop should be started in the early stage of the next phase.

1.4 Accelerator Facilities

The Accelerator Facilities' Conceptual Design was confirmed and extended during the CDE, with no substantial changes. In two top-priority task areas, information from other programs provided important confirming feasibility evidence.

RF System Development and Test

Development and testing of a 1 MW, 175 MHz cw rf system is identified as the highest impact development item in terms of technical capability, costs and RAM. Existing operating experience with amplifiers appropriate to the IFMIF frequency of 175 MHz is with pulses of a few seconds to the order of a minute, at frequencies generally lower (easier) than the IFMIF frequency. At frequencies higher by a factor of two or more, klystrons are used to achieve a high duty-factor and cw operation. A gap existed in the commercial tube availability for the IFMIF frequency range. A lifetime test of 100 hours at full 1 MW cw power into a resistive load with an availability of 95% or better is defined as the design confirmation goal.

No resources were available for this task. However, very good news has been received from Thomson Tubes, who have reported 1 MW cw operation of a 200 MHz diacrode amplifier for one hour. This scales to an even better result at 175 MHz (frequency to 5/2 power). Acceptance tests for LANL (200 MHz), including a 24 hours "heat run test", have demonstrated the compliance of this TH628 diacrode with LANL specification. During the 24 hours test, the diacrode has been successfully operated with 600 kW mean power (pulsed operation with 20% duty cycle, 3.0 MW peak power, 2.27 ms – 88 Hz). Therefore, our first priority task has almost been demonstrated. Thomson could make the 100 hour test for us and have provided a cost estimate.

Injector System Development and Test

The injector system has the second highest impact in terms of reaching the required performance and RAM goals for IFMIF. Two technical approaches (the ECR and volume type ion sources) are to be developed, because the present status precludes a decision between them, and because substantial ongoing efforts mainly supported by other programs can, with IFMIF augmentation, be expected to progress to a decision point.

Important confirming progress was reported by other projects during the CDE period. The basic IFMIF source requirement is a 140 mA cw deuteron beam delivered through the low-energy-beam-transport RFQ entrance, with suitable quality, confirmed by a 100-h cw demonstration with availability approaching 98%.

The IAP Frankfurt volume type source was experimentally studied using a deuteron beam. A maximum current density of 210 mA/cm^2 has been achieved, and so far 80 mA deuteron current has been measured using an extraction hole with a diameter of 8 mm. A 200 mA cw 94% proton beam (corresponds by scaling to 140 mA deuterons) was extracted in July 1998 from the IAP Frankfurt AMFIS source in cw operation. The extracted current density is 390 mA/cm^2 and the noise level is less than 1%.

A 126 mA cw proton beam was extracted from the SILHI ECR source at CEA-Saclay through a 10 mm diameter extraction aperture. With the appropriate conditions, a plasma density J = 213 mA/cm^2 can be achieved, which is close to the requirement for the IFMIF source. LEBT performance was also shown to be well suited to IFMIF. The CEA-Saclay SILHI source has been operated for 100 hours with 96% availability (99% after a conditioning period of 20 hours).

The LANL ECR proton ion source was operated at ~100 mA for 170 hours with 96% availability.

In Japan, proton ion source tests are being conducted, concentrating on potential lifetime and efficiency benefits of LaB_6 filaments in comparison to tungsten filaments. The volume source with a long-life filament, LaB_6 cathode assembly model, developed at KEK, is under development at JAERI. A performance test using a proton beam resulted in excellent comparison with the conventional tungsten filament.

All Other Conceptual Design Activity

There are many other tasks necessary to reach a stage where productive preliminary design activity can start. An overall category for these detailed design tasks is maintaining beam loss and activation low enough that remote handling is not necessary. The tasks involve a detailed design of the accelerator beam transport from ion source to target, fundamental investigations to gain understanding of the loss mechanisms, coordination with neutronics calculations and shielding design, engineering design of the accelerator, and so on.

Limited activity was possible on this comprehensive task during the CDE, and effort focused on specific items. The principal IFMIF requirement for 70% availability was addressed by extending the development of the Accelerator System Model (ASM) RAM component to a systematic gathering and analysis of world-wide accelerator reliability and availability.

A very detailed review of the accelerator beam dynamics simulation codes was accomplished, and progress made on code improvements, new capabilities, and application to the accelerator design process. The stringent IFMIF beam loss requirement necessitates continued emphasis on advanced methods.

The reference conceptual design for the 8-40 MeV linac uses room-temperature rf-cavity technology. Superconducting cavities offer several potential advantages; work was accomplished in Japan to further develop and explore this option. Important confirming accelerator technology demonstration is in progress with the construction of a full-scale cw 100 mA proton linac prototype to ~10 MeV at Los Alamos.

1.5 Design Integration

Safety Assessment

An activity aimed at the safety assessment of the entire IFMIF plant and its subsystems (Test Cell, Target, Accelerator and Conventional Facilities) has been carried out using the PRA (Probabilistic Risk Assessment) methodology. Results show that the IFMIF plant is quite safe and presents no significant hazard to the environment. Additional safety analysis is required as soon as a more detailed design is available because the level of detail for the conceptual design is not sufficient to reach a final assessment.

RAM Summary

An overall facility availability goal of 70% is a primary IFMIF specification. This requirement constitutes a new major design factor. Existing accelerator-driven facilities typically operate with much reduced yearly operating hours than intended for IFMIF, and therefore more time for maintenance, but these facilities do represent the available experience base with relevant components. However, none of the information from major existing facilities had ever been systematically collected and analyzed. Intending to put the RAM aspect, along with physics, engineering and cost aspects, on a systematic and inter-correlated basis, during the CDA the IFMIF team conceived and developed the powerful Accelerator System Model (ASM), and used it to guide conceptual design choices and the development of a credible RAM model.

During the CDE, the subsystem and component RAM database was systematically developed by obtaining voluminous data from a number of operating accelerator facilities, and by beginning the task of translating the information into a consistent format and performing the required analyses.

Already at the stage achieved by the CDE, important and new insight into the reliability requirement has resulted. The initial objectives were to study the operating procedures employed in these facilities to achieve the recorded availability, and to collect performance data. It was found that the organization of operations across the facilities is remarkably similar, with differences mainly reflecting more or less formality depending on the facility size. A preferred database format for future data capture has been proposed and endorsed by a number of facilities.

At this time, the state of the art in the area of reliability of repairable systems leaves a lot of uncovered ground even outside the field of accelerators. Continued development of this methodology is thus necessary to achieve the IFMIF system design with the required availability characteristics. There are three major directions recommended at this time for future activities: continued data collection, continued statistical inference analysis, and development of modeling approaches for accelerators as repairable systems (in the form of stochastic process simulations).

Central Control System

Two instruments have been evaluated by JAERI that are important for the interface between the accelerator , target and test cell.

Neutron Monitor

Two detector concepts have been evaluated for calibration and operation of the neutron monitor. The concept is based on a compact multi-channel neutron detector which is calibrated by an activation wire detector.

Infrared Camera

An infrared camera concept has been evaluated to measure the beam position and temperature distribution on the target.

2 Test Facilities

2.1 Introduction

It has been agreed at the beginning of 1997 that instead of a broad based engineering evaluation phase a smaller reviewing phase, named Conceptual Design Evaluation (CDE) and covering the period until the end of 1998 should follow the CDA phase. This is why only a fraction of the necessary tasks originally specified for an engineering oriented evaluation phase could be handled during this CDE phase. Due to the nature of the CDE phase, the main objectives for the Test Facilities/Users group during 1997-98 were (i) to review the baseline design concept of the former Conceptual Design Activity (CDA) period, (ii) to present the progress made in the design and neutronics fields and to discuss the consequences, (iii) to implement additional requirements of the users community, (iv) to improve the design of key devices, (v) to calculate in more detail relevant nuclear responses of the neutrons, and (vi) to assess the possibility for using real-time neutron/gamma detectors. Major goals of the CDE phase were therefore:

1) Component design and development:

- Validation of CDA design and specification of a sub-sized test apparatus for the helium cooled high flux test module
- Calculation of thermo-hydraulics and temperature distribution in specimens, capsules and rigs
- Detailed design of a sub-sized test apparatus equipped with rigs and instrumented specimen capsules
- Fabricability of specimens, specimen capsules and test module
- Handling tests to demonstrate assembling and disassembling as well as initial thermo-hydraulic tests
- Design of an improved reference high flux test module
- Validation of present design and improvement of the test module for in-situ tritium release tests on breeders in the medium flux position
- Feasibility of the VTA2 concept taking into account all ducts and helium gas tubes
- Design of improved reference VTA2 equipped with test modules for creep-fatigue and tritium release tests

2) Neutronics:

- Improvement of the D-Li nuclear model to reduce the neutron yield uncertainty
- Evaluation and preparation of a D-Li cross-section data file
- Assessment of γ-ray and by-products generated from the D-Li reaction
- Evaluation and processing of further neutron cross-section data (E>20 MeV) as needed for the neutronics design calculations
- Preparation of a first version of an Activation Cross-Section File (E>20 MeV)
- Re-evaluation of irradiation parameters for the high flux test region taking into account the recent results of the detailed neutronics calculations
- Improved assessments for the medium flux region with breeder material samples
- Qualification of the IFMIF displacement damage characteristics in the High Flux Test Module in comparison with ITER and DEMO irradiation conditions

- Shielding and activation analyses (thickness of walls for access cell, hot cells etc., gamma and total heat generation in test modules, decay heat evaluation for NaK and helium gas coolant)
- On-line neutron and gamma detectors, and data base (E_n < 50 MeV) for dosimetry.

User specific tasks were added and discussed in detail during a related Users meeting on November 1 1997 in Sendai, Japan. Although the user tasks are basically not related to design requirements, they represent important activities in the present phase because of their outstanding relevance for the overall IFMIF performance. The development program that has been specified is structured into 9 component design tasks, 4 neutronics tasks, and 3 user tasks.

The table gives a task overview and indicates whether there were activities during the CDE phase.

	Component Design & Development	**Priority***	**Tasks During CDE (1997-98)**
1	He cooled high-flux test module	High	Yes
2	Tritium release test module[2]	High	Yes
3	Creep-fatigue test module	Medium	
4	VTA handling mock-up	Medium	
5	VIT system mock-up	Low	
6	Universal robot system	Medium	
7	Integral test cell design	Low	
8	Remote handling PIE	Medium	
9	Tritium laboratory[3]	Medium	
	Neutronics		
10	Source term of D-Li reaction	High	Yes
11	20-50 MeV data evaluation	High	Yes
12	Shielding and activation analysis[3]	High	Yes
13	On-line gamma monitors	High	Yes
	User group		
14	Re-evaluate irrad. parameters	High	Yes
15	Evaluation of Li-target backwall	High	Yes
16	Small specimen test technology	High	Yes

*) Priority for CDE phase, according to the Subcommittee Meeting, Brussels, Jan 30-31, 1997.

2.2 CDE Tasks

2.2.1 Helium cooled high flux test module

Description and justification:

Providing a test module for specimen temperatures of up to 1000 °C is one of the most challenging design requirements for the IFMIF test facilities. The successful development of a He-cooled test module would provide for any material a broad temperature window as well as flexible and very safe operating conditions. It is necessary to demonstrate (1) the fabricability of specimen encapsulation, helium gas pipes, active ohmic heating elements, and rigs, (2) the remote handling of all assembly and disassembly procedures, (3) the thermal hydraulics under different loading conditions, (4) the structural integrity, as well as (5) the proper function of the instrumentation equipment. All these requirements have to be demonstrated under relevant conditions on a suitable test module mock-up assembled with an adequate number of completely instrumented rigs.

Contributors:

Organization	Principal Investigator
FZK	A. Moeslang, G. Schmitz
ORNL	J. Haines

Main responsibility: FZK

Milestones:

1) Validation of present design	July 1997
2) Prototype development and testing of sub-sized test module	
- Define test apparatus	Oct. 1997
- Calculate thermo-hydraulics and temperature distributions in specimens, capsules and rigs	Dec. 1997
- Detailed design of capsules and actively heated specimens	March 1998
- Detailed design of instrumented rigs and dummy rigs	March 1998
- Detailed design of simple test module with flow paths	Sept. 1998
- Fabricate test specimens	Dec. 1997
- Fabricate capsules and rigs	Oct. 1998
- Fabricate test module	Dec 1998
3) Documentation	Dec 1998

2.2.1.1 Impact on CDA

The general validation of the CDA design taking into account a preliminary improved reference HFTM based on new neutronics results has confirmed largely the existing, highly modular concept.

The main activity during the CDE-phase, however, was dedicated to a prototype development of a sub-sized test module to verify experimentally details of the design, the handling and the thermal hydraulic calculations. The development of that sub-test module has also verified the reference design concept, that is, there has not yet been any need to modify the general HFTM reference design developed during the CDA phase.

2.2.1.2 Results & Conclusions

Providing a test module for specimen temperatures of up to about 1000 °C is one of the most challenging design requirements for the IFMIF test facilities. The successful development of a He-cooled test module would provide for any material a broad temperature window as well as flexible and very safe operating conditions.

HFTM reference design

The reference design done during the CDA phase for major components of the test cell has been evaluated mainly to implement additional requirements of the users community, and to take into account more recent flux/volume and heat deposition calculations from the neutronics group.

During the early stage of the CDE phase,- the hydraulic calculation of the helium pressure drop (PD) in the helium-cooled high flux Vertical Test Assembly (VTA1) as specified in Section 2.4 of the IFMIF CDA final report was carried out. As this calculation has given a too high PD of greater than 0.8 bar in that reference design, the form and dimension of the helium pipes were optimized and changed from circular form with a diameter of 30 mm to a rectangular form of about 50 mm side length. Also the shape of the rigs in helium flow direction was changed resulting in a lower hydraulic resistance. These updates of the reference design are shown in Fig. 2.2.1.2.1.

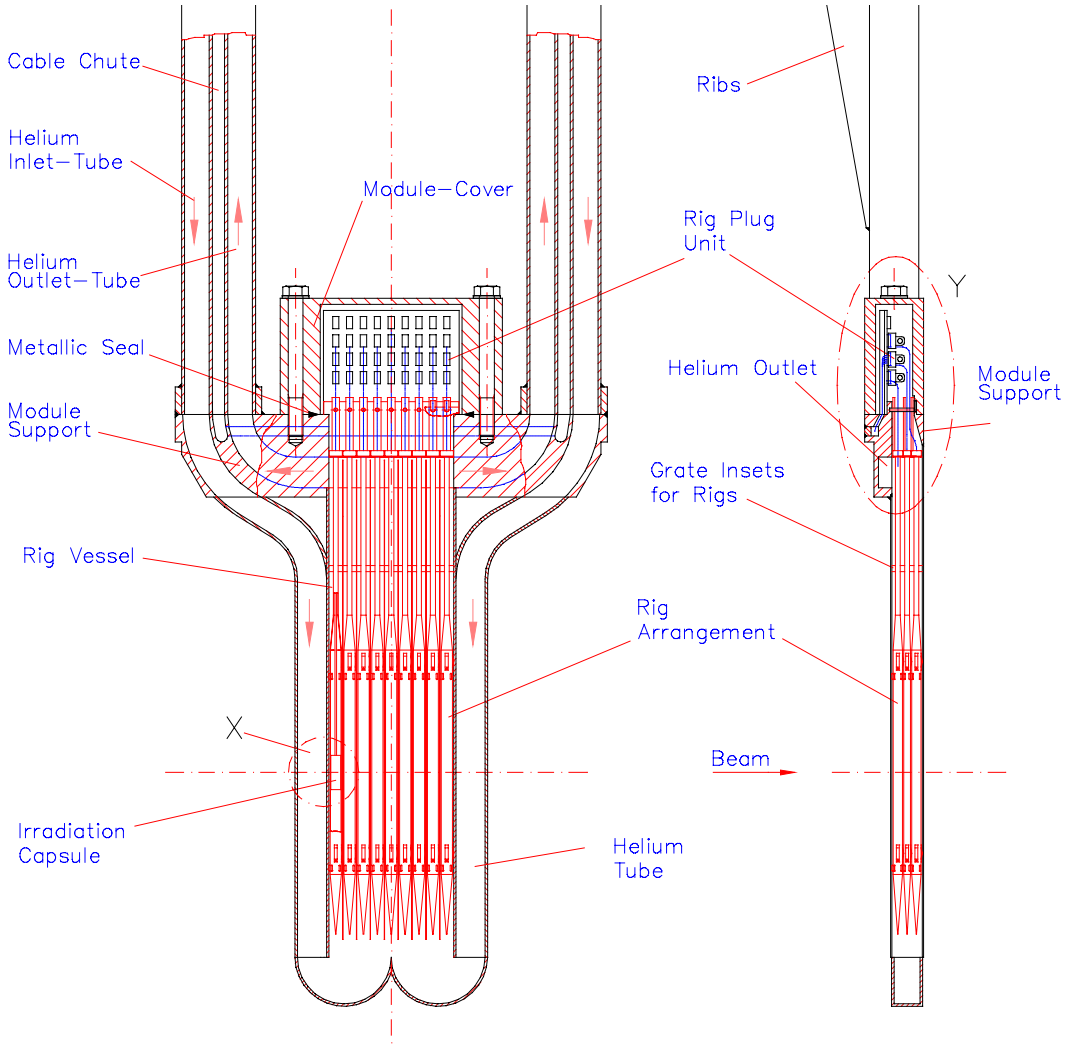

Fig. 2.2.1.2.1: Front and elevation view of the updated design configuration for the helium gas cooled high flux test module.

The helium is now streaming from the bottom of the rigs upwards, it flows along both sides of the test modules (better cooling efficiency) and the rigs are opened at the top and bottom to guarantee for a similar helium pressure inside and outside the rig walls. Another important feature is that all rigs can be disassembled and re-assembled individually after the module cover is opened and the electrical signals are disconnected from the rig plug unit. In the revised reference design the HFTM has 27 vertical rigs arranged in three rows, each consisting of 9 rigs.

Prototype development and fabrication of a sub-sized test module

In order to test the fabricability, remote handling, heat removal etc., a detailed design for a sub-sized test apparatus has been done [1]. The developed design is a test module that is in the geometry and the material very similar to the reference design but has only 9 instead of 27 rigs. That is, the helium flow channels, hydraulic diameter, wall thickness etc. basically reflects the reference design. Fig. 2.2.1.2.2 shows FE-calculations of this sub-test module. The geometry can be interpreted as the left side of the front view in Fig. 2.2.1.2.1, that is, as one third of the reference design.

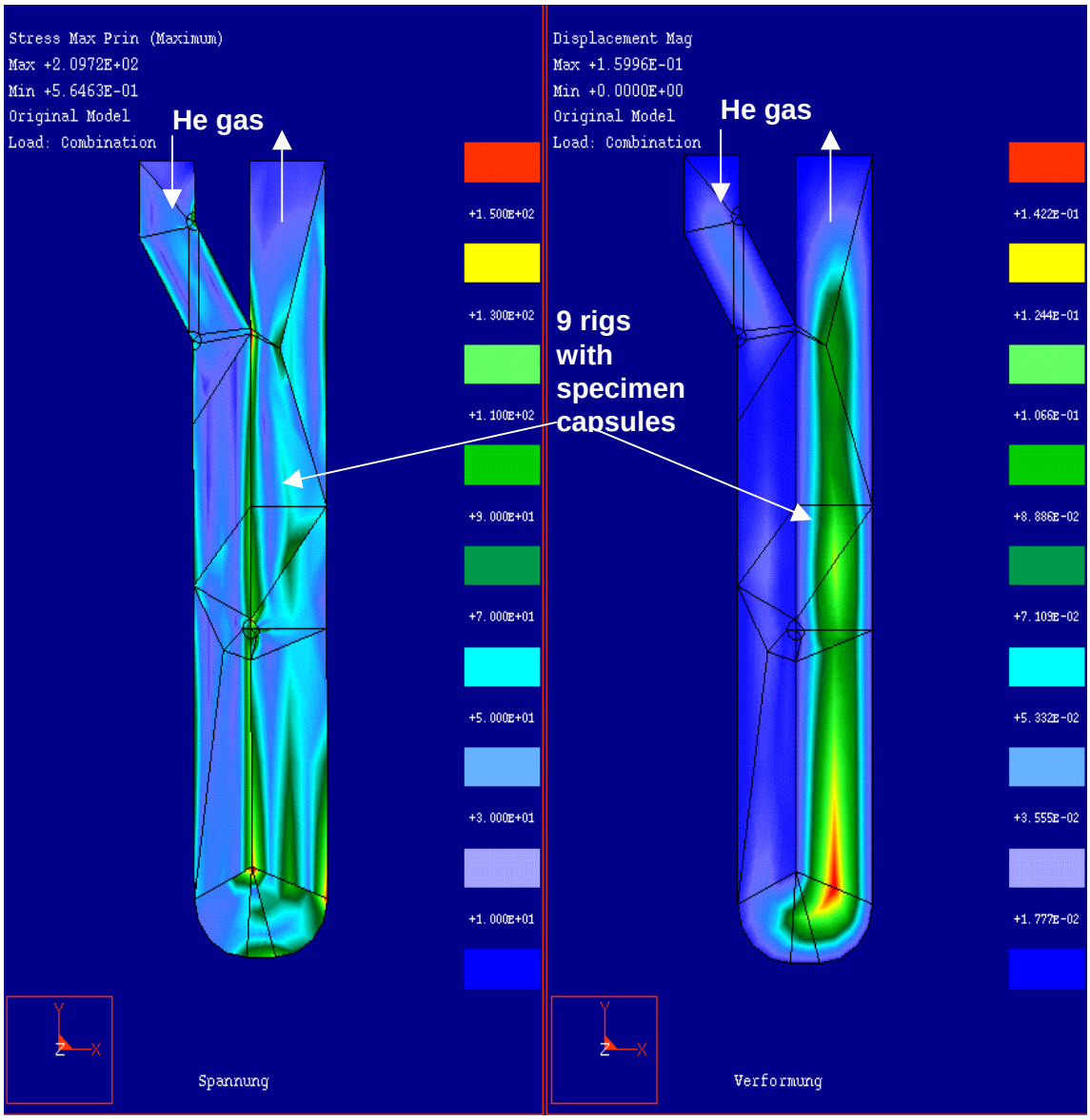

Fig. 2.2.1.2.2: Stress analyses (left, numbers in MPa) and strain analyses (right, numbers in mm) of a sub-sized test module that houses 9 rigs with instrumented specimen capsules.

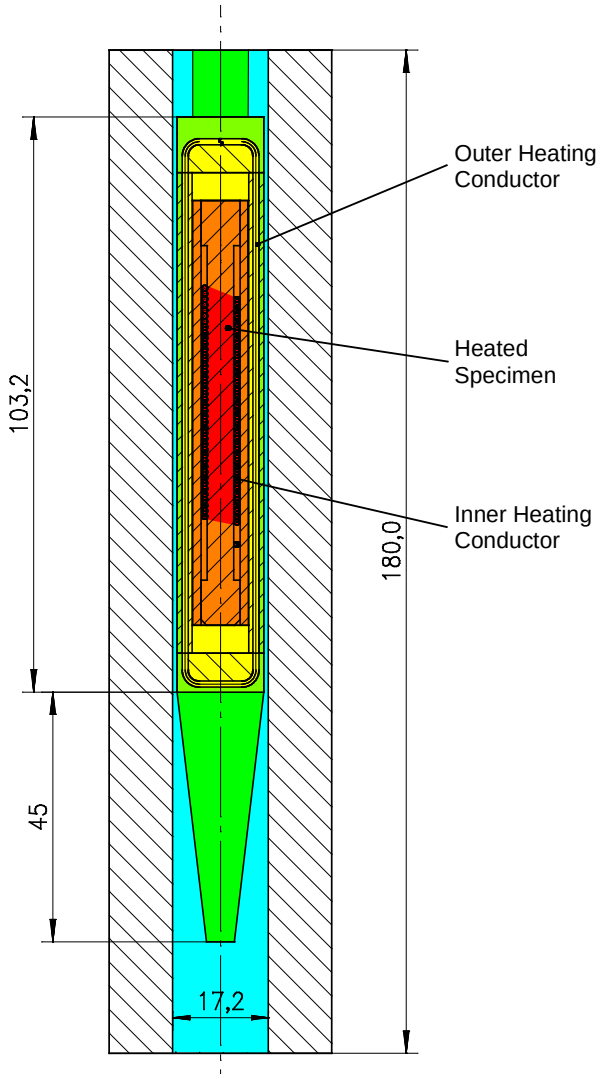

Fig. 2.2.1.2.3: Fabricated single-rig test module housing one rig instrumented with a specimen dummy.

The FE-analyses of the sub-sized test module have shown that for reference helium-gas coolant conditions and a wall thickness of 2 mm (reduced activation steel F82H-mod, unirradiated) the maximum stress does not exceed 210 MPa and therefore is considered to be not critical. The maximum displacement was calculated to be 0.16 mm at the turning point of the helium coolant and hence, is also very moderate. Although it might not be necessary, both values could be reduced further by dedicated design improvements.

However, due to the nature of the CDE phase, this sub-sized test module could not be fabricated. This is why a smaller test module with one rig only has been selected as the test object to verify the key parameters of the helium gas coolant concept.

As obvious from Fig. 2.2.1.2.3, this single-rig test module consists of a hollow canister with a square cross section (gray hatched) and houses the specimen capsule (green) which has an integrated ohmic heating system. Inside this rig the specimens are replaced by one specimen dummy (yellow and orange) that is also heated by ohmic heaters. The heated zone of the specimen dummy has a length of about 50 mm (red color) and therefore adequately reflects the height of the IFMIF beam foot print. In this way both, the nuclear heating in the specimens and in the specimen capsule can be simulated in a manner that is representative for expected IFMIF heat loadings. The gas gaps, the wall thickness of all structural materials (reduced activation ferritic/martensitic (RAFM) steel F82H-mod), the overall rig, capsule and specimen dummy dimensions are practically identical with the IFMIF reference design.

The blue color in Fig. 2.2.1.2.3 shows the helium gas inlet (bottom) and outlet (top). Presently this single-rig test module is fabricated and assembled at FZK. After the integration of this test module in a suitable helium gas loop, a variety of parameter studies are foreseen to verify experimentally (i) the fabricability of devices with RAFM steels, thermo-hydraulic calculations, and (iii) the structural integrity during and after thermal cycling test to high specimen and capsule temperatures.

2.2.1.3 Future Directions

- Presently, the first version of the sub-sized test module is fabricated. After assembling and integration of thermocouples it will be tested in a helium coolant loop at FZK in order to verify the thermo-hydraulic calculations experimentally and to confirm the overall gaseous coolant concept.
- With that knowledge and with the results of the advanced neutronics calculations, the existing reference design concept of the HFTM can be modified, if necessary. As soon as the database for a suitable reduced activation material will be available, 3D stress calculations will have to be performed in order to further optimize the reference test module design.
- Although the suggested helium coolant concept is based on long-term experience from high energy accelerators and mixed spectrum reactor irradiations, it should be verified in a suitable neutron environment mainly because of its degree of miniaturization. Therefore, it is suggested to construct, fabricate and irradiate in a fission reactor a sub-test module that represents all relevant features of an IFMIF high flux test module. That rig would already be equipped with a representative number of miniaturized specimens and would be suitable to do parameter studies under realistic heat production conditions.

References

[1] M. Class; Layout and design of a helium gas cooled test module for IFMIF); unpublished FZK report IMF-050, 1998.

[2] A. Möslang and R. Lindau, Proceedings of the IEA-Technical Workshop on the IFMIF Test Facilities, Karlsruhe, Germany, July 7 - 9, 1997, Forschungszentrum Karlsruhe, FZKA 5993, 1997

[3] A. Möslang, C. Antonnucci, E. Daum, J.R. Haines, S. Jitsukawa, K. Noda and S. Zinkle, Overview of the IFMIF Test Facility, ICFRM-8, Sendai, Japan, October 1997, Journal of Nuclear Materials 258-263 (1998) 427.

[4] E. Daum, A. Möslang, M. Sokcic-Kostic, 2nd Topical International Meeting on Nuclear applications on Accelerator Technology (AccApp98) Gatlinburg, TN, USA, September 20-23 1998; Proceedings American Nuclear Society 1998, p. 534.

[5] K. Noda, K. Ehrlich, S. Jitsukawa, A. Möslang and S. Zinkle, User's requirements for IFMIF, ICFRM-8, Sendai, Japan, October 1997, Journal of Nuclear Materials 258-263 (1998)

[6] T.E. Shannon, R.A. Jameson, H. Katsuta, H. Maekawa, M. Martone, A. Möslang, V. Teplyakov and M.J. Rennich „Conceptual Design of the International Fusion Materials Irradiation facility (IFMIF)", Journ. Nucl. Mater. 258-263 (1998) 106.

[7] T. Kondo "IFMIF, its facility concept and technology" Joun. Nucl. Mater 258-263 (1998) 47.

[8] J.R. Haines, S. Jitsukawa, A. Möslang, K. Noda, R. Viola, S.J. „Design concept of the IFMIF test assemblies", Journ. Nucl. Mater. 258-263 (1998) 400.

[9] K. Ehrlich and A. Möslang, „IFMIF - An international fusion materials irradiation facility“, Nucl. Instr. and Meth. In Phys. Res. B 139 (1998) 72.

[10] T. E. Shannon, H. Katsuta, H. Maekawa, R. A. Jameson, M. Martone, A. Möslang, M. J. Rennich, V. Teplyakow; „IFMIF: A High Intensity Deuteron Beam Application“, EPAC’98, June 22-26 1998, Stockholm; Proceedings in press.

[11] K. Ehrlich and A. Möslang, “International Fusion Materials Irradiation facility (IFMIF): User requirements and test cell design”, Annual Meeting on Nuclear Technology ’97, May 13-15 1997, Aachen, Germany, Inforum Verlag Bonn (1997); ISSN 0720-9207; p. 550.

[12] A. Möslang, K. Ehrlich, T. E. Shannon, H. Katsuta, H. Maekawa, R. A. Jameson, M. Martone, A. Möslang, M. J. Rennich, V. Teplyakow, „Suitability and Feasibility of the International Fusion Materials Irradiation Facility (IFMIF) for Fusion Materials“; Internat. IAEA Conference on Fusion Technology, Yokohama, 18-24 Oktober 1998, Proceedings.

[13] K. Ehrlich and A. Möslang, “IFMIF – An international fusion materials irradiation facility” Nucl. Instr. and Methods in Physics Research B139 (1998) 72.

2.2.2 Tritium release test module

Description and justification:

The availability of suitable tritium breeder materials that have been tested and developed under real loading conditions is a major requirement for a fusion reactor. Tritium release experiments using several different types of breeding material candidates are planned for the medium flux region of the Test Cell. To function properly, the temperature of the tritium-release test specimens must be kept at a prescribed value, while the temperature of the structural material should be maintained as low as possible (ambient temperature) to avoid tritium permeation and a large degradation of the mechanical integrity of the structural materials due to irradiation.

For this purpose and to perform the tritium gas release experiment, pipes, six or more in number, with a diameter of about 1 to 2 mm will be attached to a capsule. The capsules are further complicated by the need to easily connect and disconnect these pipes for re-encapsulation. One full scale sub-test module includes four kinds of capsules for disk, pellet, and pebble shaped specimens and compatibility test specimens. The design of the sub-test module is carried out based on the evaluation of the thermal behavior of the design concept and taking into consideration the degradation of capsules/sub-test module due to the irradiation and swelling of the irradiated breeder materials.

Contributors:

Organization	Principal Investigator
JAERI	S. Jitsukawa
ENEA	G. Mercurio, P. Turroni
FZK	A. Möslang

Main responsibility: ENEA and JAERI

Milestones:

- Validation of present design	Sept 1997
- Design study of specimen temperature control	Dec. 1997
- Design study for easy attachment/detachment to VTA	Dec. 1997
- Design of one full scale sub-test module	July 1998
- Feasibility of VTA2 concept with two test modules	July 1998
- Design integration: Concept to combine VTA2 with 2 test modules	Dec 1998
- Detailed analyses of tritium release test module concept	Dec 1998

2.2.2.1 Design Integration

2.2.2.1.1 Impact on CDA

The Tritium Release Test Sub-module (TRTS) of the VTA 2 is conceived to admit simultaneous tests at different temperatures for several specimens. Specimens are made of a ceramic material that, according to the specific scope of the test, will be selected carefully and

shaped to different geometries. The expected specimen and test types are listed in the following table.

Table 2.2.2.1-1 - Specimens and test condition frame to be used in the TRTS

Specimen	Diameter (mm)	Thickness (mm)	Temperature (°C)	Test type	Dose (dpa)
Disk	10	2	400/600/800	In-situ tritium release Neutron radiography	10, 20, 30
Pellet	10	10	Temp. grad.	Mechanical integrity Dimensional change	
Pebble	1		Temp. grad.	Microstructure change Tritium/He retention Fracture strength, etc.	
Breeder	5	1,5	400/600/800	Compatibility	
Structural	5	0,5	400/600/800	Compatibility	10, 20, 30

All specimens will be put inside probes that must be lodged within a volume in the Test Cell where the neutron flux presents the adequate characteristics for the testing conditions (that is a rate of ~10 dpa/y equivalent for standard ferritic steel). The volume size and shape is roughly 50 mm thick, 50 mm high and 220 mm wide.

Within this restricted volume, the probes must also be supplied with cooling, temperature control, temperature monitoring and tritium release rate sensors.

The TRTS is divided into parallel coolant sections with an independent control of the cooling helium flow according to the temperature to be maintained for the specimens and the internal generated heat. A tuning of the heat transfer rate from the test probes to the coolant gas for obtaining the desired test temperature for the specimens is basically made by a gas layer surrounding the probes where the conditions affecting its thermal conductivity can be controlled. Also the coolant gas flow rate that must be adapted to the level of internal heat generation, may affect the global heat transfer coefficient, but only significantly in the turbulent flow regime and in a way difficult to control. The transition from laminar flow to turbulent flow will be characterized by a dramatic change.

The regulation of the heat transfer should allow to keep constant the desired specimen temperature during the test campaign, and uniform within a TRTS section. The regulation should be flexible to set the right temperature for different specimen materials inside a coolant section, and accommodate the geometrical and physical modification during the irradiation campaign. In particular, it should be capable to cope with varying levels of heat generation due to ion beam modulation or a reduced rated power regime (i.e. reduced by 50% due to one beam of the two being off.).

Measurements of tritium release rate must be carried out during the test campaign. In order to do this, a filler gas inside the capsules is swept out through a specific connected line. The released tritium mixes with the sweep gas and is transported to the proper measuring equipment. A quite low sweeping gas flow will be sufficient to measure the present tritium and not to affect the specimen temperature significantly.

The capsule inner wall, being separated from the specimen only by the thin sweep—gas layer, will have a temperature not too far from that of the specimen. So, in case of a specimen temperature of 800 °C, the effectiveness of a tritium permeation barrier envisaged for the high penetration of tritium in solid metal at high temperatures, is questionable and this point remains to be assessed with specific research on tritium barriers.

Thermo-hydraulic analyses have been performed with two-dimensional models for a section of the TRTS where the specimens, the sweep—gas and gas—gap layers, the structural walls of the capsule and the TRTS section have been represented with their thickness and their relevant

physical characteristics (code FLUENT). A parametric set of cases has been analyzed by changing the helium coolant velocity, the rate of the internal heat generation, and the gas-gap thermal conductivity. For some peculiar case an analysis with a three-dimensional model (code CFX) was performed.

The TRTS, assembled and set-up for a test campaign that will presumably last one year, is mounted on the VTA 2 shielding body. Because the large and heavy VTA 2 shielding body may have been contaminated due to the previous test campaign, the mounting operation has to be carried-out with remote handling techniques in the Service Cell. After the test campaign, the activated TRTS again has to be dismounted with remote handling operations in the Service Cell and moved to the Hot Cell for its disassembly. The TRTS design with such different and multiple hydraulic and instrumental lines should consider an arrangement and reversible connectors that can be operated adequately by remote handling. With that aim the TRTS geometrical lay—out has been reviewed to obtain a configuration that better combines these aspects together with the structural compliance of the differential thermal expansion and swelling, and the feasibility of the TRTS assembly itself.

2.2.2.1.2 Results & Conclusions

ANALYSES - Analyses have been carried out with a 2D model varying: a) the coolant He gas velocity in the range of 1 to 6 m/sec; b) the thermal heat generation from 30 and 15 W/cm^3, respectively on the specimen and on the structural material to the half generation regime that is 15 and 7.,5 W/cm^3; c) the gas-gap thermal conductivity coefficient from the condition of pure helium at a normal pressure to a condition of pure argon. Concerning this last parameter, it has to be pointed out that the amplitude of the variation range corresponds to a factor of 10 and a variation within this range may be realized more easily with a varying binary mixture of helium and argon gases instead of a pure helium with a pressure of down to only some hundreds Pa. Efforts to attain a lower thermal conductivity are worthwhile only, if accompanied by a limitation of the thermal radiation that plays a more significant role. The results of analyses with Fluent are summarized in the table 2.2.2—2. The results regarding their absolute values are to be taken with care due to the simple 2D model. In fact, the real “thermal exchange surface” to “heat generation volume” ratio is larger than that represented on the 2D model, so the real specimen and outlet temperatures are expected to be lower.

Table 2.2.2.1-2 – Summary of the results from the 2D analyses with FLUENT code

Case ident.	**v (m/s)**	**Heat Gen. (W/cm3)**	**Emissivity**	**k Gas Gap (W/mK)**	**T Spec. °C**	**T outlet °C**
c	3	30-15		He	709	144
a	2	30-15		He	761	206
b	1	30-15		He	876	391
o	6	30-15	0.3	He	640	82
m	6	30-15	0.3	Double GG*	641	82
n	6	30-15	0.3	He(50%)+Ar	874	82
e	3	30-15	0.3	He	706	144
d	1	30-15	0.3	He	848	389
f	1	15-7.5	0.3	He	505	206
g	1	15-7.5	0.3	He (95%)+Ar	512	206
h	0.5	15-7.5	0.3	He (95%)+Ar	614	383
p	1	15-7.5	0.3	Ar	1094	205
l	1	15-7.5	0.3	Double GG	505	205

* Gas Gap section thickness=4 mm with He.

Regarding the above results with their relative meaning, a few points still remain to be added:

- in order to control the specimen temperature, it is more effective to act on the gas gap conductivity than on the coolant flow velocity (cases "e" and "o" velocity reduction of one half rises the specimen temperature by 65 °C, while reducing the gas gap conductivity by 50% (case "o" and "n"), the increase is 234 °C; for all cases a pure linear coolant flow is assumed);
- to control the specimen temperature, the pure helium gas-gap must change in terms of pressure by a factor of the order of “hundreds”, while an helium/argon mixture has to change within the two extremes;
- assuming a full power rate and a gas-gap of pure helium, the thermal radiation plays only a minor role of a few percent at a specimen temperature of about 800 °C, while an argon gas-gap would lead to a much stronger impact.

Results for more specific cases are also obtained with a 3D model based on the CFX code. The model represents a TRTS section containing two capsules. Some contribution from turbulence has been assumed for the coefficient convection on the cooling gas. The cases analyzed and the summary of the results are given in table 2.2.2—3. Case 2 is also illustrated by Fig. 2.2.2—1 showing the map of the temperature distribution. Results show the difficulty to maintain the specimen at ~800 °C, while keeping the structural wall at less than 100 °C. The wall containing the cooling gas has to rise in temperature in order to keep the specimen temperature high. Also the capsule wall has a temperature very close to the specimen temperature. This justifies the concerns regarding the efficiency of the tritium barrier.

Table 2.2.2.1-3 – Summary of the cases and results from the 3D analyses with the CFX code

Case ident.	v (m/s)	Heat Gen. (W/cm3)	Turbulence	Gas Gap	$T_{Spec.}$ °C	T_{outlet} °C
1	3	30-15	none	He 10% + Ar 90%	614	217
2	1,5	30-15	none	He 10% + Ar 90%	687	327
3	2	30-15	10%	Ar 100%	727	227
4	1,5	30-15	10%	Ar 100%	759	327
5	1	30-15	10%	Ar 100%	827	477

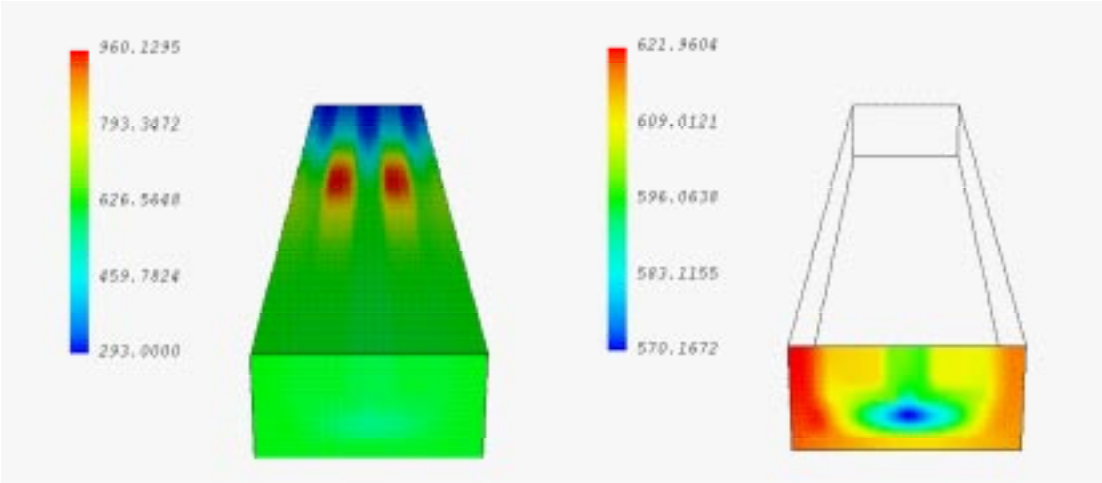

Figure 2.2.2.1-1 Temperature distribution map of a cooling section containing 2 capsules. Case with cooling gas flow velocity of 1,5 m/sec, no turbulence and a gas-gap mixture of 10% helium + 90% argon. Temperature unit is °K

LAY-OUT: The structural lay-out of TRTS is mostly influenced by the convergence of a number of hydraulic lines and thermocouple cables to small components confined in a small room. When replacing a TRTS in the VTA 2, manipulators with remote handling operations are required and all line connections must be equipped with quick and reliable connectors by robots. Special attention must be paid to the tritium containment in the sweep—gas line connectors. The tritium having a high permeation through the pipe walls at high temperatures (> 400 °C) requires a special "barrier" in the capsule containing the specimens. The following assumptions were made when reviewing the geometrical lay-out:

1. Special pipe joints suitable for R.H. technology must be used.
2. A containment cover device is foreseen around the pipe connections of the sweep gas circuit in order to ensure a better leak tightness of tritium towards the surroundings
3. Thermocouples on each cell are used to control the temperature
4. The thermal displacement produced during the experiments in the gas gap and in the gas sweep pipes is, as a general provision, compensated by means of bellows. Figure 2.2.2.1—2 illustrates the provisional lay-out of the TRTS at this stage.

2.2.2.1.3 Future Directions

In order to rely on the gas—gap layer to control the temperature of the specimen within the envisaged range for all expected levels of heat generation, and to keep the structural wall temperature low, the layer thickness must exceed the 2 mm actually considered, such as to produce the thermal gradient corresponding to a differential temperature of the coolant section wall of ~100 °C and the capsule wall of close to 800 °C. Attempts to limit the thermal radiation across such a layer should also be made.

Alternatively, the tritium sweeping may be made with the same gas-gap by unifying it with the actual sweep-gas layer . Thus, the thermal conductivity can be modified over a more important thickness. The capsule wall would simply became a thermal baffle to protect the specimen from the hardest temperature non-uniformity. The tritium containment will be featured by the gas-gap wall and the permeation barrier will be applied at the colder side of the gas gap layer, thus making the barrier more effective. The lines to be connected to the TRTS will be reduced by a merging of the gas-gap and the sweep-gas lines. On the other hand, assuming that the gas-gap is filled with the changing mixture of He and Ar, the feasibility of the tritium measures and separation during the transport of such a gas mixture must be verified.

If for both alternatives the gas-gap mixture is selected instead of pure He with a changing pressure, helium and argon must be separated in order to be able to recycle the two components.

The options outlined above will constitute the leading points for the next design activities with thermo-hydraulic analyses and coherent and feasible lay—out development.

A final and definite assessment of the thermo-hydraulic behavior may be further pursued with a simplified TRTS mock-up construction and test. Also specific quick connector tightness reliability and operability by remote handling are arguments to be assessed by tests.

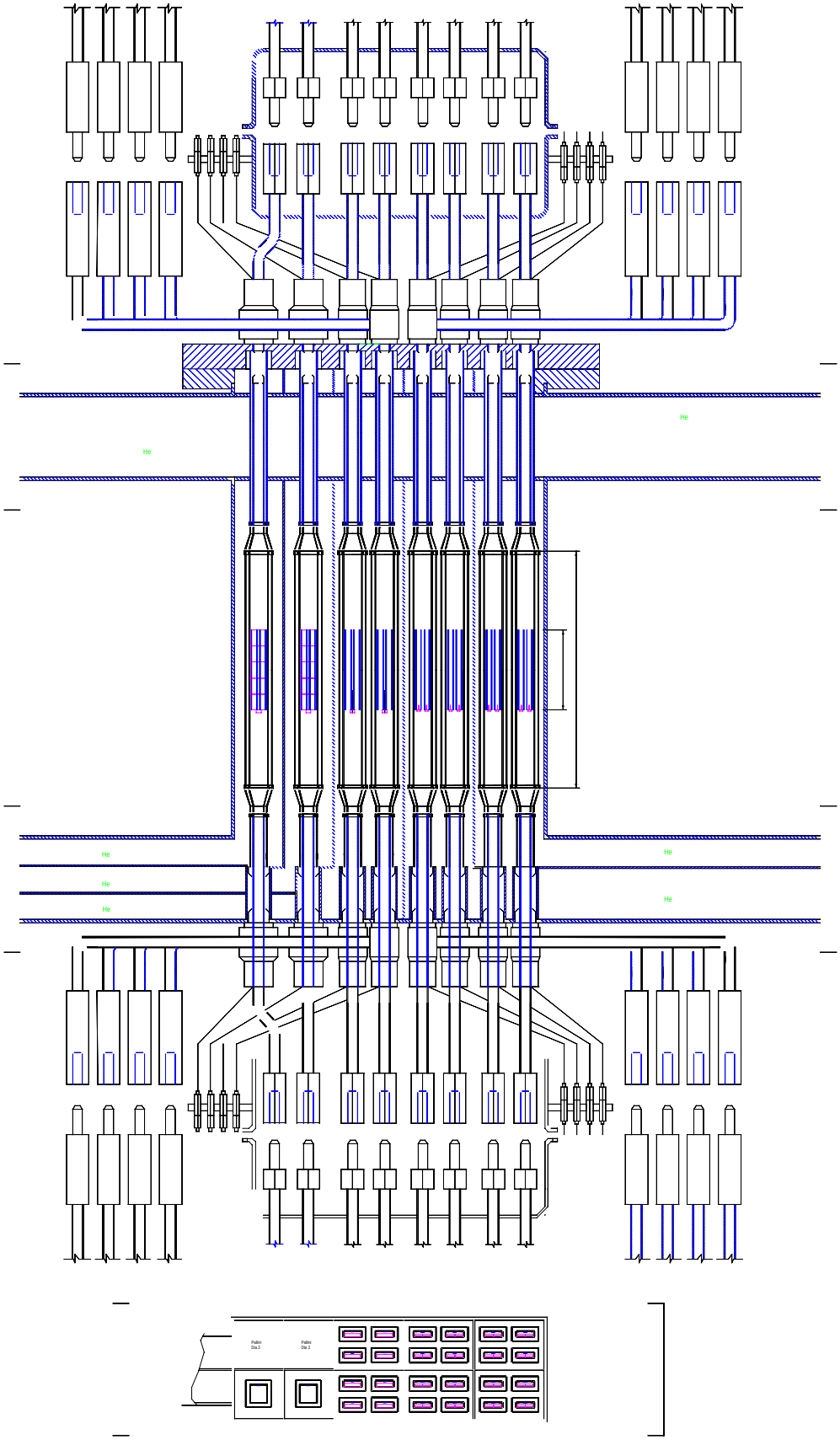

Figure 2.2.2.1 – 2 Lay-out of the TRTS

2.2.2.2 Design Analysis of the Tritium Release Test Module Concept

2.2.2.2.1 Impact on CDA

It is suggested to reduce the number of individual specimen capsules in order to simplify the fabricability. Tritium production and displacement damage production rates are evaluated. They confirm basically the parameters reported in the CDA report.

2.2.2.2.2 Results & Conclusions

The in-situ tritium release test module was designed considering the loading capacity to be maximized for the better efficiency of the IFMIF. On the other hand, the capacity of VTA 2 became a concern while increasing the number of specimens and the complexity of the module. Two test modules of the tritium release and creep-fatigue experiments needed to be pout into the VTA 2 simultaneously. The evaluation of the capacity should be conducted during the detailed design of VTA 2.

The sub-test module design for the pebble specimen has been modified. Changes are done mainly due to the results of the re-evaluation of heat generation from the specimen (neutron flux at relatively low energy levels is evaluated) and to improve accessibility to the specimen for re-encapsulation. Candidate breeding materials are also reviewed to reduce the test matrix. Priority for the experiments with pebble specimens seems to be high. And, loading of single sub-test module for pebble specimens may be recognized as the minimum requirement for an in situ tritium release experiment. Scattered neutrons by the test cell wall are evaluated in the re-evaluation of the tritium breeding reaction. Also, the displacement damage is re-evaluated.

The sizes of the pebble specimens, irradiation temperature, sweep gas parameter and the structural materials of the modules are summarized in table 2.2.2.2.1. The pebble size and its distribution determinate the tritium release rate, thermal stress in a pebble and the loading density. The diameter of the package affects the temperature distribution. The pebble sizes, diameter of the specimen package and sweep gas velocity are determined by the ITER DEMO blanket design.

The specimen temperature is defined at the wall of the package. The temperature at the outer surface of the pipe in the first breeding layer of the ITER DEMO blanket has been designed to be a relatively low temperature of 150C. Contrary to the relatively low temperature in the ITER design, the temperature of the package wall is determined to be about 450 °C according to the conceptual design of a prototype reactor (SSTR) at JAERI. One of the objectives of the tritium release experiment is to demonstrate the availability of the breeding material. Therefore, the design and the irradiation conditions should be changed with the progress of DEMO and prototype reactor design. This is also true for the selection of the candidate breeding materials. Li_2O with large heat generation density in the reactor is selected as a reference material here. Ceramic breeding materials of Li_2TiO_3, Li_2ZrO_3, Li_4SiO_4 and $LiAlO_2$ have also been developed.

A schematic cross-sectional view of the sub-test module is shown in Fig. 2.2.2.2.1. Pebbles are loaded to a height of 50 mm. Ducts of six in number are attached to the module for sweep gas, gap gas, coolant gas and thermocouples. The temperature of the material, except for that of the specimen package, is designed relatively low to reduce tritium leakage and to minimize irradiation damage of the structural material of the module. For the re-encapsulation operation of the pebble specimens, (i) pebbles are loaded in the specimen package with meshes at the top and the bottom, and (ii) the sub-test module is designed so as to remove the specimen package by only unscrewing the bottom plate.

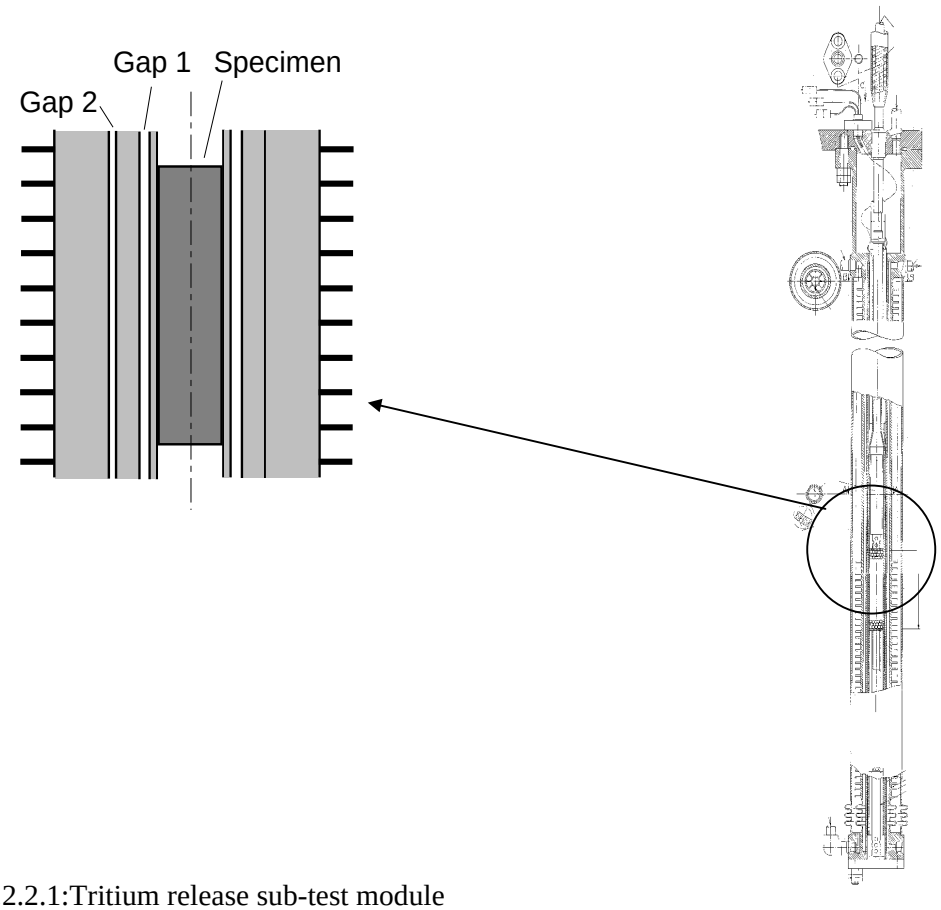

Fig. 2.2.2.2.1:Tritium release sub-test module

The test module is filled with flowing He gas to keep the outside of the sub-test module at about 150 °C. The velocity of the He gas is 0.5 l/s for one sub-test module. The temperature and the pressure of the He gas coolant is 20 °C (at the inlet) and 1 bar, respectively. Gas gap 2 is filled with stagnant He gas (>1 bar). The gas gap is designed to adjust the irradiation temperature by changing the gas pressure. Sweep gas is supplied to gas gap 1 to remove tritium from pebble specimens leaked through the wall of the pipe by diffusion. The sweep gas also flows into the pipe 1 at the bottom of the sub-test module and through the pebble specimen layer to sweep released tritium. Thermocouples of three in number are located at the top, the center and the bottom of the packed specimen. Released tritium is often occurs in the form of tritium water (HTO). To reduce the absorption of water at the surface, the temperature of the sub-test module is designed to be kept above 150 °C.

Table 2.2.2.2.1: Parameters of the in-situ tritium release experiment

Pebble specimen	60% of 2.0mm-diameter pebbles and 25% of 0.2mm-diameter pebbles
Irradiation temperature	400-500 °C at the surface of the specimen package
Sweep gas	Helium gas with water to 1000 appm Pressure: ~ 1 bar Flow rate: 3-5 cc/s (1 bar)
Structural material	Reduced activation ferritic/martensitic steel (F82H as a reference)

A schematic diagram of the He gas system is shown in Fig. 2.2.2.2.2. The flow rate of the coolant He gas for the test module is relatively large. Hydrogen may be added to 1000 ppm to the sweep He gas to enhance tritium release from the specimen. Dual concentric pipes with an electric heater wrapped inner pipe may be used as a duct from the sub-test module for the sweep gas. The duct is designed so as to reduce the absorption of HTO on the inner surface of the pipe by heating to 150 °C with an electric heater.

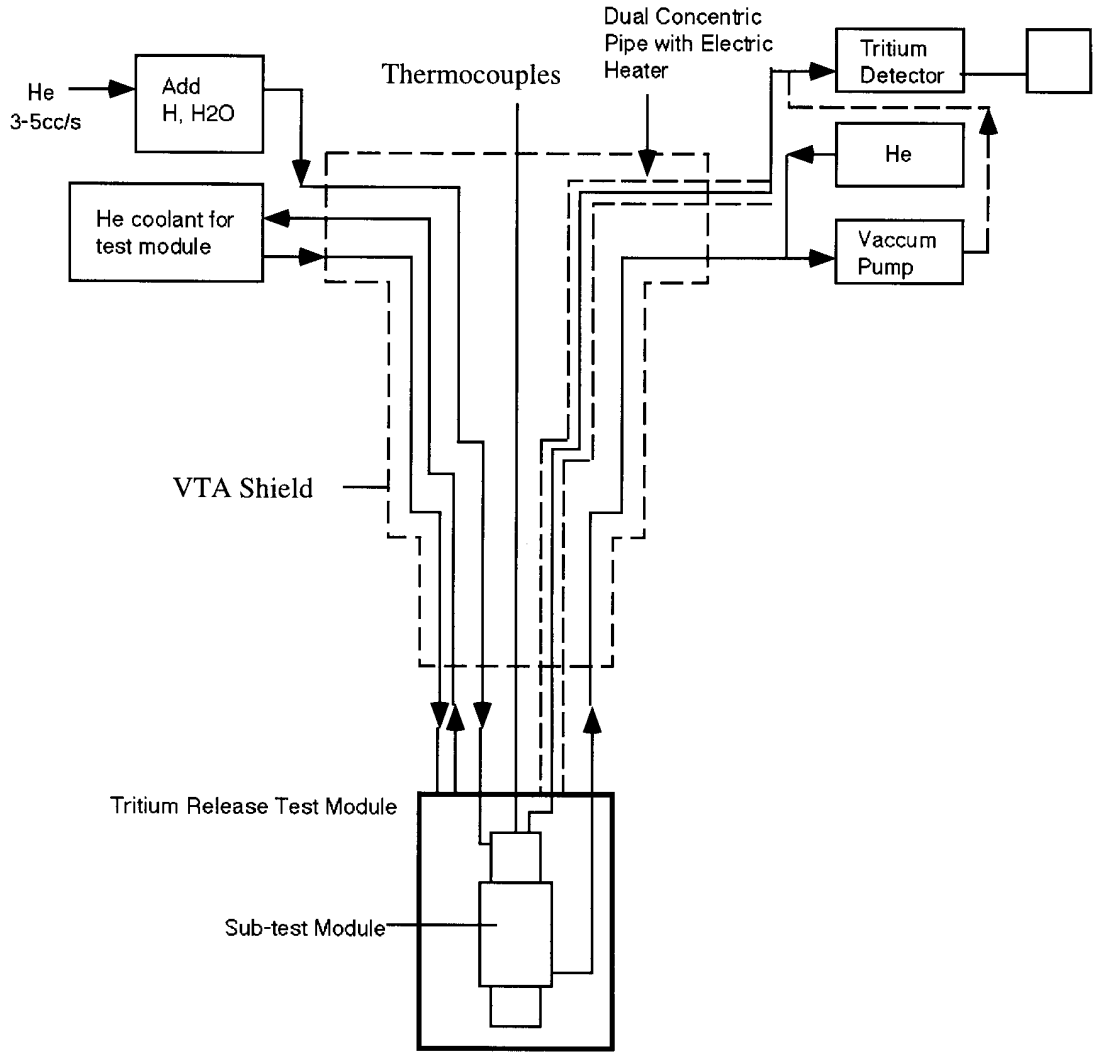

Fig. 2.2.2.2.2: Schematic flow diagram of the helium gas coolant system

Figure 2.2.2.2.3 shows the neutron spectrum near the center of the test cell including the component scattered by the wall (concrete). The cross section for the reaction 6Li(n, a) becomes large in the energy range below 1 keV, and the flux is not strongly dependant on the position in the test cell. The ^{6}Li burnup rate is estimated to be about 4% in the test module region. The rate for the ^{7}Li(n, a) reaction is smaller by two orders.

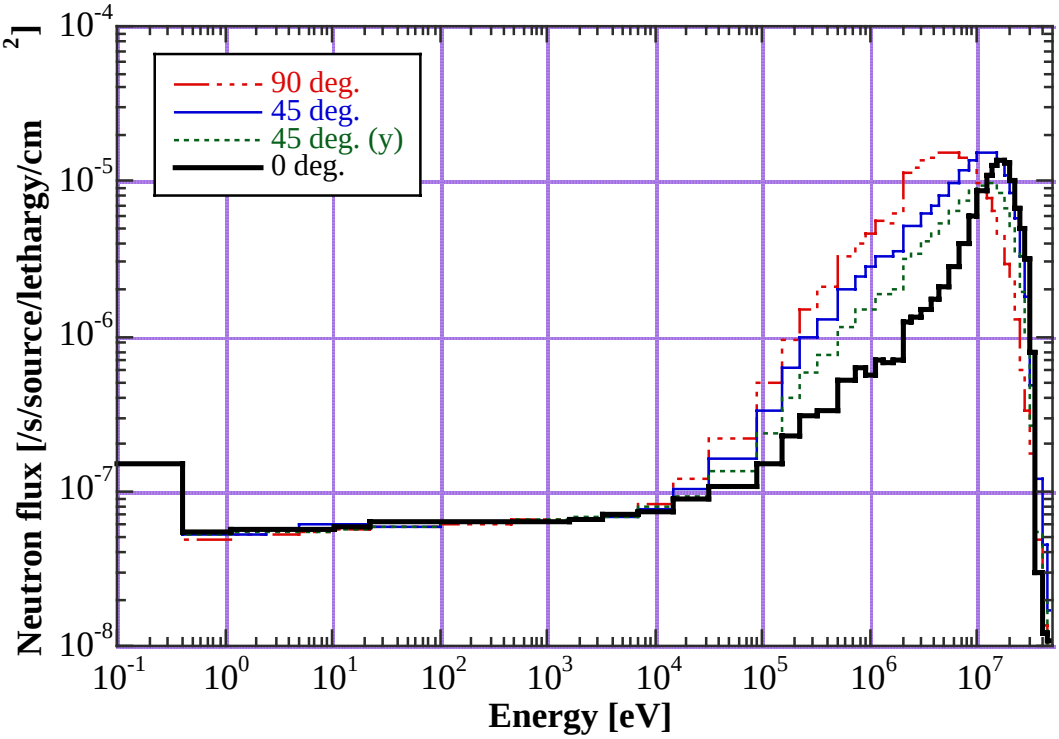

Fig. 2.2.2.2.3 Neutron spectra at the position where the damage rate is 0.1 dpa/fpy. The calculations are based on a NaK-cooled high flux test module (Fe50%/NaK30%) and also include neutrons back-scattered from the concrete wall.

The burn up of the 50%-enriched 6Li specimen attains 15% for 7.5 fpy irradiation. For the two modules of the tritium release experiment, it will take 15 fpy to complete the irradiation. High flux test modules are also planned to be irradiated at 15 fpy to complete the irradiation.

The maximum displacement damage level for breeding materials loaded in the first breeding layer of the DEMO reactor is estimated to be approximately 20 dpa (for O in Li2O). The damage level of iron loaded in the same position may attain 70 dpa. It is feasible to attain both a 15% burn up and 22 dpa of displacement damage simultaneously in the medium flux region.

Heat generated from 50%-6Li Li_2O is estimated to be 15 W/g. The gap size for the heat generation rate of 30 W/g (with 10 W/g for structural material) is calculated to be equal to or greater than 0.1 mm.

2.2.2.2.3 Future Directions

- Fabrication of a sub-test module mock-up
- Re-evaluation of nuclear data (e.g. tritium and displacement damage production rate)

2.2.3 Source Term of D-Li- Reaction

Description and justification:

The d-Li neutron source term is of primary importance for calculating the neutron flux, the spectrum and the nuclear responses in the IFMIF Test Cell. Currently there is an uncertainty band of 20 % in the total neutron yield that is directly transmitted into the neutronic responses calculated for the test module. The uncertainty has to be reduced to a tolerable level for the Engineering Design Evaluation phase of IFMIF. In addition to neutrons, the d-Li reaction generates gamma radiation and other by-products like tritium that accumulate in the lithium system during operation and must be removed. Currently, cross-section data needed to assess the generation of these products are lacking.

To assess and reduce the uncertainties in the neutron yield of the d-Li reaction state-of-the-art theoretical tools will be applied to analyze the d-Li interaction processes. An improved nuclear model will be developed to better simulate the d-Li reaction and the parameters of the nuclear model will be adjusted to the experimental data available. New results are expected from a thick lithium target experiment planned to be performed at the Karlsruhe cyclotron. As a medium-term goal, an evaluated set of d-Li cross-section data will be produced for deuteron energies from 0 to 50 MeV.

To assess the γ-ray and by-products generated from the d-Li reaction, a data file will be prepared that is suitable for γ-ray transport. Production cross-section data for by-products of the d-Li reaction (e. g. Be-7, tritium) will be both evaluated and measured.

Contributors:

Organization	Principal Investigator
FZK	U. Fischer, U. v. Möllendorff, P. Wilson
JAERI	Y. Oyama

Main responsibility: FZK

Milestones:

- Uncertainty assessment of d-Li neutron yield	June 1997
- Improved d-Li nuclear model	June 1998
- Experimental results on tritium and Be-7 production	Oct. 1998
- D-Li cross-section data set and file preparation (postponed)	Dec. 1998
- Assessment of g-ray and by-products (JAERI)	May 1998
- Reduce yield uncertainty (ongoing)	Dec. 1998

2.2.3.1 Impact on CDA

Based on the detailed 3D distribution of all important nuclear responses, the geometric form of the high flux test module can be reshaped partly in order to optimize further the available volumes for the test specimens.

2.2.3.2 Results & Conclusions

Improved d-Li Nuclear Model

A complete reassessment of the various components of the nuclear model was carried out, resulting in a physically sounder model for the neutron source term.

The "Serber" stripping component, which is responsible for the majority of the high-energy forward-directed neutrons, saw the largest improvement to the physical basis for the model. Previous implementations of the stripping model, including those for the IFMIF CDA, were drawn directly from the original research by Serber and based heavily on assumptions that are not valid given the physical parameters of IFMIF. In particular, IFMIF has a relatively low initial deuteron energy (40 MeV compared to Serber's 190 MeV) and the thick target means that stripping reactions occur at energies down to about 6 MeV. The assumption of high energy deuterons was implemented primarily to reduce the semi-classical momentum distribution to either a closed-form angular cross-section or closed-form energy cross-section. These results from Serber were then simply multiplied to create a double-differential cross-section, making a further (and incorrect) assumption that the two distributions are independent. By removing the original assumption of high energy and implementing the model by directly sampling the semi-classical momentum distribution, the physical basis for the model is improved considerably.

Although the use of an evaporation model for the compound reaction component has been recognized as inappropriate for such light nuclei, the lack of any more physically valid models which can be implemented on the same scale has required its continued use. As a result, the theoretical development of the model was reconsidered with assumptions and approximations made to suit the specific conditions of the d-Li reaction at energies between the Coulomb barrier energy (~1.5 MeV), used as a lower energy threshold for this reaction, and an upper energy threshold of 15 MeV, as first suggested by Oyama. More importantly, a simplistic linear model was added to roughly include the contributions from all neutrons which may be emitted after the primary evaporation, so-called "subsequent evaporations", as first suggested during the FMIT analysis.

While some of the models continue to be rough approximations to the real physics of the reaction, they have been fit to experimental data sets with more rigorous requirements on the fitting process than in previous models. For example, the total cross-sections were required to have realistic shapes and conversions between inertial reference frames were applied directly rather than approximated.

The most important result from this assessment, however, is that the need for a complete and physically sound measurement and evaluation of the Li(d,xn) cross-section is ever-present. Given the importance of having a reasonable prediction of neutron flux throughout the test facility and throughout the design and operation of IFMIF, this task is vital for determining how well the facility meets its design requirements!

Measurement of Be-7 and H-3 production

An IFMIF simulation experiment was performed at the Karlsruhe Isochronous Cyclotron for measuring the neutron yield, neutron spectrum and Be-7 and tritium yields. The analysis of the neutron yield and spectrum (in FZK/JAERI collaboration) is in progress. The Be-7 and tritium measurements are reported in the following.

Two identical stainless steel containers having 1.1 mm wall thickness and 9.7 cm^3 volume (Fig. 2.2.3.1) were filled in an argon atmosphere with pure lithium metal and then closed by laser beam welding. The austenitic steel type 1.4571 was selected because it exhibits very low tritium permeation. The Li thickness in the beam direction was 21.8 mm, slightly more than the range of 40 MeV deuterons. The containers were irradiated as internal targets within the cyclotron by the full-energy beam of 52 MeV. Since 52 MeV deuterons lose about 12 MeV in traversing 1.1 mm of steel, the deuterons entering the lithium had the correct energy.

One container (target A) was used to find empirically the suitable beam current that would not damage the target. This was done by irradiating for about 15-20 minutes each at 1, 2, ... μA

and visually inspecting the target after each irradiation. After the beam current of 3 μA had been found to be safe, a fresh container (target B) was irradiated for 16.5 hours at 3 μA. The beam current was always recorded by a current digitizer and scaler to determine the total charge, i.e., number of deuterons. More details about the experiment are found in Ref. [1].

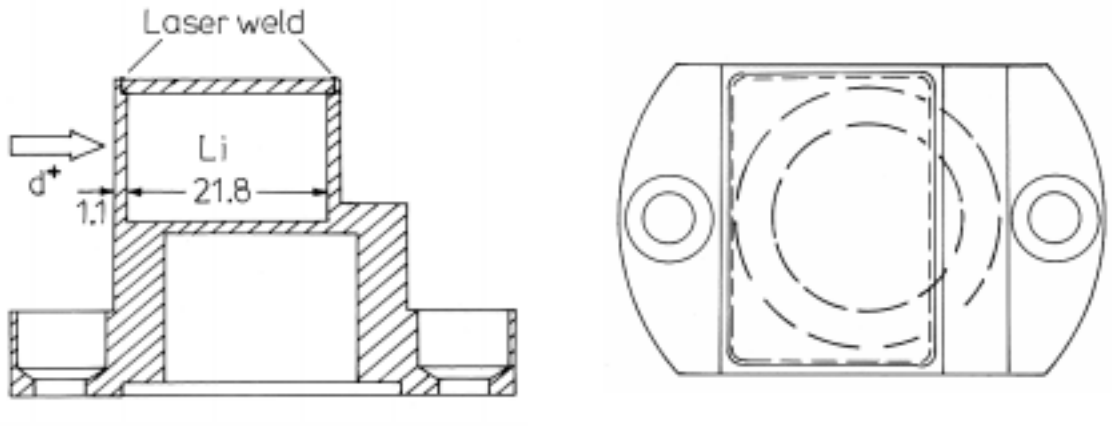

Fig. 2.2.3. 1: Lithium-filled cyclotron target (dimensions in mm)

Beryllium-7 measurement

After a cooling time of about 100 days to decrease the considerable activity induced in the steel, the 478 keV γ ray line from target B was measured with a 25% efficiency, high purity germanium γ spectrometer. The spectrometer, which usually is employed for analysing much weaker samples, had to be reduced in counting efficiency for this measurement by using a lead collimator in front of the detector. Two separate sets of measurements were taken with collimators of different dimensions, a 50 mm thick slab with a 10 mm dia. bore and a 30 mm thick slab with a 12 mm dia. bore. The spectrometer was re-calibrated in either case with a Eu-152 γ ray source. Either collimator had a different position in front of the detector, but always eccentric with respect to the detector axis to avoid the centre with its reduced efficiency. The distance between radiation source and collimator was 65 cm. The correct source position was found by seeking, in several series of short measurements, the maximum 487 keV counting rate as a function of source position along a horizontal or vertical scale at right angles to the collimator axis.

The measurement constitutes a comparison of the unknown Be-7 activity with the known activity of the calibration source. As the Eu-152 calibration source is practically point shaped, the unknown spatial distribution of the Be-7 within the Li target of finite size causes a small systematic uncertainty in view of shadowing effects of the collimator. For a homogeneous distribution, a counting rate reduction of <5% as compared to the point-source case is expected with the narrower collimator. Experimentally, no systematic difference between Be-7 activities measured with the two collimators was found.

The emitted γ radiation is reduced by absorption in the steel case by about 8%. The absorption within the lithium, assuming all radiation to be emitted at a depth of 7 mm (half the lithium thickness in the direction of measurement), amounts to about 4%. Corresponding corrections were applied.

One major difference between IFMIF and the present simulation experiment is the steel target wall on the beam entrance side. A very rough estimation, assuming a similar mean cross-

section per nucleus for deuteron loss in steel at 40 to 52 MeV as in lithium at 0 to 40 MeV, gives a deuteron beam loss of about 1%.

The result is given in Table 2.2.3.1. The 'production cross section' given is the average over deuteron energy, assuming that all Be-7 originates from the $^{6}Li(d,n)^{7}Be$ reaction. From the scatter of several Be-7 and calibration measurements and the uncertainties of the corrections, an overall 1-sigma uncertainty of ±10% is estimated.

Tritium measurement

For the tritium measurement, both of the targets were subjected to a well established standard procedure. The tritium was released by heating the target to several hundred °C in a quartz tube through which a gas stream of 95% Ar + 5% H_2 was flowing at 50 ml/min. The gas was subsequently oxidized in passing through a CuO bed. The resulting H_2O+HTO was absorbed in a molecular sieve. The molecular sieve was periodically changed and eluted with water. This water was then analyzed for tritium in an automated liquid scintillation system (Beckman Instruments LS 6000TA). The result (tritons per 100 incident deuterons), after correcting for decay and for the estimated 1% deuteron loss in the steel case (see above), is 2.45 in target A and 2.32 in target B, with an uncertainty of ± 5% in either measurement. The final result is given in Table 2.2.3.1. The production cross-section given there is analogous to the one for Be-7, but refers to the $^{7}Li(d,t)^{6}Li$ reaction.

Table 2.2.3.1. Experimental results of radionuclide production in the target

	Atoms per 100 deuterons	Mass per full-power year	Production cross section[1)]
Be-7 ($T_{1/2}$ = 53.29 d)	0.274 ±10%	1.57 g	362 mb per Li-6 atom
H-3 ($T_{1/2}$ = 12.32 a)	2.39 ±4%	5.89 g	255 mb per Li-7 atom

[1)] see text

Reference

[1] U. von Möllendorff, H. Feuerstein and H. Giese, Measurements of radioactivity production in the IFMIF target, Proc. 20th Symp. on Fusion Technology (Marseille, France, 7-11 Sept. 1998), pp. 1445-1448

2.2.3.3 Future Directions

The results of the FZK/JAERI measurement of neutron yield and spectrum will be compared with McDeLi-MCNP calculations and will likely lead to modifications of coefficients in the McDeLi model.

The evaluation of d+Li cross-sections, including gamma ray and radioactivity production, from theory and existing differential experimental data remains a major goal within this task.

2.2.4 20-50 MeV data evaluation

Description and justification:

In the IFMIF Test Cell there will be a considerable amount of neutrons produced above 20 MeV. Neutron nuclear data files for energies above 20 MeV are lacking. They need to be developed and processed for use with the calculational tools available for IFMIF design analyses. This includes two different types of files: cross section data for collided spectrum calculations and important nuclear responses like dpa, nuclear heating and gas production ('neutron transport files', to be used mainly with the MCNP Monte Carlo code, but also with discrete-ordinate transport codes) as well as transmutation/activation cross section data ('activation files', to be used with inventory codes such as ALARA).

During the IFMIF CDA phase, data evaluation activities were launched to extend the energy range of the nuclear data files to energies up to 50 MeV. So far, transport files for only a few nuclides have been prepared, both as basic data files in the ENDF-6 format and as processed files for use with the MCNP Monte Carlo transport code.

It is planned to continue this activity during the CDE phase with the final aim of producing a full IFMIF nuclear data file including all the nuclides and data types of interest to IFMIF neutronics analyses. During the CDE phase, the evaluation will focus primarily on activation files for the most relevant nuclides for IFMIF, but in parallel also on the continued buildup of the transport library. The work includes the processing of the evaluated nuclear data into suitable working files and test calculations for the IFMIF high flux test module applying those files. The data evaluation and processing effort will have to be continued after the CDE phase to meet the final goal of making available a full data library for IFMIF.

Contributors:

Organization	Principal Investigator
FZK	U. Fischer, U. v. Möllendorff, P. Wilson
JAERI	T. Fukahori, Y. Oyama

Main responsibility: FZK

Milestones:

- Data evaluation for major nuclides	Jan. 97 - Dec. 98
- Processing of data files, test calculations	Jan. 97 - Dec. 98
- Activation calculations for the IFMIF high flux test module	Sept. 98
- Evaluation of tritium production and heat generation in breeder materials (relevance of IFMIF spectrum)	Dec. 1998

2.2.4.1 Impact on CDA

No impact on CDA.

2.2.4.2 Results & Conclusions

At the time of writing, complete transport files in the above sense (i.e., including PKA and gamma production data) from the FZK/INPE Obninsk evaluation work are available for O-16, V-51, Cr-52 and Fe-56. Incomplete transport files (lacking gamma production data, but useful for neutron transport proper) are available for C-12, NA-23, Si-28 and K-39 [1]. Independently

of our efforts, complete transport files for H-2, C-12, O-16, Al-27, Ca-40, Fe-54, -56, -57, -58, W-182, -183, -184 -186 and Pb-206, 207, 208 were released by LANL in 1997. All the mentioned files were successfully processed for use with MCNP.

Activation files from the FZK/INPE Obninsk evaluation work are available so far for the elements Z = 9 - 42, 49, 69, 72 - 75, 79 and 83 up to 150 MeV neutron energy [2]. For each of these elements, all isotopes contained in the European Activation Library EAF-97 are included. EAF-97 also is the source of the data below the neutron energy of 20 MeV. The new activation and transmutation cross-section files were prepared according to ENDF-6 format rules using the option MT=5 with LAW=0 file on MF=6. This has the advantage that, while the total excitation function is given on file 3 as a regular cross-section dependent on the neutron incidence energy, the individual product yields are stored separately for each reaction product on file MF=6 using the LAW=0 option. As the reaction products are specified by Z,A identifiers and not by MT-numbers, there are no restrictions to the number of activation and transmutation reactions that can be handled. This is vital in view of the multitude of reaction channels existing at energies above 20 MeV.

Activation calculations with intermediate energy data

Following the delivery of the above mentioned intermediate activation files [IEAF], it became apparent that activation calculations at these higher energies required an activation/inventory code which was able to accommodate the numerous reaction channels (up to 170 per isotope). As a result, the recently developed and benchmarked ALARA activation code[3] was chosen. Using the McDeLi neutron source model referred to in Task 10, a 205 group flux was calculated (175 vitamin-j groups plus 30 groups spaced uniformly in lethargy) and used together with the new data as input for ALARA-calculations for the IFMIF high flux test module.

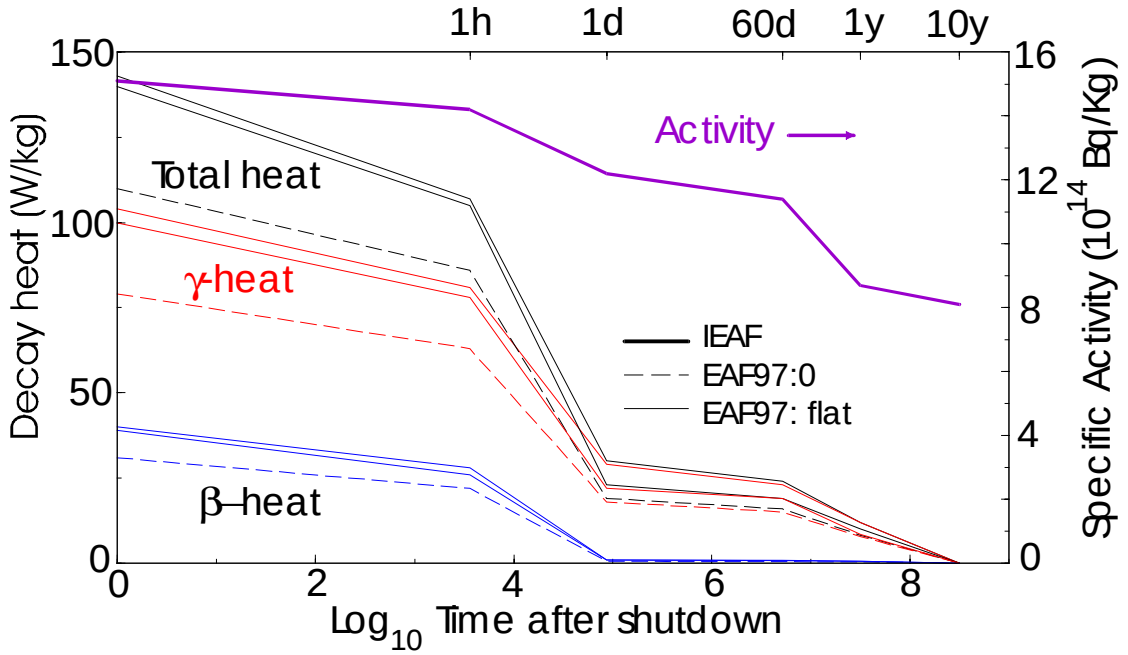

Fig. 2.2.4.1: Activity and decay heat for one position of the high flux test module

In addition to the activation and decay heat results themselves, shown for one position in the high flux test region in Figure 2.2.4.1, the importance and completeness of the libraries was shown by comparison with various other libraries. In particular, this comparison showed that various approximations, such as assuming that the activation cross-section is either zero or constant at energies above 20 MeV, were not able to accurately calculate the activation or decay

heat for iron in the high flux test region. In addition, by comparing one library consisting of the IEAF data alone with another library consisting of the IEAF data supplemented by data from EAF97 for those isotopes which are not yet available, it was shown that the set of isotopes which are currently available are sufficiently complete for the activation analysis of iron.

2.2.4.3 Future Directions

The evaluation work for both neutron transport and activation data will have to be continued throughout the KEP, and likely even beyond the KEP, to reach the final goal of a complete nuclear data library for IFMIF. The task is facilitated by the emerging European activity to create a common intermediate-energy nuclear data library.

Experimental verifications (benchmark tests) of both the transport and the activation data will be essential for quality control. As a first step, the activation of different structural material samples was measured in the IFMIF simulation experiment at Karlsruhe (see Section 2.2.3). The analysis of these measurements is in progress.

References

[1] Yu. Korovin et al.: Evaluation and Test of Nuclear Data for Investigations of Neutron Transport, Activation and Transmutation in Materials by Intermediate and High Energy Particles, Proc. Int. Conf. on Nuclear Data for Science and Technology NDST'97, Trieste, Italy, 1997

[2] Yu. Korovin et al.: Radiation Damage and Processes of Activation and Transmutation In Materials Irradiated By Intermediate and High Energy Particles, Int. Conf. on Emerging Nuclear Energy Systems, Jerusalem, July, 1998

[3] P.P.H. Wilson: Activation Characterization of the High Flux Region of the International Fusion Materials Irradiation Facility [IFMIF], 20th Symp. on Fusion Technology, Marseille, France, September 7-11, 1998

2.2.4.4 APPENDIX: Status of JENDL High Energy File ANd JENDL PKA/KERMA FILE

The JENDL High Energy File for the IFMIF and JENDL PKA/KERMA File supplies relevant fundamental data for many of IFMIF equipment designs. The energy range of JENDL High Energy File for IFMIF is up to 50 MeV. Below 20 MeV, the data of JENDL Fusion File [1] or JENDL-3.2 [2] are adopted basically. The elements included in the JENDL High Energy File for IFMIF are summarized in Table 2.2.4.4.1.

Table 2.2.4.4.1: Elements included in JENDL High Energy File for IFMIF

Compiled (48 nuclides):
H-1(< 1 GeV), C-12(< 80 MeV), Na-23, Mg-24,25,26, Al-27, Si-28,29,30, K-39, Ca-40,42,43,44,46,48, Ti-46,47,48,49,50, V-51, Cr-50,52,53,54, Mn-55, Fe-54,56,57,58, Ni-58,60,61,62,64, Cu-63,65, Y-89, Nb-93, Mo-92,94,95,96,97,98,100,
Evaluating (33 nuclides):
Li-6,7, Be-9, B-10,11, N-14, O-16, Cl-35,37, K-41, V-50, Co-59, Ge-70,72,73,74,76, Zr-90,91,92,94,96, W-180,182,183,184,186, Au-197, Pb-204,206,207,208, Bi-209

SINCROS-II [3] is mainly used for the phase-I evaluation. For light mass nuclei, the SCINFUL/DDX [4] code which considers break-up reactions with primary knock-on atom (PKA) spectra is used as well as the EXIFON [5] code. The JENDL PKA/KERMA File contains

primary knock-on atom (PKA) spectra, KERMA factors and displacement per atom (DPA) cross sections for 78 isotopes of 29 elements in the energy range between 10^{-5} eV and 50 MeV. Table 2.2.4.4.2 shows physical quantities included in PKA/KERMA File as well as the MF number defined in the ENDF-6 format.

Table 2.2.4.4.2: Physical quantities included in the JENDL PKA/KERMA File

MF	Quantities
3	Cross-sections and KERMA factor
4	Angular distributions for discrete levels
6	Double-differential light particles and PKA cross-sections
63	DPA cross-sections
66	Damage energy spectra

The processing code system, ESPERANT, was developed to calculate PKA, KERMA and DPA profiles from evaluated nuclear data for medium and heavy elements by using an effective single-particle emission approximation (ESPEA) [6]. As a trial task of ESPERANT, a file for 69 nuclides from ^{19}F to ^{209}Bi in the energy region up to 20 MeV has been generated for fusion application from the JENDL Fusion File [1] by ESPERANT. The calculated PKA spectra were compared with the results of Monte Carlo calculation code, MCEXCITON [7], and of Doran's processing [8] from ENDF/B-IV [9]. The DPA cross-sections were compared with calculations by RADHEAT-V4 [10] and Doran. The KERMA factors were also compared with Howerton's calculation [11] as a data and method check of ESPERANT. For example, the DPA cross sections and KERMA factors for ^{27}Al and ^{56}Fe compared with other calculations are shown in Figs. 2.2.4.4.1 and 2.2.4.4.2. It was concluded that the processed result of ESPERANT had a good accuracy.

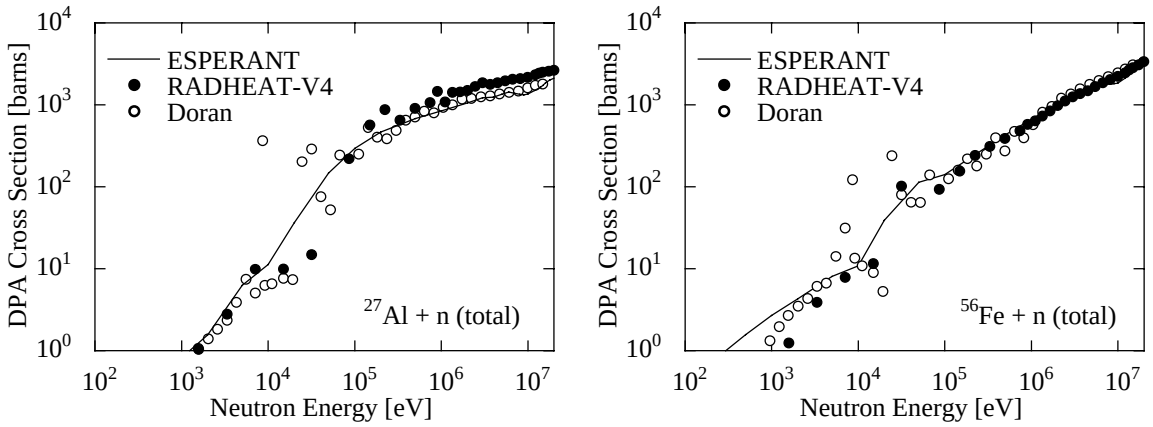

Fig.2.2.4.4.1: ^{27}Al and ^{56}Fe DPA cross-sections of the KERMA File compared with calculations by Doran [8] and RADHEAT-V4 [10]

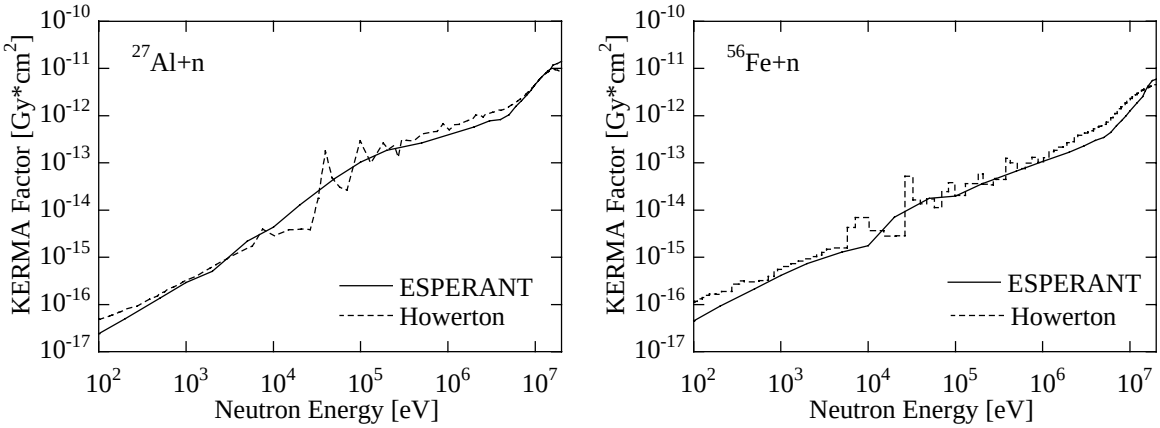

Fig.2.2.4.4.2: ^{27}Al and ^{56}Fe KERMA factors of the KERMA File compared with calculations by Howerton [11]

Future Directions

The evaluation of nuclear data for the JENDL High Energy File for IFMIF is now in the final stage. The JENDL PKA/KERMA file will be processed from the file. Using the FNS experiments of nuclear heating, the benchmark test of the KERMA data for C, Ti, Cu, Mo, etc. will be made. After the test, the PKA/KERMA file will be released.

References

[1] Y. Baosheng, et al., J. Nucl. Sci. Technol., **29** (1992) 677.

[2] T. Nakagawa, et al., ibid., **32** (1995) 1259.

[3] N. Yamamuro, "A Nuclear Cross Section Calculation System with Simplified Input-Format Version II (SINCROS-II)," JAERI-M 90-006 (1990).

[4] H. Kashimoto, et al., Proc. of 1992 Symposium on Nuclear Data, Tokai, Japan, Nov. 26-27, 1992, JAERI-M 93-046, p.287 (1993).

[5] H. Kalka, Proc. Int. Conf. on Nuclear Data for Science and Technology, Julich, May 13-17, 1991, p.897 (Springer-Verlag, Berlin, Heidelberg, 1992).

[6] T. Fukahori, et al., Proc. the Ninth International Symposium on Reactor Dosimetry, September 2-6, 1996, Prague, Czech Republic, p.449 (World Scientific Publishing, Singapore, 1998).

[7] N. Kishida and H. Kadotani, Proc. Int. Conf. on Nuclear Data for Science and Technology, Mito, May 30 - June 3, 1988 (Saikon Publishing, Tokyo, 1988) p.1209.

[8] D.G. Doran and N.J. Graves, HEDL-TME 7670, Hanford Engineering Development Laboratory (1976).

[9] (Ed.) D. Garber, BNL-17541, 2nd Edition, Brookhaven National Laboratory (1975).

[10] N. Yamano et al., JAERI-1316, Japan Atomic Energy Research Institute (1989).

[11] R.J. Howerton, UCRL-50400 Vol. 27 (1986).

2.2.5 Activation foils and Real-time Neutron/Gamma Monitors

Description and justification:

The task is to provide reliable methods to measure the gamma/neutron field in the test cell and test assembly.

Activation foils: This is a dosimetric method largely used in fission reactors. Its application to IFMIF requires to improve the available dosimetry database for high energy neutrons. A review of dosimetric cross sections with their uncertainties (as available in the published literature or existing databases) for each one of the selected high priority reactions (see IFMIF CDA Final Report) will be performed. The reactions and energy ranges, for which cross-sections measurements are necessary, will be pointed out. It is important to note that a relatively low number of well-measured dosimetry cross sections can guarantee an accurate measurement of the actual neutron field characteristics (fluence and energy spectrum) in the hostile environment of the test cell/test assembly (high temperature and radiation level).

Real-time neutron/gamma detectors: The option of using real-time detectors for spatial and time-resolved flux monitoring will be examined by means of a survey of the present status of in-core reactor monitoring instrumentation (micro fission chambers and self-powered detectors) at EU/US nuclear sites. An assessment of these detectors for their application to IFMIF (where sensitivity to neutrons up to 50 MeV is required) will be provided.

Contributors:

Organization	Principal Investigator
ENEA	B. Esposito, L. Bertalot

Milestones:

Assessment of applicability of existing real-time in-core reactor neutron/gamma monitoring systems to IFMIF	Jan. 1999
Review of available data for high priority cross sections; list of cross sections to be accurately measured; sensitivity analysis of spectrum with covariances	Mar. 1999

2.2.5.1 Impact on CDA

The work on dosimetry [1] for IFMIF, necessary for the characterization of the specimens' irradiation, carried out during the CDA Phase was mainly concentrated on the definition of a proper set of activation reactions for passive neutron dosimetry by means of activation foils (multifoil activation). The principal advantage of the dosimetry foils is their compactness (few mg of various materials are sufficient for neutron fluence and spectrum measurements) together with the fact that they are passive sensors, not requiring any control during the irradiation. In the CDE phase this part of the activity will be further continued, concentrating on the qualification of the dosimetric foil package and the use of cross section covariances for further tests on the sensitivity of the IFMIF neutron spectrum determination to cross section uncertainties.

The passive detectors may be complemented by on-line active miniaturized neutron/gamma monitors (miniaturized fission chambers and/or SPNDs) similar to those used for in-core fission reactor applications. The possibility of having an on-line neutron/gamma detection system within the High Flux Test Module (HFTM) is attractive for various reasons:

a) the conditions of the irradiation test can be monitored continuously and locally, very close to the irradiated samples;
b) beam control and optimization, especially during facility commissioning;

c) in the case of frequent removal of parts of the sample set, it would be advantageous to know the exact dose accumulated in the samples before and not after the removal;
d) redundancy of detectors: as on-line monitors are a totally independent measuring system, they can be used to cross-check other measurements (e.g. dosimetry foils).

During the CDE phase the concept of on-line miniaturized radiation monitors as viable diagnostic tools for the HFTM is considered, representing a major new item with respect to the previous CDA phase. In particular, a study will be performed on the possibility of adapting present on-line miniaturized neutron/gamma monitors to IFMIF: these detectors should be located at several positions inside the test cell for beam control, safety and diagnostic purposes.

All activities of the dosimetry task will be completed within early 1999. Preliminary results available at the time of writing [2] are presented hereafter.

2.2.5.2 Results & Conclusions

Miniaturized fission chambers

Already within the framework of the NET (Next European Torus) project, studies were performed [3] on the possibility of using miniaturized fission chambers within the blanket components, whose environment (high radiation field and high temperature) is not dissimilar, except for the different energy distribution of the neutrons, from that of the IFMIF HFTM [4]. Nowadays, the miniaturized fission chamber technology is available worldwide and micro-fission chambers are considered for use as neutron yield monitors for ITER (International Thermonuclear Experimental Reactor) [5].

Very recently, new technology sub-miniature fission chambers have been developed by CEA (Commissariat de l'Energie Atomique, France). These detectors, with a maximum external diameter of 1.5 mm and 12 mm length [6] have been designed as fixed in-core instrumentation for light water reactors. Tests were made at the SILOE water reactor (35 MW) to check their properties under intense (thermal) neutron flux (~10^{14}n/cm^{2}s), fluence of 10^{21}n/cm^2 and high temperature (350 °C). Due to their reduced size and characteristics, these sub-miniature fission chambers look particularly promising for application to IFMIF, although some modifications are necessary.

In order to assess the possibility of using these newly developed on-line in-core detectors in the IFMIF HFTM, a meeting was held in Cadarache in December 1997 with CEA experts [7]. A set of requirements, which should be met by sub-miniature fission chambers suitable for IFMIF application, was prepared for open discussion. The main specifications were: miniaturization (≤ 2 mm diameter), neutron sensitivity in the range 10^{13}-10^{15} n/cm^{2}s, capability of spectral response, reduced burn-up, accuracy ~10%, low gamma sensitivity, capability of withstanding high nuclear heating (~60 W/cm^3) and high temperature (250-1000 °C), accessibility through remote handling. In particular, as ~85% of the neutrons in the HFTM are above 1 MeV, chambers sensitive to fast neutrons are required.

It was pointed out that a considerable effort is needed to meet the IFMIF requirements as the present sub-miniature fission chamber technology is optimized for the detection of thermal neutrons and not for high energy neutrons. The following points were considered to be worth of being investigated:

- *characteristics of the gamma field in the HFTM*: an evaluation of the gamma flux and spectrum within the HFTM (both gamma-rays generated directly by the D-Li source and those induced by neutron activation in HFTM) is necessary as input for a proper feasibility study of IFMIF on-line neutron/gamma sub-miniature monitors (effects due to photofission and γ,e reactions particularly on the cables). This aspect is addressed below (par. *Gamma Field within the HFTM*) where an evaluation of the gamma field in the HFTM is presented.

- *nuclear damage* due to high energy neutrons (resistivity decrease of insulating components) is a concern and should be investigated in detail (see par. *Radiation Effects*).

- *the location of the monitors* is a major issue: existing sub-miniature fission chambers have been tested at a maximum temperature of 350 °C only. If operation at higher temperature is required, an additional development is strictly necessary (investigation of appropriate detector and cable materials), while if the temperature is kept below 350 °C the present technology is sufficient and only studies on fissile coating and gas pressure are needed.

- *selection of the appropriate fissile energy*: the best choice of coating for high energy neutron detection (E>1 MeV) must be carefully studied: ^{238}U, ^{237}Np, ^{238}Pu, ^{232}Th are among the possible nuclides which have a fission cross section with an energy threshold in the MeV region. However, it is very important to take into account the effect of daughter nuclides (produced in the coating during the irradiation) which may have high cross section at thermal energy.

- the detectors to be developed for the HFTM may not necessarily operate in the lower flux test modules; the knowledge of neutron/gamma fields in these regions is important for a proper detector design.

A preliminary investigation on the integration of the sub-miniature fission chambers in the HFTM has been also performed considering the small room available and the high-temperature environment. Two possible configurations are suggested:

a) up to three sub-miniature fission chambers might be accommodated, one on top of the other, in the 5 cm of vertical extension of the HFTM; each chamber would have 1.5 mm diameter (sensitive length ~12 mm), but an overall 3-5 mm diameter space would be necessary also for cables and plugs. This arrangement would permit a 3-D neutron flux mapping.

b) if only one sub-miniature fission chamber is used in the vertical extension, then only about 2 mm diameter room would be necessary and the chambers may just fit into the gas gaps of the helium-cooled HFTM (according to the updated design [8] the gaps have a 2 mm width).

The temperature constraint is a critical issue. In order to avoid excessive additional development to adapt present CEA sub-miniature fission chambers to IFMIF (capability of withstanding high temperatures) it would be important not to exceed the maximum operating temperature of 350 °C. This is probably possible if the detectors can be located directly inside the gas gaps. In fact, the temperature in these gaps would always be much lower than the temperature at which the irradiated samples are kept. Since in the present design the gaps have 2 mm width (more or less as the diameter of the chambers) it may be necessary to round the corners of the rigs in order to increase the space available for the chambers and to accommodate them more easily. Of course, the thermo-hydraulic implications of the inclusion of the chambers in the gaps should be studied carefully. On the other hand, if the chambers are located inside the rigs (within the specimens' capsules, together with other instrumentation like thermocouples and dosimetry foils) the temperature of many capsules would be too high. In this case, a possible solution is to install the chambers only in those capsules which, according to the irradiation program, must remain below 350 °C.

Self-powered neutron detectors

The Self-Powered Neutron Detectors (SPNDs) represent an additional possibility for on-line neutron/gamma detection in IFMIF. This kind of detectors, as in-core flux monitors, has been used extensively in nuclear power reactors for over 25 years [9]. So far, their application has been limited to thermal or epithermal neutrons. Recently, a rhodium SPND has been tested successfully as fast neutron monitor in a Russian fission reactor core (see [2] for details). For the application of this SPND as a fast neutron detector, however, some methodological problems

remain to be solved, in particular the separation between the fast and thermal neutron signal components and the γ-ray contribution to the total signal.

Gamma field within the HFTM

A Monte Carlo neutron and photon transport calculation using the MCNP code [10] has been performed in order to evaluate the absorbed gamma dose within the HFTM, which has been simply modeled by subdividing it into 30 cells with equal stainless steel content (70% stainless steel + 30% void). The uncollided expected IFMIF neutron spectrum at the front cell has been used as input [4, 11] with a flux of 9.18×10^{14} n/cm^{2}s. In our evaluation only the part of the neutron spectrum up to 20 MeV has been used. Gamma rays produced by the deuteron beam directly in the lithium target are not included. The total absorbed gamma dose as a function of distance from the front cell is plotted in Fig. 2.2.6.1, while the energy spectrum of the absorbed gamma dose in the front cell is shown in Fig. 2.2.6.2. It is found that the peak value of the gamma dose (about 7×10^4 Gy/hr) is at 2 cm within the HFTM. The main contribution to the gamma emission comes from the spectral region between 1 and 10 MeV. No significant variation of the spectrum with the cell position has been found. The total gamma dose values obtained in the present calculation for the HFTM (4-7×10^4 Gy/hr) are consistent with those evaluated in calculations for shielding and activation analysis [12] at the test cell walls ~3 m far from the HFTM (5-9×10^3 Gy/hr).

A preliminary evaluation of the minimum detection current, due to γ rays, produced in miniaturized fission chambers or SPNDs (for example, the smallest commercially available fission chamber from CEA-Philips (CFUR 43) and the SPND with rhodium emitter used in the Russian experiment) would give detection currents which are smaller by three orders of magnitude than those due to the thermal neutrons. It must be noted that an additional spurious current is also produced in the cable part exposed to the irradiation field (about 3 m length).

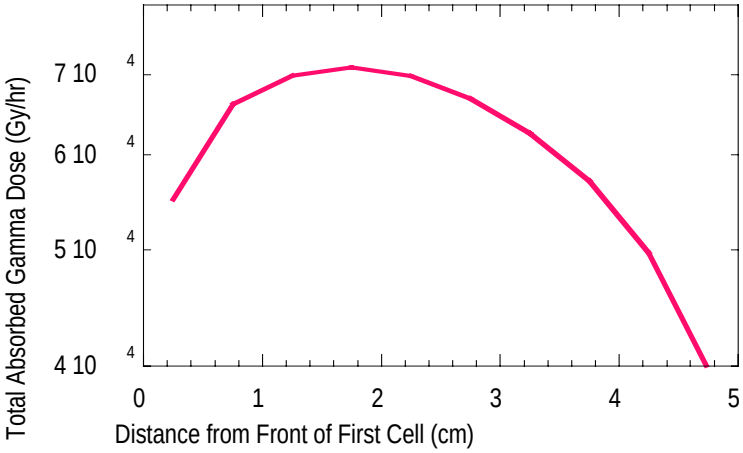

Fig. 2.2.6.1: Total absorbed gamma dose as a function of distance from the front cell

Radiation effects

The neutron and gamma monitors in the HFTM will also be affected by the radiation effects and it is expected that these detectors will behave differently from normal operating conditions.

Recent work [13] was performed under the ITER Project dealing with an overview of irradiation tests (at high operating temperatures) on ITER diagnostics components and with a comprehensive irradiation database for application on ITER.

The radiation effects depend on the incident radiation energy: therefore, different types of irradiations have been carried out for these ITER tests using spallation and fission neutron sources, a 14 MeV neutron generator, electron and ion beams and gamma sources.

With respect to ceramics (i.e. the insulation material), Radiation Induced Conductivity (RIC) and Radiation Induced Electrical Degradation (RIED), which is a permanent degradation observed in ceramics insulators under the applied voltage, have been investigated for the following materials: alumina, silica glass, BeO, AlN, Si_3N_4, $MgAl_2O_4$, MgO, pyrolitic BN. As far as cables/wires are concerned, RIC, RIED, Radiation Induced Electro-Motive Force (RIEMF) between sheath and centre conductor of mineral insulated (MI) cables and conductor resistance, dielectric breakdown strength have been measured for: Al_2O_3, MgO-insulation; Ni, NiCr, SS-central conductor; SS-shield. The main results of this ITER investigation are shortly reported below.

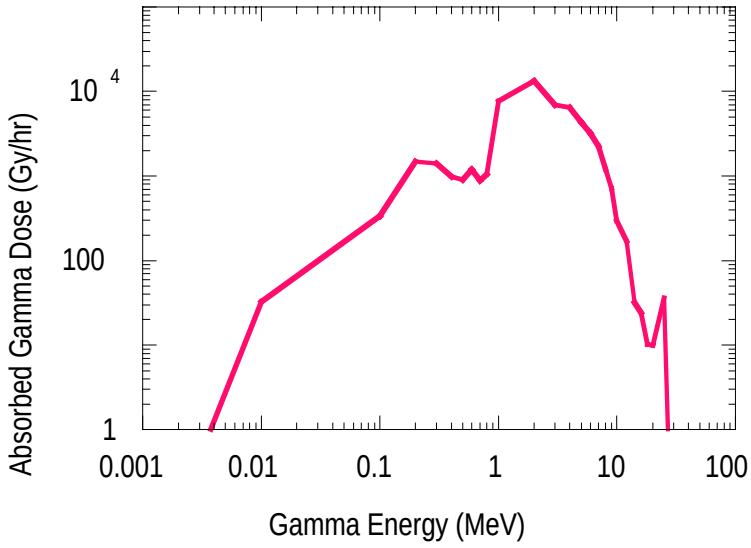

Fig. 2.2.6.2: Energy spectrum of the absorbed gamma dose in the front cell

Ceramics: the main recommended material is *polycrystalline alumina*, which has a RIC value $<10^{-6}$ S/m at 450°C and at 700 Gy/s (~2×10^6 Gy/hr). The dependence on dose rates of 14 MeV neutrons is the same as obtained from other sources (fission neutron, electron beam, ion beam or gamma irradiations). This material does not show permanent damage, RIED, up to 3 dpa. In particular, the Al_2O_4-WESGO candidate (99.5% purity) achieves a value $<10^{-7}$ S/m and no RIED was observed neither under electron beam at 450 °C nor neutron irradiations (spallation and fission sources) up to 600 °C.

Wires: *MgO* and *Al_2O_3* are the recommended materials. Al_2O_3 performs better than MgO. In particular two cables with 99.99% purity of Al_2O_3 powder having a particles size of 0.3 and 5 μm respectively show a total conductivity value of 10^{-10} S/m at temperatures of 450 and 600 °C respectively, for an irradiation dose of 42 Gy/s (~1.5 10^6 Gy/hr). No catastrophic degradation up to 1.8 dpa has been observed for temperatures up to 440 °C.

2.2.5.3 Future Directions

On the basis of the results of the Cadarache meeting, it was decided to pursue the investigation on the possible use of miniaturized on-line neutron/gamma monitors in IFMIF. A contract has been assigned by ENEA to CEA for a feasibility analysis of the modifications

required to adapt existing sub-miniature fission chambers to the HFTM. The option of using SPND monitors will also be investigated. The contract was signed by CEA in June 1998 and the research activity should be completed in early 1999. The main items are as follows:

1) Bibliographic search limited to sub-miniature fission chamber and SPND detectors;
2) Verification of the application pertinence to IFMIF of sub-miniature fission chambers and/or SPNDs;
3) Gross definition of the physical characteristics of the detectors according to the specifications described in Section 2.2.6.2 (with the exception of the maximum operating temperature, limited to 350 °C). Such definition will entail the selection of the suitable fissile material and an estimate of the detector behavior as a function of the neutron fluence.

This activity is expected to be continued further on according to the time schedule presented in the following table.

Table 2.2.6.1: Time schedule of R&D for IFMIF neutron/gamma on-line monitors

Year	Action
early 1999	feasibility study + preliminary specifications
end 1999	design + detailed specifications evaluation performance (accuracy and calculations)
2000-2003	prototype construction test on heavy ion accelerator and fast breeder reactor
2003-2005	engineering improvements

Moreover, ENEA will carry on further work regarding the improvement and optimization of the passive dosimetry for HTFM by means of multifoil activation. This technique, routinely used in fission reactors up to ~10 MeV energy, must be extended to higher neutron energy (~50 MeV) for IFMIF application. Some experimental work on this has been done so far in accelerators, allowing the measurement of suitable activation cross sections: see for example refs [14] (a ^{9}Be(d,n) source was used to produce neutrons up to 20 MeV), [15] (^{7}Li(d,n) source producing neutrons limited to 17 MeV energy) and [16] (^{7}Li(p,n) source producing neutrons up to 40 MeV). Recently, the multifoil activation technique was applied successfully also in the two largest fusion experiments (TFTR and JET) operating in reactor condition, i.e. with deuterium and tritium fuelling, and producing up to 16 MW of fusion power. Neutron fluences and spectra (in the range 1-16 MeV) have been measured for different plasma operating scenarios [17, 18, 19].
The details of the CDE on-going work on passive dosimetry are as follows:

a) optimization of the data set of dosimetric cross sections (as described in [1]) and related covariances by means of a bibliographical search in the present literature and in nuclear libraries;
b) sensitivity analysis of the IFMIF neutron spectrum to the cross sections uncertainties with the inclusion of the covariances. Such analysis will be performed with the LSL-M2 code [20] which optimizes the spectrum by means of a least-squares technique using the covariance matrices;
c) determination by means of the SNL-SAND-II code [21] of the detectable/measuring range of neutron fluxes in the HFTM with the selected set of reactions. Integration of the dosimetry capsules in the HFTM will be considered.

References

[1] B. Esposito, "*Define Design Concept for Dosimetry, 1996 Final Report*", ENEA Report ERB5004 CT 960061, NET/96-419, Frascati, Italy, (1997).

[2] B. Esposito, L. Bertalot, L. Petrizzi, Y. Kaschuck, "*Activation Foils and Real Time Neutron/Gamma Detectors, CDE Intermediate Report*", ENEA Report ERB5004 CT 970071, NET/97-452, Frascati, Italy, (June 1998).
[3] L. Bertalot, M. Martone, L. Pillon, "*Analysis and Preliminary Design of Neutron Diagnostics for NET (Second Part): Blanket-Diagnostics*", EUR-FU/XII-80/88-87, (1988).
[4] E. Daum et al, "*Neutronics of the High Flux Test Region of the International Fusion Materials Irradiation Facility (IFMIF)*", FZKA Report 5868, Karlsruhe, Germany, (1997).
[5] T. Nishitami et al., Fusion Eng. Design, **34-35**, 567, (1997).
[6] G. Bignan, J.C Guyard, C. Blandin, H. Petitcolas, "*Direct Experimental Tests and Comparisons between Sub-moniature Fission Chambers and SPND for Fixed In-Core Instrumentation of LWR*", OECD Proceedings of a Specialist Meeting Mito-shi, Japan, (16-17 October 1996).
[7] G. Bignam, J.P. Trapp, A. Lebrun, O. Poujade, private communication (1997).
[8] G. Schmitz and A. Möslang, "*Helium Cooled High Flux Test Module*", in FZKA Report 5993 (Proceedings of the IEA-Technical Workshop on the IFMIF Test Facilities), Karlsruhe, Germany, (7-9 July 1997).
[9] W.H. Todt, "*Characteristics of Self-Powered Neutron Detectors Used in Power Reactors*", OECD Proceedings of a Specialist Meeting Mito-shi, Japan, (16-17 October 1996).
[10] "MCNP- A General Monte Carlo N-Particle Transport Code", Version 4B, J. Briesmeister ed., Los Alamos National Laboratory, (1997).
[11] U. Fischer, private communication (1997).
[12] S. Monti, "*IFMIF-CDA Shielding and Activation Analysis Final Report*", ENEA Report CT-SBT-00001, (1997).
[13] ITER Design Description Document - DDD 5.5M RV5, "*Radiation effects"*, Garching, (1998).
[14] L.R Greenwood, R.R Heinrich, R.J. Kennerley and R. Medrzychowski, "*Development and Testing of Neutron Dosimetry Techniques for Accelerator-Based Irradiation Facilities*", Nuclear Technology, **41**, 109, (1978).
[15] J.R. Dumais et al., "*Measurement of Average Cross Sections for Several Dosimetry Reactions in a Thick Target Li(d,n) Neutron Field*", Proceedings of the 7th ASTM-EURATOM Symposium on Reactor Dosimetry, Strasbourg, France, (27-31 August 1990).
[16] Y. Uno, Y. Uwamino, and T.S. Soewarsono and T. Nakamura, "*Measurement of the Neutron Activation Cross Sections of ^{12}C, ^{30}Si, ^{47}Ti, ^{52}Cr, ^{59}Co and ^{58}Ni between 15 and 40 MeV*", Nucl. Sci. Eng. **122**, 247, (1996).
[17] D.L. Jassby et al., "*Determination of TFTR far-field Neutron Detector Efficiencies by Local Neutron Flux Spectrum Measurement*", Rev. Sci. Instrum. **68**(1), 540 (1997).
[18] L. Roquemore, "*Performance of the 14 MeV Diagnostics on TFTR and JET*", paper GI-III presented at the 12 th Topical Conference on High Temperature Plasma Diagnostics, Princeton, USA, (June 7-11 1998), to be published in Rev. Sci. Instrum.
[19] B. Esposito, L. Bertalot, M. Loughlin, L. Roquemore, "*Neutron Spectrum Measurements in DT Discharges using Activation Techniques*", paper G-10 presented at the 12th Topical Conference on High Temperature Plasma Diagnostics, Princeton, USA, (June 7-11 1998), to be published in Rev. Sci. Instrum.
[20] F.W. Stallmann, "*LSL-M2: A Computer Program for Least Squares Logarithmic Adjustement of Neutron Spectra*", ORNL Report, ORNL/TM-9933, (1985).
[21] P.J. Griffin, J.G. Kelly, J. VanDenburg, "*User's Manual for SNL-SAND-II code*", SANDIA Report, SAND93-3957 UC-713, (1994).

2.2.6 Re-evaluation of Irradiation Parameters

Description and justification:

During the CDE phase, more accurate nuclear data will become available that will allow more reliable neutronics calculations. As a consequence, a re-evaluation of the preliminary assessment of nuclear responses for the irradiation modules will be necessary. This task is also needed as the design develops and more detailed description of the test modules and the whole facility will be available. Also an assessment of the tritium production and inventory in the facility is to be performed. MCNP based calculations will be performed for the dpa, gas production, nuclear heat deposition, and neutron/gamma flux distributions in the test cell on the basis of the newly available nuclear data and the D-Li neutron source term. Detailed 3d-models of the target, the test modules and the test cell itself will be developed and applied in the MCNP neutronics calculations. In addition to the DPA calculations, a better characterization of the materials damage is needed. This includes the investigation of PKA spectra for elastic and non-elastic interactions and their impact on the calculations of the damage characteristics of IFMIF. A comparison of the IFMIF, ITER, and DEMO damage characteristics is necessary to demonstrate the adequacy of IFMIF for fusion irradiation simulations.

Contributors:

Organization	Principal Investigator
FZK	E. Daum, K. Ehrlich, U. Fischer, P. Wilson,
JAERI	Y. Oyama

Main responsibility: FZK

Milestones:

- Processing of elastic and non-elastic PKA-spectra for ^{56}Fe (Aug. 97)
- Evaluation & qualification of damage characteristics for IFMIF, ITER and DEMO (Dec. 97)
- Extended damage qualification for other important elements (e.g. Cr, V) (Dec. 98)

2.2.6.1 Impact on CDA

The characterization of the irradiation parameters and the high flux irradiation volume show that due to improvements by the nuclear transport and physical response data the responses have increased. On the other hand the uncertainties, e.g. approximations in the high energy domain, have been reduced. Especially by the neutron source function the comparison of the different neutron source data and models reveal the uncertainty in the total neutron yield. The overall results confirm that the IFMIF irradiation conditions are very well suited for the DEMO 1st wall, as was assumed during CDA. This is valid for both, quantity and quality.

2.2.6.2 Results & Conclusions

Characterization of the irradiation parameters in the high flux test region

In order to demonstrate the suitability of IFMIF for irradiation experiments, a comprehensive characterization of the neutronics of the high flux test region (HFTR) has been

carried out for the high flux test region and for Fe as the major constituent of ferritic-martensitic iron-based alloys.

During the CDA and the CDE phase significant progress has been achieved in the neutronics. The neutron transport and engineering response data, used for neutronic calculations during CDA, (H-, He-, damage production and nuclear heating) in the ENDF-B VI data file were good up to 20 MeV and with some approximations above 20 MeV. For neutronic calculations, data up to 50 MeV were provided at the end of the CDA in a comprehensive data evaluation program for ^{56}Fe, ^{23}Na, ^{39}K, ^{52}Cr, ^{51}V, ^{28}Si and ^{12}C. For detailed three-dimensional Monte Carlo calculations a neutron source model based on the Li(d,xn) nuclear reaction was developed (7.3 % total neutron yield) and applied with the Monte Carlo Neutron and Photon Transport Code (MCNP). For the high flux test module (HFTM) a He-cooled and a NaK-cooled design have been set up. On this basis detailed investigations of the irradiation parameters by extensive MCNP calculations for the high flux test region have been performed [1,2,3,5].

For the analysis of the HFTM under a 20° angle between the impinging deuteron beams, a test region filled with 50% ^{56}Fe and 50% void and a non-uniform beam profile were assumed for the MCNP calculations. The results are volume averaged over $(0.5\ \text{cm})^3$ cells. The HFTM in the present design has the dimensions (x, y, z) of (5 cm, 20 cm, 5 cm). In the following figures, the x-axis points downstream and the z-y-plane covers the Li-target backplate.

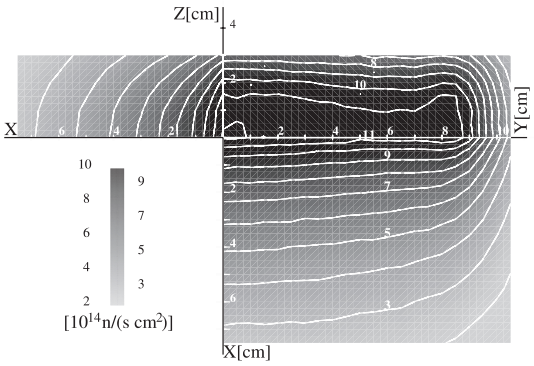

Fig. 2.2.6.1: Neutron flux distribution in units of 10^{14} n/(s cm^2).

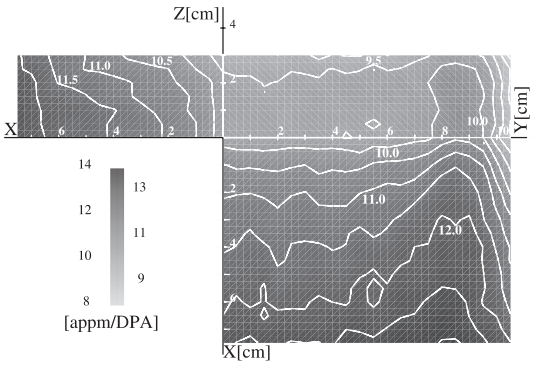

Fig. 2.2.6.2: Ratio of helium to damage production in units of appm/DPA.

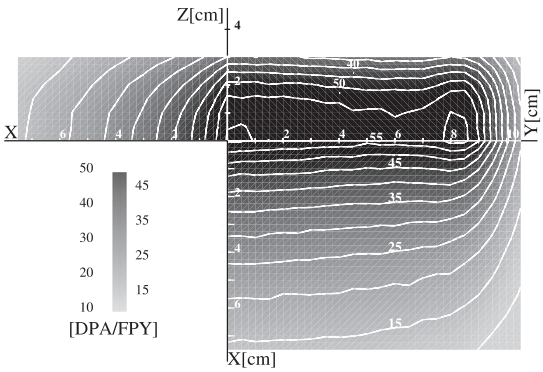

Fig. 2.2.6.3: Displacement damage rate in units of DPA/FPY.

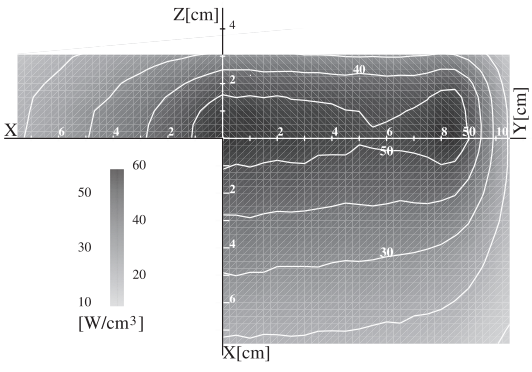

Fig. 2.2.6.4: Nuclear heating production in units of W/cm^3.

Throughout most of the HFTR the neutron flux is greater than 4 x 10^{14} n/(s cm^2). Close to the target the flux is greater than 10^{15} n/(s cm^2). The peaked edges effect of the non-uniform beam profile can be seen in the z-y-plane. The total neutron flux gradient is between 20 %/cm - 30 %/cm in a large portion of the proposed HFTR. Further results are listed in the table.

Table 2.2.6.1: Comparison of irradiation parameters in the High Flux Test Region of IFMIF and the first wall data in ITER and DEMO

Irradiation parameter	IFMIF	ITER	DEMO
Total neutron flux [n/(s cm^2)]	4 x 10^{14} - 10^{15}	4 x 10^{14}	7.1 x 10^{14}
Neutron flux, E_n >14.6 MeV [n/(s cm^2)]	4 x 10^{13} - 2 x 10^{14}	-	-
Hydrogen production [appm/FPY]	1000 - 2500	445	780
Helium production [appm/FPY]	250 - 600	114	198
Displacement production [DPA/FPY]	20 - 55	10	19
H/DPA ratio [appm/DPA]	35 - 50	44.5	41
He/DPA ratio [appm/DPA]	9.5 - 12.5	11.4	10.4
Nuclear heating [W/cm^3]	30 - 55	10	22
Wall load [MW/m^2]	3 - 8	1.0	2.2

Characterization of the volume for high-dose irradiations

One of the major design criteria of IFMIF is to provide a volume of at least 0.5 liter for high dose irradiations (> 20 DPA/FPY). A comprehensive characterization of the irradiation volume of the HFTR has been carried out [4].

The main purpose of this analysis was to characterize the impact of the calculation parameters - beam profile, beam footprint, neutron source data, material loadings and engineering response data - on the HFTM irradiation volume. The investigated conditions are listed below. More detailed information can be found in [4].

- INS and MCNP calculations
- Uniform (20 x 5 cm^2 footprint) and non-uniform (22 x 7 cm^2 footprint) beam profile
- The available data sets for the neutron source function differ in total neutron yield and angular distribution and give a total neutron yield of (6.4 ± 0.9) %.
- Material loadings: Uncollided (100% void) and collided (50% Fe / 50% void) calculation.

The irradiation volumes for certain DPA/FPY levels under reference conditions are listed in table 2. In the third column the volume portions inside the proposed HFTM, cutout of the total volume by HFTM design limits, are given. In Fig. 2.2.6.5 the envelopes for the volumes for different DPA/FPY levels are shown. The physical border of the present HFTM design is shown by the grid. The valuable high-dose volume can be identified above and below the grid.

Using a total neutron yield of 6.7%, the uniform beam profile and the uncollided option, a comparison between INS and MCNP shows that INS underestimates the MCNP total volume by approx. 10 - 15 % and the volume inside the HFTM by approx. < 5 %, see fig. 2.2.6.3.

Between the uniform and non-uniform beam profile the footprint varies from 5 x 20 cm^2 to 7 x 22 cm^2. This slightly affects the available volume, as shown by the values of table 2.2.6.1.

MCNP calculations generate appropriate results if the material is loaded in the test cell. The maximum volume is attained with no material (uncollided). The realistic loading parameters of 50% Fe / 50% void (collided) cause a volume drop of about 20% as listed in Table 3.

The uncertainty of the total neutron yield of (6.4 ± 0.9)% causes the greatest volume impact. Volumes for INS / MCNP calculations (uncollided, uniform beam profile) are shown in Fig. 2.2.7.6 as a function of their total neutron yield. The neutron yield uncertainty domain between 5.5% and 7.3% causes an average total volume (uncollided) of 550 cm^3 with an uncertainty of ± 180 cm^3 and an average total volume (collided) of 455 cm^3 with an uncertainty of ± 145. This large uncertainty in the volume indicates that a considerable effort is required to improve the neutron source function in the future in order to obtain more accurate results.

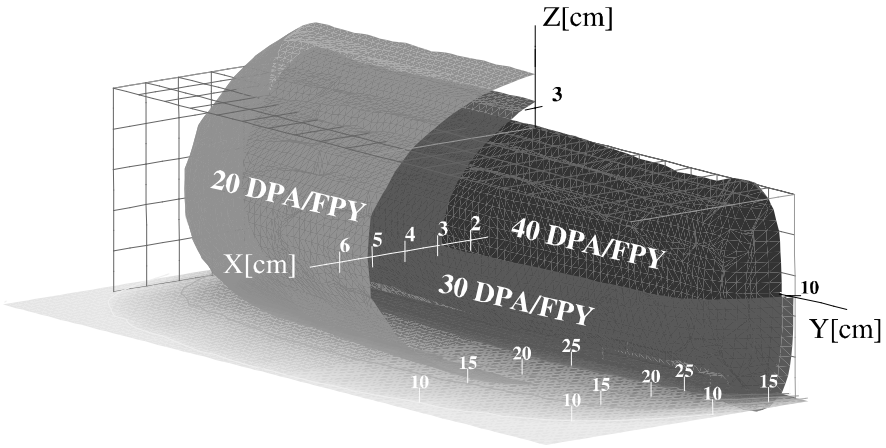

Fig. 2.2.6.5: Irradiation volumes in the HFTM based on minimum damage rates.

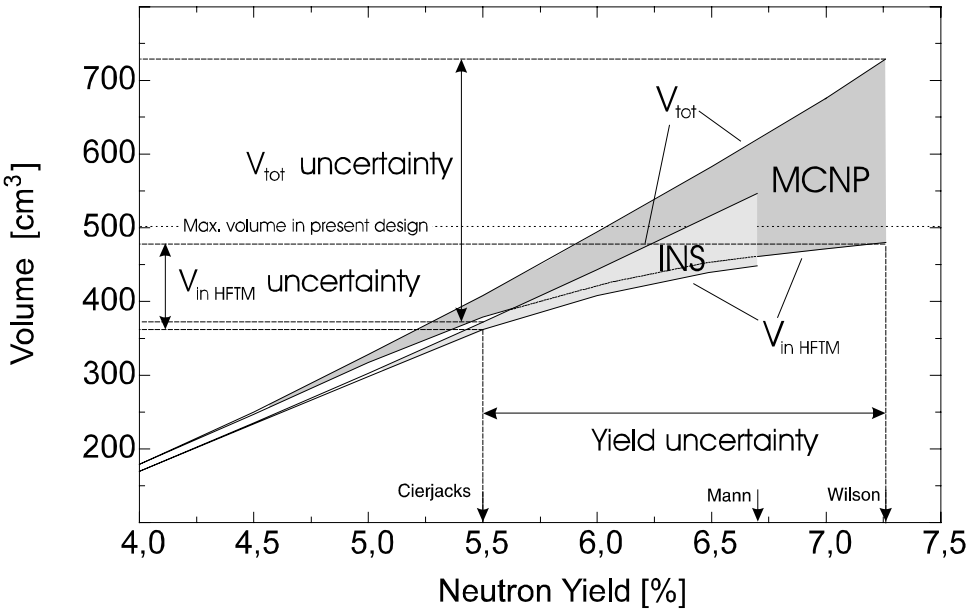

Fig. 2.2.6.6: Irradiation volumes in the HFTM with damage rates > 20 DPA/FPY as a function of the total neutron yield (uncollided case only, the collided case is not shown here).

Table 2.2.6.2: Irradiation volumes as a function of the minimum displacement damage calculated with MCNP, collided, non-uniform beam profile, 6.7% yield.

Displacement Damage [DPA/FPY]	Total Volume [cm^3]	Volume Inside the Proposed HFTM [cm^3]
20	512	415
30	213	201
40	76	76
50	11	11

Table 2.2.6.3: Comparison of irradiation volumes for displacement damage > 20DPA/FPY calculated with MCNP for 7.3 % neutron yield.

	Total Volume [cm^3]	Volume Inside HFTM [cm^3]
uniform, uncollided	732	478
non-uniform, uncollided	716	480
uniform, collided	594	460
non-uniform, collided	590	452

Characterization of the impact of the material loading and composition variation

In order to obtain a better understanding of how the test modules can influence the neutronics field in the test cell, further neutronics evaluations have been carried out [6]. According to materials testing needs the irradiation volume has been divided into four flux regions covered by different test modules. The high flux test module (HFTM) has an irradiation damage rate of greater than 20 DPA/FPY, the medium flux test module (MFTM) with 1-20 DPA/FPY, the low flux test module (LFTM) with displacement damage levels between 0.1-1 DPA/FPY, and the very low flux test module (VLFTM) with less than 0.1 DPA/FPY.

Detailed three dimensional geometry models were developed for use with MCNP on the basis of the reference design at the end of the CDA. For the specimen loading reasonable average material densities depending on the packing and loading pattern were assumed and also the structure supporting the specimens is modeled as detailed as possible. The main focus is put on the neutronics change due to the material composition change. Iron and an iron / chromium mixture are used. Four different cases were investigated:

Case 1: Only the HFTM is in the test cell (Fe only)
Case 2: All test modules are in the test cell (Fe only)
Case 3: Complete geometry (as case 2 and with test cell walls scattering neutrons)
Case 4: Complete geometry with Fe (92%) + Cr (8%) material combination

The physical responses show that in the HFTM almost no change appears. In the MFTM an increase of about 10 - 20%, at the LFTM position an increase of 30 - 50% and at the VLFTM an increase of more than a factor of 2 appears if neutron scattering at the test cell walls is considered. However no effect is observed if the material composition is changed from pure Fe to 92% Fe and 8%Cr.

In the low flux and the very low flux positions the calculated damage rates are significantly higher than assumed at the time of definition.

A comparison of the IFMIF results with ITER or DEMO at a first wall position shows that especially the He/DPA and the H/DPA ratios throughout all test modules are in the right domain for the cases 3 and 4. This makes IFMIF a very valuable and powerful tool for irradiation experiments under fusion-typical conditions.

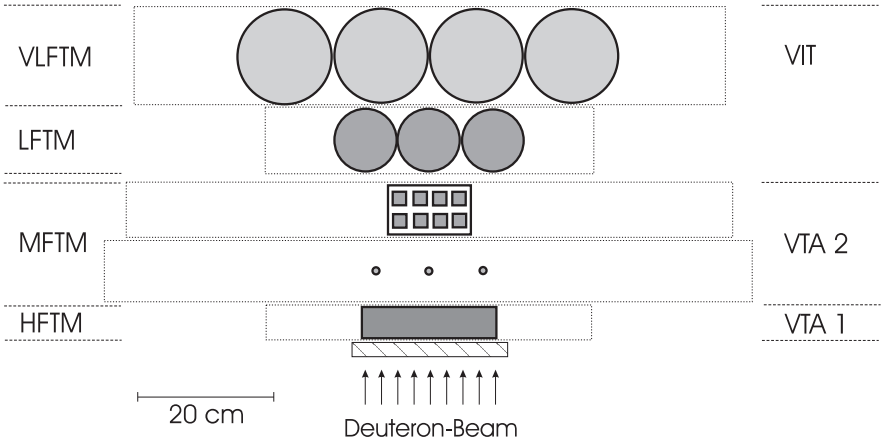

Fig. 2.2.6.7: Horizontal cross sectional view throughout the test modules in the test cell. The hatched area shows the liquid Li-jet flowing perpendicular to the paper. The dotted lines characterize the physical borders of the test modules. The specimens are placed in the shaded areas. VTA 1 houses the HFTM for the instrumented post irradiation experiments (PIE) specimen. VTA 2 houses the universal testing machine for three in-situ creep-fatigue specimens and behind them the capsules for the in-situ tritium-release test specimen. The VIT consists of the LFTM and the VLFTM designed for irradiation of a variety of special purpose materials.

Table 2.2.6.4: Displacement damage rates in units of DPA/FPY, hydrogen production rates in units of appm H/FPY and helium production rates in units of appm He/FPY at representative positions.

	HFTM			MFTM			LFTM			VLFTM		
	DPA	H	He	DPA	H	He	DPA	H	He	DPA	H	He
Case 1	37.5	1662	427	-	-	-	-	-	-	-	-	-
Case 2	37.7	1674	431	11.0	612	157	3,3	179	46	0.57	28	7
Case 3	38.4	1679	432	13,4	680	174	4,9	233	60	1,4	58	15
Case 4	38.4	1678	432	13,4	680	174	4,9	233	60	1,4	59	15

Table 2.2.6.5: Hydrogen to DPA and helium to DPA ratios at representative positions.

	HFTM		MFTM		LFTM		VLFTM	
	He/DPA	H/DPA	He/DPA	H/DPA	He/DPA	H/DPA	He/DPA	H/DPA
Case 1	11,4	44,3	-	-	-	-	-	-
Case 2	11,4	44,4	14,3	55,6	14,1	55,1	12,8	49,8
Case 3	11,3	43,7	13,0	50,7	12,2	47,5	10,6	41,3
Case 4	11,3	43,7	13,0	50,7	12,2	47,4	10,6	41,2

Table 2.2.6.6: Displacement damage and gas production rates for ITER and DEMO first wall spectra

	Displacement damage [DPA/FPY]	Helium production [appm/FPY]	Hydrogen production [appm/ FPY]	He/DPA ratio [appm/DPA]	H/DPA ratio [appm/DPA]
ITER	20	230	891	11.5	45
DEMO	17	180	709	10.6	42

Qualification of the displacement damage in the high flux test region

As it is shown above, IFMIF is very well suited for a fusion reactor environment if the gas to DPA ratios are considered. However , these values are generated only on a gross DPA scale. For a more quantitative evaluation of the effects of displacements on different radiation damage phenomena, the analysis of the transferred damage energy as a function of the primary knock-on atom (PKA) energy is important. Low energy PKA's produce primarily Frenkel pairs. For high energy PKA's two aspects have to be considered. First, the instantaneous recombination of single defects is larger in defect cascades and therefore the concentration of mobile Frenkel defects is reduced. This leads mainly to a reduced supersaturation of single defects and hence suppresses point defect agglomeration phenomena like void formation. Secondly, the formation of cascades and subcascades becomes more probable which can lead to a more intense irradiation hardening. Therefore, the effect on mechanical properties for the low-energy PKA's is different from that of high energy PKA's, because of the varying defect morphology. This explains that irradiation damage does not only depend on the DPA scale but also on the normalized energy transfer function W(T) in a nontrivial way. W(T) describes the fraction of damage energy produced by PKA's as a function of their kinetic energy.

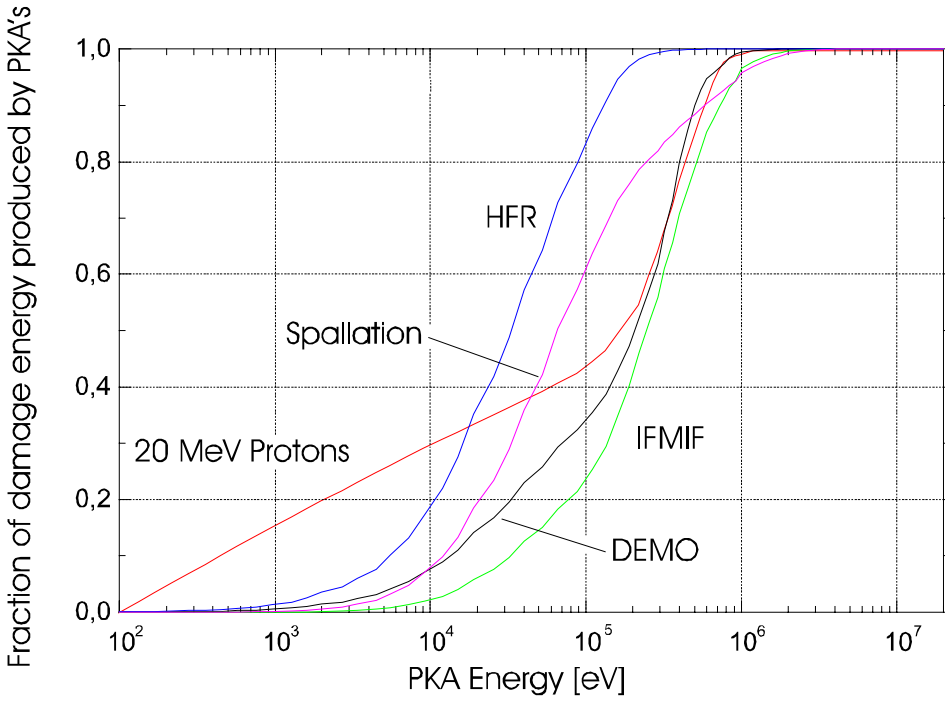

Fig. 2.2.6.8: Irradiation facility comparison

$$W(T) = \frac{\int \sigma_{dam}(E_n, T)\ \frac{\phi_n(E_n)}{dE_n} dE_n}{\int \sigma_{dam}(E_n, T_{\max})\ \frac{\phi_n(E_n)}{dE_n} dE_n} \qquad \sigma_{dam}(E_n, T) = \int^{T} \frac{d\sigma_{PKA}(E_n, T)}{dT}\ T_{dam}(T)\ dT$$

E_n = neutron energy, T = PKA energy, $T_{dam}(T)$ damage energy, $\sigma_{dam}(E_n, T)$ = damage energy cross section, $d\sigma_{PKA}(E_n, T)/dT$ = PKA spectrum, $d\phi_n(E_n)/dE_n$ = differential neutron flux.

The comparison shows that IFMIF very well suits the DEMO and ITER function. IFMIF is much better than the fission reactor HFR Petten, a 800 MeV proton spallation source and a pure 14 MeV neutron peak.

Conclusions

- The neutronics of the high-flux test region (HFTR) is well investigated.
- The total neutron flux gradient in the HFTR is between 20 %/cm - 30 %/cm. One of the HFTR requirements is a limit on the flux gradient of less than 10 %/cm over the specimen width (which was assumed to be 1 cm). This means that miniaturized specimens are required and, additionally, the HFTM design needs to allow the orientation of the samples in the direction of minimized gradients.
- The high-energy fraction of the neutron flux (E_n > 14.6 MeV) is between 15 % - 20 % of the total neutron flux throughout the HFTR. This high energy fraction increases the displacement and gas production responses significantly and allows IFMIF to provide accelerated material irradiations as compared to fusion reactors.
- The comparison of the gas to DPA ratios between IFMIF and the situation in ITER or DEMO at a first wall position shows that the values are in the right domain. This makes IFMIF a very valuable and powerful tool for irradiation experiments under fusion typical conditions.
- The evaluated uncertainty of the neutron source function causes large volume uncertainties.
- A valuable high flux volume above and below the proposed high-flux test module design is available.
- The neutron flux in the LFTM and VLFTM is increased significantly by considering the neutrons backscattered by the test cell walls.
- The displacement damage qualification shows that IFMIF fits best to the DEMO damage characteristics.

2.2.6.3 Future Directions

Improvement of the HFTM design

It is shown with the He-cooled HFTM design as an example, that the present design simply covers a box-shaped volume of 0.5 liters (5 x 5 x 20 cm^3). The MCNP calculations predict, however, a great portion of the available high dose volume to exist above and below the physical borders of the present HFTM design. In order to enlarge the utilized irradiation volume the irradiation capsules need to be extended in vertical direction. This change in the design can be

done without great effort, but will make about 25% - 30% more volume usable above 20 DPA/FPY.

Improvement of the neutron source function

The investigation of the uncertainty of the neutron source function shows a (6.4 ± 0.9)% total neutron yield. This results in uncertainties for all neutronics responses (except gradients) and the estimated irradiation volumes. Improvements on the neutron source function have to be worked out in order to increase the accuracy for the neutronics.

Improvement of the irradiation conditions in the test cell

The above presented results show for iron and an iron/chromium combination that IFMIF very well covers the irradiation conditions in quantity in the high flux test volume as it is required for the DEMO 1st wall. Additionally the damage qualification for iron shows a really good agreement with the DEMO 1st wall. In the future, this investigations need to be extended to other elements and other flux zones. One idea is to increase the effect of the backscattered neutrons by applying a neutron reflector component relatively close to the test modules. This can improve the neutronics condition: Firstly, the total number of neutrons will increase and secondly, the neutron spectrum will become softer.

Activation and element transmutation investigations

Due to the high neutron energy in IFMIF, as compared to max. 14 MeV in DEMO, a large number of nuclear reaction channels are opened additionally. This can change the activation and element transmutation behavior. A comparison between IFMIF and DEMO conditions should be made in order to see, whether there are critical aspects.

References

[1] E. Daum, U. Fischer, A. Yu. Konobeyev, Yu. A. Korovin, V.P. Lunev, U. von Möllendorff, P.E. Pereslavtsev, M. Sokcic-Kostic, A. Yu. Stankovsky, P.P.H. Wilson, D. Woll, Neutronics of the High Flux Test Region of the International Fusion Materials Irradiation Facility (IFMIF), Bericht FZKA 5868, Forschungszentrum Karlsruhe, Januar 1997.

[2] P. Wilson, E. Daum. U. Fischer, U. von Möllendorf, D. Woll, Neutronics Analysis of The International Fusion Materials Irradiation Facility [IFMIF] High Flux Test Volume, contribution at ANS Accelerator Applications Topical Meeting, Albuquerque, New Mexico, November 1997, Fusion Technology, Vol.33 March 1998 pp. 136-145.

[3] E. Daum, P.P.H. Wilson, U. Fischer and K. Ehrlich, Characterization of the Irradiation Parameters in the IFMIF High Flux Test Region, Contribution to ICFRM-8, Sendai, Japan, October 1997, Proceedings in JNM.

[4] E. Daum, P.P.H. Wilson and A. Möslang, Characterization of the Volume for High Dose Irradiations with IFMIF, Contribution to ICFRM-8, Sendai, Japan, October 1997, Proceedings in JNM.

[5] E. Daum, Damage characterization in IFMIF and comparison with ITER and DEMO devices, Contribution to the IFMIF User Group Meeting held in Sendai, Japan, November 1st, 1997, Proceedings as a JAERI Report in print.

[6] E. Daum, A. Möslang and M. Sokcic-Kostic, NEUTRONIC CALCULATIONS FOR IFMIF TEST MODULESContribution to ANS Conference AccApp 98 (Accelerator Applications), September 20 - 23, 1998, Gatlinburg, TN, USA, to appear in the conference proceedings.

[7] Yukio Oyama, Kazuaki Kosako and Kenji Noda, Neutronics analysis of International Fusion Material Irradiation Facility (IFMIF) - Japanese Contributions -, Report JAERI-Research 97-065(1997).
[8] K. Ehrlich and A. Möslang, European Conference on Accelerators in Applied Research and Technology, ECAART 5, August 26 - 30, 1997, Netherlands; Nucl. Instr. and Methods in Phys Research B 139 (1998) 72-81.
[9] K. Ehrlich und A. Möslang, International Fusion Materials Irradiation Test Facility (IFMIF) : User requirements and test cell design, Jahrestagung Kerntechnik, Aachen, 13.-15. May 1997, Bonn, INFORUM GmbH, 1997, S. 550 – 553.
[10] T. Kondo, T.E. Shannon, K. Ehrlich, Materials development and testing aspects of IFMIF in the conceptual design stage, Journal of Nuclear Materials, 233-237(1996) p.82-91.

2.2.7 Availability of RAFM steels for IFMIF target back-wall

Description and justification

The solid Li-target backwall has to withstand more than 55dpa/fpy, at the same time it accumulates – depending at the alloy – about 500 appm Helium and more than 2000 appm hydrogen, and is the device with the highest neutron and gamma wall load of the overall facility. Besides safety aspects, the structural integrity of that backwall governs the availability of the IFMIF test facilities and is therefore a matter of concern.

Specialists of radiation damage of structural materials will be nominated as members of a working group to evaluate the lifetime of the candidate materials for the Li-target backwall.

Contributors:

Organization	Principal investigator
JAERI	S. Jitsukawa, K. Shiba
FZK	E. Diegele, A. Möslang
ORNL	S. Zinkle
ENEA	G. Benamati, I. Ricapito

Milestones

- Activity planning	June 1997
- Collection of materials data currently available	ongoing
- Establishment of materials database for evaluation of the lifetime	Dec.1997
- Stress-strain analyses of the Li-backwall geometries under real loadings	June 1998
- Suitable experiments to the low temperature irradiation, He, H embrittlement of potential materials (e.g. RAFM steel, V-4Cr-4Ti)	Dec. 1998
- Results of the structural integrity including the lifetime	Dec. 1998

2.2.7.1 Impact on CDA

The results achieved and presented here regarding candidate materials for the backwall target do not have any influence on the design and work planning as discussed in CDA.

2.2.7.2 Results and Conclusions

The target backwall will contain a jet of lithium flowing at a velocity of around 15 m/s with an inlet and outlet temperature of about 250-300 °C. The mean temperature of the target backwall has been estimated in 270 °C, but a more detailed calculation will be made in the future. Considering the high neutron fluence to be withstood and the foreseen thermal regime, fully martensitic steels of the 8-9 % Cr family appear to be the most attractive solution for IFMIF target backwall among the different candidate materials. The main advantages of this class of materials are:

a) better thermo-physical properties under irradiation as compared to austenitic steels;
b) better corrosion properties with respect to liquid metals as compared to austeitic steels;
c) lower susceptibility to impurities as compared to vanadium alloys;
d) much higher swelling and helium embrittlement resistance than austenitic steels

Reduced activation ferritic/martensitic (RAF/M) steel is therefore one of the candidate for the IFMIF target backwall. However, the thermal and loading conditions of the component have not yet been calculated in detail. Material properties and loading conditions listed below are used for the evaluation of the Li-target backwall lifetime. Necessary data for lifetime evaluations are:

A. Physical Properties
- · Elastic modulus
- · Poisson's ratio
- · Thermal conductivity
- · Thermal expansion coefficient
- · Specific heat:

B. Mechanical Properties
- · Tensile properties (irradiated/unirradiated)
- · Charpy impact properties (irradiated/unirradiated)
- · Fracture toughness (irradiated/unirradiated)
- · Creep properties (irradiated)
- · Fatigue properties (irradiated/unirradiated)
- · Swelling behavior (irradiated)
- · Corrosion/erosion behavior in Li (irradiated/unirradiated)

C. Condition and Criteria
- · Stress distribution
- · Temperature distribution and thermal cycles
- · Allowable deformation
- · Allowable fracture toughness

The main activities involved in the task can be summarized as follows:

- collection of data currently available on the mechanical properties of irradiated materials
- establishment of a materials database for evaluation of the lifetime
- stress-strain analysis of the Li-backwall geometry under operative conditions
- assessment of the structural integrity including the lifetime

IN 1998, the main part of the work focused on a collection of data for irradiated materials under conditions as close as possible to those foreseen for the IFMIF backwall target, with the aim of selecting the most suitable ones. Moreover, some preliminary calculations were carried out in collaboration with the University of Pisa to evaluate the stress-strain behavior of the Li backwall target under the loading conditions, just at the beginning of its operation (low absorbed dose).

2.2.7.2.1 Physical Properties

Physical properties of reduced activation ferritic steel of F82H are reported in reference [1]. Following equations are used for approximation in this report. The irradiation effects on these physical properties are expected to be small except for density.

- Elastic modulus E (GPa) (T: RT-973K)
  $E(T) = -2.134\times10^{-7}T^3 + 3.195\times10^{-4}T^2 - 2.075\times10^{-1}T + 256.157$ (1)
- Poisson ratio m (T: RT-773K)
  $m = 0.29$ (constant) (2)
- Thermal conductivity λ (W/mK)
  $\lambda(T) = 1.778\times10^{-7}T^3 - 2.530\times10^{-4}T^2 + 1.243\times10^{-1}T + 12.093$ (T: RT-573K) (3a)
  $\lambda(T) = 1.016\times10^{-10}T^3 - 2.439\times10^{-6}T^2 + 1.088\times10^{-3}T + 33.850$ (T: 573-973K) (3b)

- Thermal expansion coefficient (RT vs. T): α (K^{-1}) (T: RT-973K)
  $\alpha(T) = (1.099E\text{-}11T^4 - 3.975E\text{-}08T^3 + 4.891E\text{-}05T^2 - 0.0215T + 13.901)*10^{-6}$ (4)
- Specific heat *c* (J/kgK) (T: RT-823K)
  $c(T) = 1.222x10^{-6}T^3 - 1.675x10^{-3}T^2 + 1.083T + 243.5$ (T in K) (5)
- Density ρ (kg/m^3) (T: RT-973K)
  $\rho(T) = \rho_0/(1+\alpha(T))^3$, $\rho_0 = 7.87x10^3$ at T= RT (T in K) (6)

2.2.7.2.2 Irradiation Behavior

2.2.7.2.2.1 Service conditions and thermal stress

The irradiation conditions are summarized in table 2.2.7.1. Most of the results are obtained by fission reactors. The quality of damage produced by high-energy (14 MeV) neutrons may different from that of fission neutrons.

Table 2.2.7.1 Irradiation conditions [2].

Temperature	250 – 300°C
Damage	~55 dpa/y
Helium	~500 appmHe/y
Hydrogen	~2000 appm/y

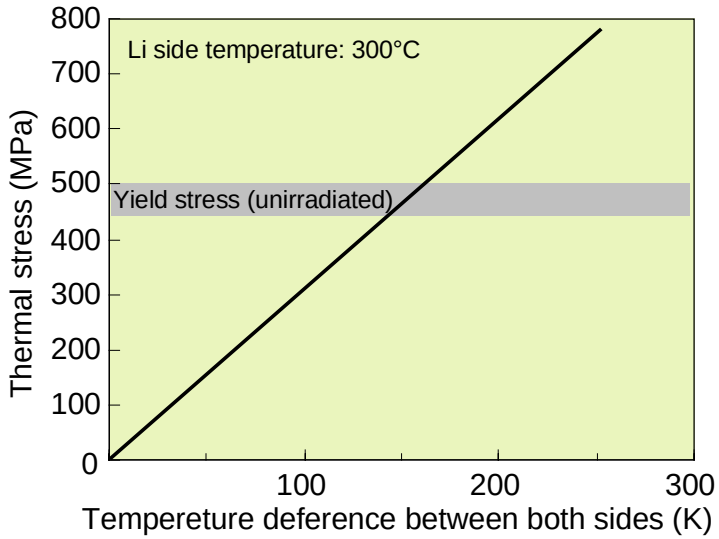

Fig. 2.2.7.1: Thermal stress due to temperature difference

Neutron beam heating in the back-wall introduces temperature gradients along the thickness direction of the back-wall. Thermal stress by the temperature difference calculated using the following equation is plotted in Figure 2.2.7.1 together with the yield stress of F82H.

Thermal Stress = $(L(T_1=573K)-L(T_2=573K-DT))*E(573K)*(1+m)$ (7)

where $L = \alpha\ (T-T_0(=293K))*L_0(=1)$. This calculation gives the temperature difference between both sides of the back-wall and should be below 130 °C. Particularly thermal shock at the onset of the Li-target system operation should be considered for the stress analysis.

From the thermal analysis carried out by a 3-D model, a weak thermal gradient through the backwall thickness (about 8°C/mm) in the irradiated area has been observed due to heat generation in the steel. The structural study of the backwall has been carried out by linear and non linear analysis.

From the linear analysis it was obvious that the material remains in the elastic region with a maximum stress of about 82 MPa. Nevertheless, the compressive stress field and a weak inflection with a maximum displacement of 0.27 mm in the direction opposite to the flowing lithium suggested to pass onto the non linear analysis in order to check a possible situation of instability of the structure.

Using the same model, a gradual increase in the thermal load has been observed, or, in other words, a gradual increase in ΔT along the lithium jet direction in the irradiated area. Consequently, until half the thermal load, a maximum displacement of some tenth of a millimeter has been observed. In this thermal load range linear and non linear analysis give nearly the same results. Afterwards there is a tendency to lose the linearity between strain and displacement with a consequent sudden increase of displacement as a function of the applied thermal load.

Under nominal operative conditions, a maximum displacement of 1.4 mm in the direction opposite to that of the flowing lithium has been found. Under these conditions, the material still remains in the elastic region with a maximum stress of about 100 MPa [10].

Considering that the vertical test assemblies must be located as closely as possible (about 2 mm) to the target backwall to receive the maximum neutron fluence, an estimated maximum displacement in that direction of 1.4 mm can produce remarkable problems as far as the operability of the whole system is concerned.

2.2.7.2.2.2 Swelling Behavior

A change in dimension due to swelling introduces some stress to the component. For example, Figure 2.2.7.2 shows the swelling of F82H after the HFIR target irradiation [3]. 300 °C irradiation with and without helium generation due to ^{10}B doping (320 appm) hardly shows any swelling after about 57 dpa. Swelling at 300°C and below is small, and is expected below 0.1% even after 100 dpa. Validation of swelling behavior by multi-ion beam (He, H and Fe ions) is also quite important. Figure 2.2.7.3 shows the calculated stress induced by swelling using the temperature dependence of the elastic modulus.

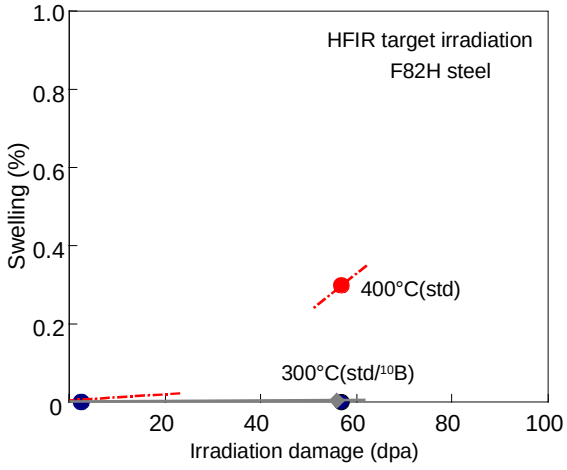

Fig. 2.2.7.2: Swelling of F82H after HFR irradiation.

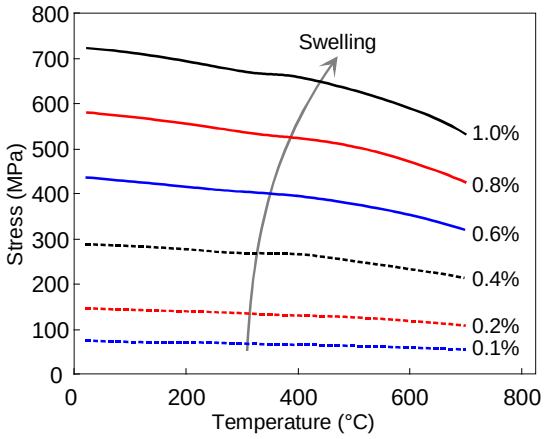

Fig. 2.2.7.3: Calculated stress during swelling

2.2.7.2.2.3 Tensile Properties

Tensile properties are the most important mechanical data of a material. Irradiation at temperatures below about 400 °C causes irradiation hardening (Figure 2.2.7.4). On the other hand, irradiation above 400°C causes hardly any irradiation hardening. Irradiation hardening at low temperature is a general feature of this alloy class and mainly due to a high density of small dislocation loops and irradiation enhanced precipitates. While irradiation hardening increases rapidly during the early phase of irradiation, the further increase beyond a few dpa is very moderate only as shown by Figure 2.2.7.5 [4,5]. Figure 2.2.7.6 shows that the yield strength can reach values as high as 980 MPa at 100 dpa. With an increase of yield stress, elongation (especially uniform elongation) decreases. Figure 2.2.7.7.7 shows examples of stress-strain curves after neutron irradiation [4]. Specimens with high yield stress (larger than 750 MPa) show hardly any uniform elongation. All specimens in this figure show a ductile fracture mode, so that ductility does not disappear even in heavily hardened specimens. The decreased work hardening capability might be the reason for the overall small uniform elongation. Another possible reason is channeled deformation. True stress-strain analysis is necessary to understand the deformation behavior of this kind of steels.

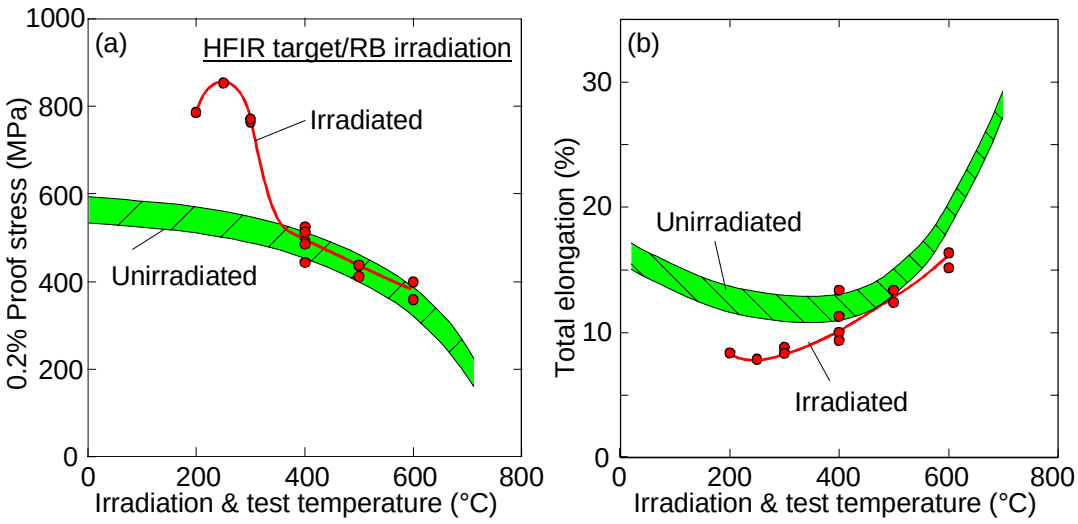

Figure 2.2.7.4: Temperature dependence of tensile properties of F82H after HFIR irradiation

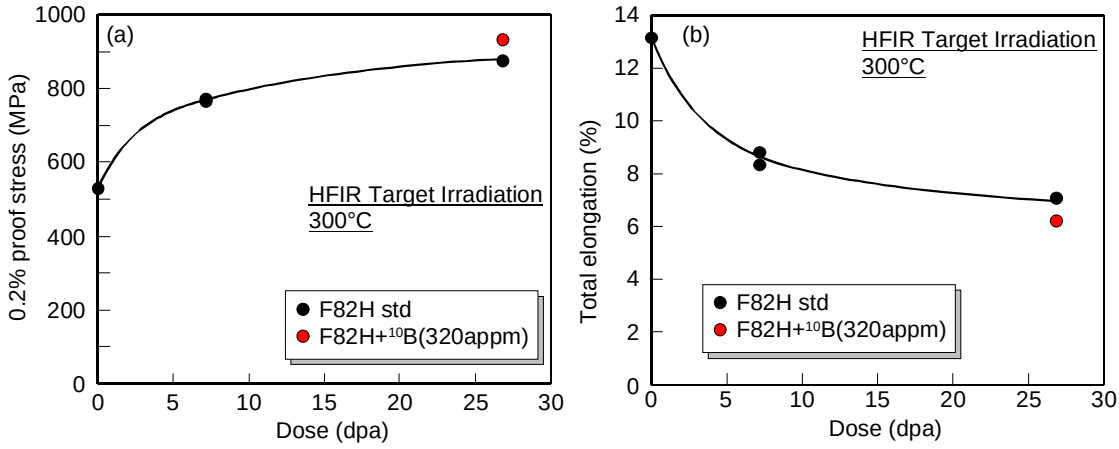

Figure 2.2.7.5: Damage dependence of tensile properties of F82H (300°C)

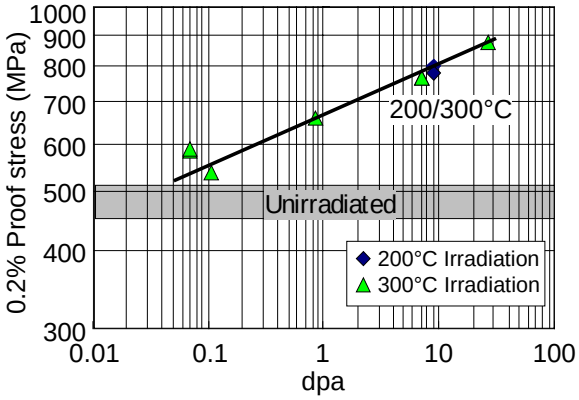

Fig. 2.2.7.6: Dose dependence of the yield stress of F82H steel

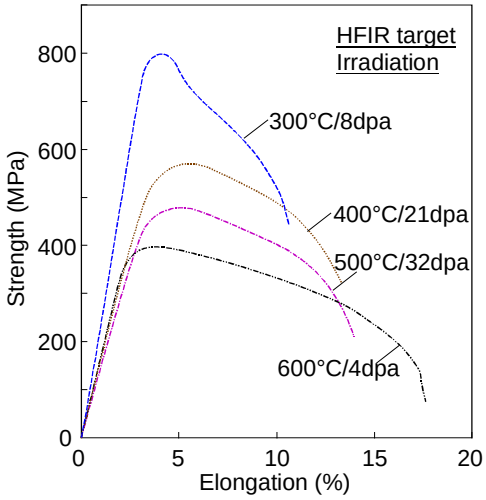

Fig. 2.2.7.7: Stress-strain curves of F82H steel after irradiation

Tab. 2.2.7.2: Tensile properties of some irradiated austenitic steels

Austenitic Steel	Material Condition	Yield Strength (MPa)	Uniform Elongation (%)
AISI 316L(N)-SPH, J316, 316 L(N) (solution annealed)	7 dpa, 250-350 °C	700-900	0.2-0.4
	18 dpa, 250-350 °C	700-900	0.4
	7 dpa, 350-400 °C	730	5-10
US 316, 20 % CW	10 dpa, 300-340 °C	1000	0.2
US 316, 20 % CW	10 dpa, 500 °C	800	1.0

It has been further shown [13] that the hardening ratio between reduced activation steels (e.g. F82H-mod) and conventional 10-12% Cr-steels (e.g.MANET-1) is about 0.44±0.09 within a wide temperature region, that is, irradiation hardening of reduced activation ferritic-martensitic steels is much smaller. Tensile properties of typical austenitic steels are given in table 2.2.7.2 for comparison.

2.2.7.2.2.4 Charpy Impact Property

Charpy properties give relevant information on dynamic brittle fracture. As shown in Figure 2.2.7.8, irradiation at temperatures below 400 °C caused an increase in the ductile to brittle transition temperature DBTT [6]. Reduced activation ferritic/martensitic steels have better Charpy properties than non-reduced activation steels before and after irradiation. Figure 9 shows the change in DBTT by irradiation [4,6,7,8]. It seems that the DBTT shift saturates at a relatively low damage level. However, the scatter is relatively large, so that irradiation experiments need too high dose levels to define the saturation level in DBTT. Transmutation produced helium is supposed to affect the Charpy property strongly around 300°C. It is reported that helium

increase DBTT, depending on the reduced activation steel, by about 60 °C after 300°C irradiation [9].

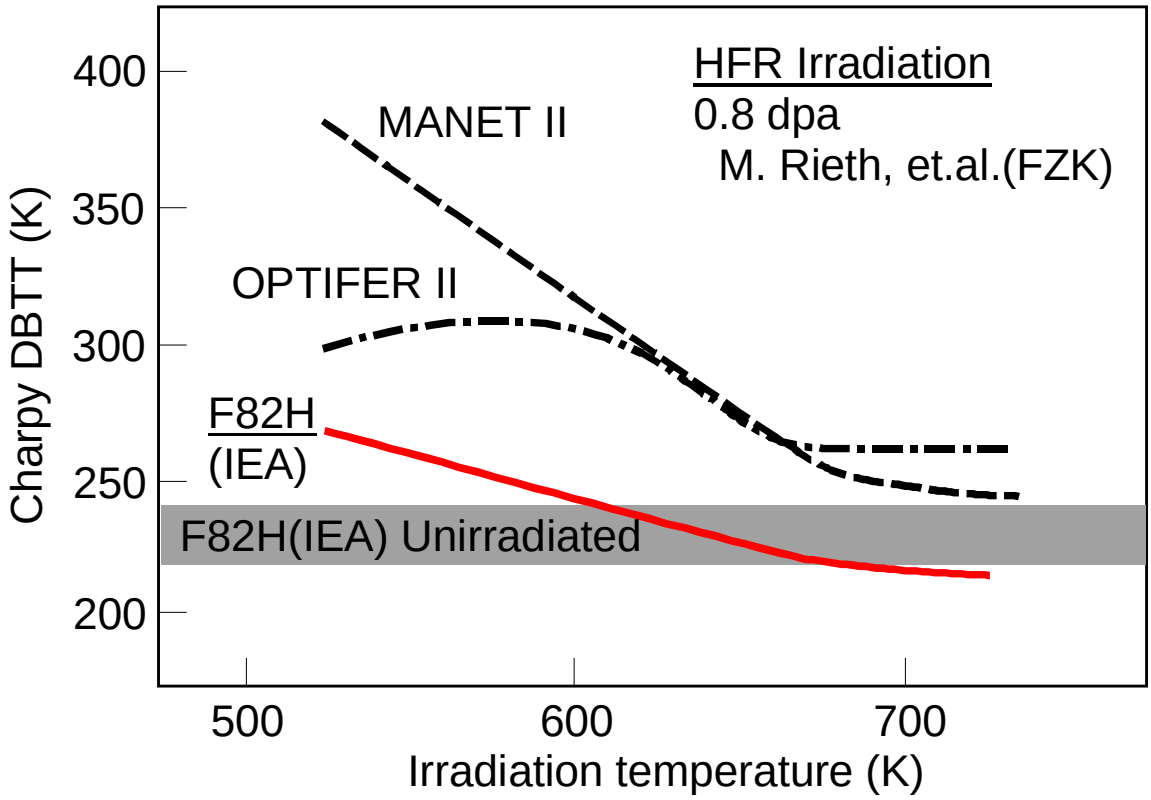

Fig. 2.2.7.8: Temperature dependence of DBTT

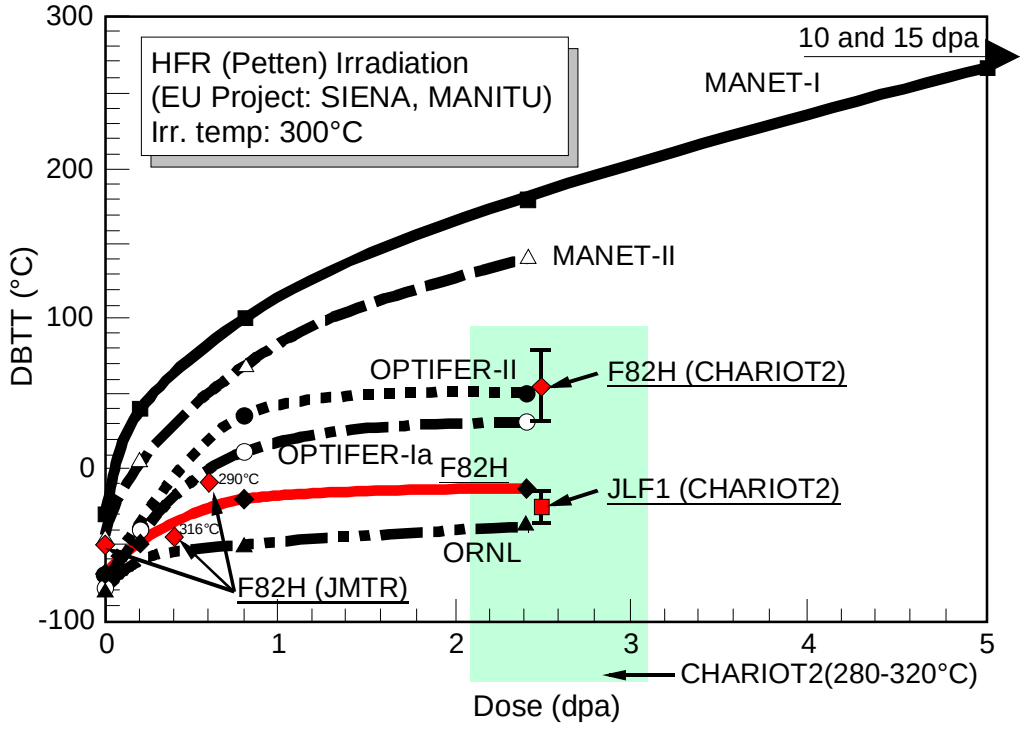

Figure 2.2.7.9: Dose dependence of DBTT (300C irradiation)

2.2.7.2.2.5 Fracture *Toughness*

Fracture toughness gives a fracture criterion concerning the resistance to crack propagation. Fracture toughness has a similar temperature dependence to Charpy impact property and a ductile-to-brittle-transition. Low fracture toughness causes an unstable fracture with low stress. There are not much irradiation data on fracture toughness, however, neutron irradiation decreases fracture toughness and shifts DBTT to a higher temperature [8,9]. There is no data reported on the helium effect on fracture toughness, but fracture toughness seems to be affected by helium as is the Charpy property. Nevertheless, the severe loss of uniform elongation after 7 dpa at irradiation temperatures of 250-350 °C would suggest a dramatic loss of fracture toughness at higher dose [14]. Therefore it is possible that fracture toughness controls the lifetime of components. Altogether it is strongly recommended to examine the dose dependence of fracture toughness and the helium effect on fracture toughness.

2.2.7.2.2.6 Creep

Creep deformation should be considered only under irradiation conditions. Limited irradiation data are available at low temperature. Irradiation creep of HT-9 was evaluated at 330°C in the ORR (7 dpa) and the HFIR (19 dpa) with a pressurized tube [10]. Creep strain seems to be linearly increased with stress, and normalized creep strains were 0.0004%/MPa and 0.0008%/MPa for 7 dpa and 19 dpa, respectively. When dose dependence is assumed to be linear with dose (evaluation for the worst case), the irradiation creep factor becomes about 4.37×10^{-5}%MPa^{-1}dpa^{-1}. Using this value, creep strain becomes 0.66% of creep strain for 300 MPa of stress in loading direction and 1.32% increase in thickness direction during irradiation to 50 dpa. Creep strain only appears in irradiated areas, so that stress relaxation may be small when irradiated area is small as compared with the whole volume. Stress equals deformation holds in the invert direction, when the component is cooled. Dose dependence of creep strain at higher dose level also needed to estimate the creep strain precisely.

2.2.7.2.2.7 Fatigue

About 2 – 3 W/cm^3 of estimated beam heating increases the temperature of the component by about 30 – 45°C/s. It is translated to 100 – 150 MPa/s in stress or about 0.05 - 0.07%/s in strain. Because the IFMIF is planed continuous operation, fatigue damage by thermal cycle during start up and shut down may be limited. Therefore, thermal fatigue is considered not to be serious fracture process for the Li-target backplate.

2.2.7.2.2.8 Helium Effects

Helium affects the microstructural evolution and materials response to mechanical loading. According to currently reported results, helium strongly affects Charpy properties, but it does not have much effect on irradiation tensile behaviors [4,5,8,12,13]. Hardly any data have been obtained on other properties. Particularly, the helium effect on irradiation creep behavior is considered important in this case. Ni-doping, boron-doping and helium injection techniques are employed to simulate the helium effect on microstructural and mechanical properties. The availability of these techniques is discussed in the IEA workshop on ferritic/martensitic steels.

2.2.7.2.2.9 Hydrogen Effects

Preliminary results obtained by shear-punch testing using the ^{54}Fe isotope tailored F82H (about 650 appmH/34 dpa at 300°C) showed some increase in shear strength [11]. It is expected that hydrogen interacts with irradiation-induced defects and helium, so that the presence of hydrogen modifies the defect morphology, depending on the irradiation temperature [12].

Hydrogen charging of the unirradiated martensitic steels MANET and F82H has brought about a significant reduction in ductility at room temperature with only a few wppm of hydrogen [15,66]. The research activity in this field is now in progress to evaluate the effect of temperature on the mechanical and microstructural properties.

2.2.7.2.2.10 Corrosion/Erosion

High-speed lithium flows over the backwall surface. Presently we do not have data on corrosion and erosion at the Li/back-wall interface. An in-pile loop corrosion test in the simultaneous conditions is needed for the estimation of corrosion at the backwall surface.

2.2.7.3 Summary

Irradiation at temperatures of about 300°C causes a rather strong decrease of the ductility and toughness and an increase of DBTT. DBTT may increase to 200°C after irradiation. There is a possibility that this limits the allowable dose and the lifetime depending on the operation scenario and the design methodology.

Irradiation creep may not be small enough to be ignored even at the relatively low temperature of 300°C. It may cause distortion of the back-wall and affect Li flow, although the allowable limit of deformation has not yet been identified. Creep deformation in irradiated areas causes some tensile stress, when the back-wall is cooled. If cracks or defects occur in the material, tensile stress works to extend cracks. Fracture toughness has a negative temperature dependence, so that there are two possible occasions for crack propagation. They are when the beam stops and when Li-flow stops.

Dimensional change due to swelling seems to be small, so that swelling will not cause a large stress. However, if the component is exposed to a higher temperature, the temperature fluctuation effect should be studied.

Yield strength increases with the increasing damage. Loss of strength is caused by fatigue (cyclic softening), but the stress amplitude and number of cycles are expected to be small. Therefore, plastic collapse due to a loss of strength is not likely. The balance of corrosion loss and thickening by creep deformation also is to be estimated to keep the wall thickness.

Loss of Li-flow may cause strong beam heating of the back-wall. Transmutation-produced He causes the ductility and fracture toughness to be decreased at high temperatures. Beam heating scenario during the loss of Li-flow event should be evaluated.

2.2.7.4 Recommendations

Probably, the backwall should be exchanged every year (~60 dpa). The following research is necessary to confirm the suitability of RAFM steels as backwall material:

- Dose dependence of fracture toughness, Charpy impact properties and creep
-· Helium effects on fracture toughness, Charpy impact properties and creep
-· Hydrogen effects on fracture toughness and Charpy impact properties
-· Corrosion loss in Li-loop

The following information is needed to determine the loading condition:

- Thermal stress (temperature distribution, time dependence)
- Allowable deformation
- Allowable minimum fracture toughness
- Temperature and stress history during off-normal event

Future work includes: - materials database for
- evaluation of lifetime
- Stress-strain analyses for Li-backwall geometries

under real loading conditions
- Assessment of the structural integrity including the lifetime.

References

[1] K. Shiba, et al, JAERI-Tech 97-038 (1997).
[2] IFMIF CDA Team, „IFMIF Conceptual Design Report“ (1997).
[3] E. Wakai, et al, to be published.
[4] K. Shiba, et al, Proc. of EUROMAT 96(1996), pp265-272.
[5] K. Shiba, et al, Proc. of IEA Working Group Meeting on Ferritic/Martensitic Steels (Tokyo) (1997)
[6] M. Rieth, et al, J Nucl. Matr. 233-237(1996), pp351-355.
[7] K. Shiba, et al, J Nucl. Matr. 233-237(1996), pp309-312.
[8] M. Rieth, et al, to be published in ASTP STP.
[9] A.F. Rowcliffe, et al, to be published in J Nucl. Matr.
[10] M.L. Grossbeck, et al, J Nucl. Matr. 233-237(1996), pp148-151.
[11] S. Ohnuki, et al, Private communication.
[12] K.K. Bae, K. Ehrlich and A. Möslang, Journ. Nucl Mater. 191-194 (1992) 905-909.
[13] R. Lindau, E. Materna-Morris, A. Möslang, D. Preininger, M. Rieth and H.D. Röhrig, Journ. Nucl. Mater. in press.
[14] R.L. Klueh et al., Journal of Nuclear Materials, 116-124, vol. 191-195, 1992
[15] G. Benamati et al., to be published in Journal of Nuclear Materials
[16] M. Beghini et al., Journal of Engineering Materials and Technology, 179-185, vol.118, 1996

2.2.8 Small specimen test technology

Description and justification

Further activities in that field are essential in order to fully utilize the available irradiation volume and to qualify all miniaturized specimens. It is assumed that also in future the SSTT activities will be mainly organized within the frameworth of dedicated IEA-workshops and also be supported within the respective materials programs.

2.2.8.1 Impact on CDA

The availability of the miniaturized hour glass type fatigue specimen has been demonstrated. No impact on CDA.

2.2.8.2 Results & Conclusions

It has been pointed out that small specimen test techniques especially for fatigue, creep and fracture properties need further development effort and discussions regarding the significance. For fatigue and pressurized creep specimens, developments of test techniques and the demonstration of the performance are required for their small sizes and the configurations. The significance of the miniaturized Charpy impact test is still in question.

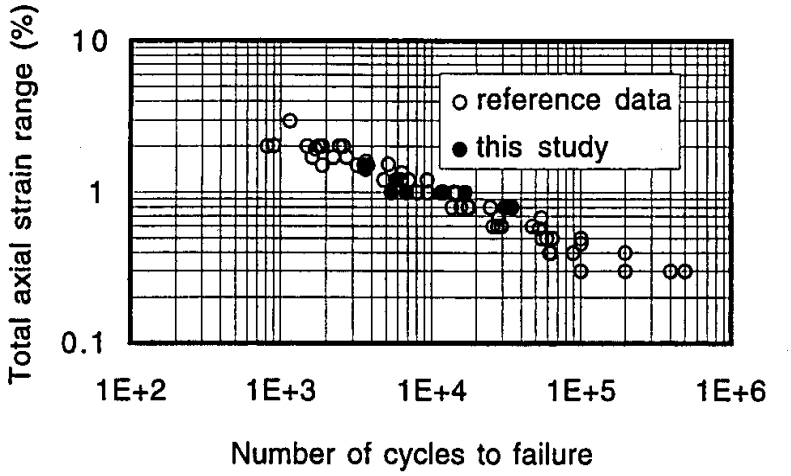

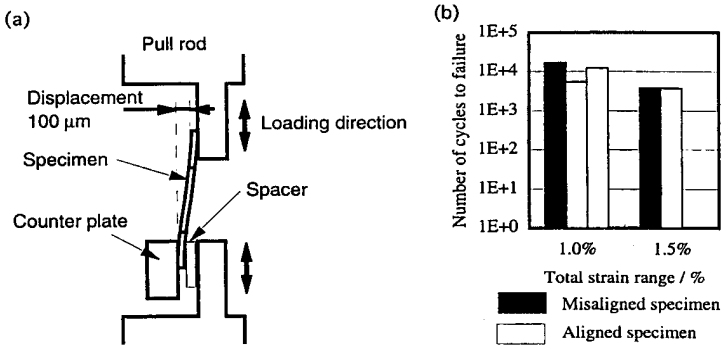

Fig. 2.2.9.1: Total strain range and number of cycles to failure for small and standard size specimens (top); Effect of misalignment on the fatigue life (bottom).

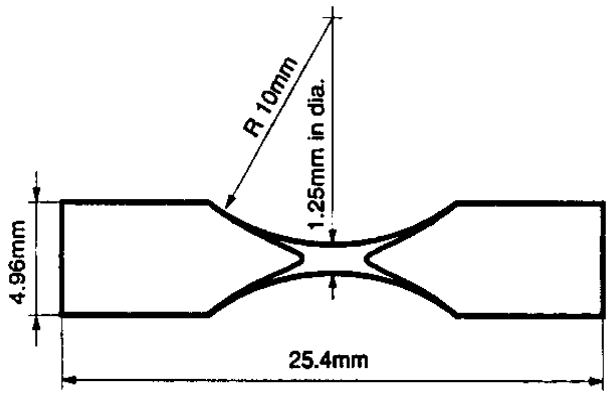

Fig. 2.2.2.9.2: Miniaturized hour-glass fatigue specimen

Fatigue testing after irradiation will be carried out in hot cells with remote handling equipment. Considering the limited specimen manipulation in the cells, the specimen and the test method need to be rather insensitive to specimen misalignment to the loading axis and simple for operation. Effects of surface preparation, specimen size and the misalignment of the specimen on the fatigue life are evaluated[1].

The configuration of the hour glass shapes miniaturized fatigue specimen is shown in Fig. 1 (a). Fatigue strain is measured at the minimum cross section. Figure 1 (b) shows the total axial strain range versus the number of cycles to failure with specimens prepared from a 0.06C-0.5Si-14Cr-16Ni-2Mo-0.25Ti austenitic stainless steel. The axial strain range $\Delta\varepsilon_a$ is obtained from diametric strain range Ded with a form of $\Delta\varepsilon_a = -2\ \Delta\varepsilon_d$. The number of cycles to failure obtained from the miniaturized specimens were almost identical to the results with standard-size specimens with cylindrical test regions. The results in Fig. 1(b) are obtained using specimens finished with electropolishing. Specimens without electropolishing exhibited a smaller number of cycles to failure. The effect of the misalignment is shown in Fig. 1(c). The effect of lateral displacement by 0.1 mm was not strong. This indicates that the fatigue damage in an hour glass shaped specimen is not very strongly affected by the misalignment.

2.2.8.3 Future Directions

Future direction for the miniaturized fatigue specimen is the development of a miniaturized specimen with cylindrical test region.

References

Y. Miwa, S. Jitsukawa and A. Hishinuma, "Development of a miniaturized hour-glass shaped fatigue specimen," J. of Nuclear Materials, in press

3 Target Facilities

3.1 Introduction

The basic design parameters for a lithium target and a loop system in the CDA are kept in the CDE task. The total deuteron beam current is 250 mA and its beam footprint on the lithium jet is 20 cm in width and 5 cm in height. So the current density onto the target is 2.5 mA/cm^2. The maximum deuteron energy is about 40 MeV and about maximum 10 MW of beam power will be deposited onto the lithium target. The main requirements of the target system are as follows:

1. Removal of this large deposit energy using a high velocity lithium jet. The jet should have stable free surface and boiling must be prevented at the beam foot print in order to provide a stable neutron field.
2. Control of the impurity level (T, ^{7}Be for the radiological safety, C, O, N, for the materials compatibility), in the lithium loop system.
3. Ensuring the safety with respect to lithium hazard and tritium release from the lithium loop system.
4. Achievement of system availability of more than 95% during the lifetime of the plant. This value is required from the overall availability budget for the IFMIF facility [1]. The evaluations and improvement for the conceptual design have been made in the CDE phase [2],[3],[4] and some results of the tasks are described as follows.

3.2 CDE Tasks

3.2.1 Optimization of System Designs

3.2.1A Target System Layout

Description and justification:

For the IFMIF target system, a complete prevention of combustion in the event of liquid lithium spill or leak is strongly required. Then in the CDA phase, a multiple confinement system was introduced to the primary lithium loop as a lithium hazard prevention plan. The primary confinement is made up of the lithium carrying components itself, such as the pipes and tanks. The secondary confinement is a simple sheet metal structure, referred to as a guard vessel, surrounding the primary confinement. The guard vessel is not required to provide a high degree of gas tightness. The space between the primary and secondary confinement is filled with an argon gas that is circulated at a low flow rate for impurity monitoring. Oxygen meters will be available to detect the lithium leak by monitoring the oxygen level change. The tertiary confinement is the lithium cell. The cell is gas-tight and maintained under argon atmosphere at a slight positive pressure. The argon gas circulating system should control its purity and the temperature under adequate conditions. To reduce the capital cost of the argon circulating system, the volume of the lithium cell should be minimized under the optimization of the target system layout. The optimization has been made together with the analysis of the thermal stress on the lithium circulating system.

Contributors:

Organization	Principal Investigator	
JAPAN	JAERI:	Y. Kato, H. Takeuchi, H. Katsuta
	IHI:	H. Kakui, et. al.
EC	ENEA:	S. Cevolani, D. Tirelli
USA	ANL	T. Hua

Main responsibility : JAERI

Milestones:

1) Validation of present design — Aug. 1997
2) Optimization design of target system layout — Oct. 1997
3) Analysis of the thermal stress on the lithium circulating system — Feb. 1998
4) Documentation — Nov. 1998

3.2.1A.1 Impact on CDA

A more practical and economical target system will be achieved by the optimization of the CDA design. The layout of the primary lithium loop of the CDA design was changed considerably. The utility space for the components maintenance, exchange and transportation was also considered. The test cell volume needs to be changed for the replacement of the target assembly.

3.2.1A.2 Results & Conclusions

As a result, the total volume of the lithium cell is about 2662 m^3 (a reduction of 37% compared to the CDA design). The lithium inventory in the main pipes of primary system decreases by about 8% but the total lithium inventory, about 20,600 liters, is only 2% less than that in the CDA design. An optimized layout of the primary loop, in which the purification loop is not included for reasons of simplification, is shown in Fig. 3.2.1A-1. In the layout of loop components, their maintenance and repair are considered with the arrangement of their lithium cell as shown in Fig. 3.2.1A-2

There are no basic changes to the flow sheet[1] of the lithium target system in CDA phase but the revised heat and flow balances on the primary lithium loop are shown in Fig. 3.2.1A-3

The average hot leg temperature of lithium in the primary loop is about 285 °C and the average cold leg temperature is about 250 °C. In normal operation, the thermal stress in the primary loop is evaluated. The maximum value is about 109 N/mm^2 at the nozzle of the quench tank outlet and it is by a factor of two lower than the permissible value (206 N/mm^2)[5].

3.2.1A.3 Future Directions

In the next phase, we should design each component cell to provide for maintenance, repair, transport, carry in or out. The argon gas circulating system should also be optimized.

References

[1] IFMIF-CDA Team (Ed.) M. Martone, "IFMIF, International Fusion Materials Irradiation Facility Conceptual Design Activity, Final Report," ENEA Frascati Report, RT/ERG/FUS/96/17 (1996).

[2] H. Katsuta, D. Smith, Y. Kato, T. Hua, L. Green, Y. Hoshi, S. Cevolani and S. Konishi, "Conceptual Design of The IFMIF Target Facility," J. of Fusion Tech, 30 (3), 1152 (1996)

[3] Y. Kato et al., “Conceptual Design Study of IFMIF Target system,” Proc. of NURETH-8, Sept. 30-Oct. 4, 1997, p.1260, Atomic Energy Society of Japan, (1997).

[4] H. Katsuta et al., “ Present status of the conceptual design of IFMIF target facility”, J. of Nucl. Mater.[1998] to be published.

[5] Y. Kato et al., “ Design study of IFMIF target system”, Proc. of AccApp-98, Sept.20-23, American Nuclear Society, [1998], to be published.

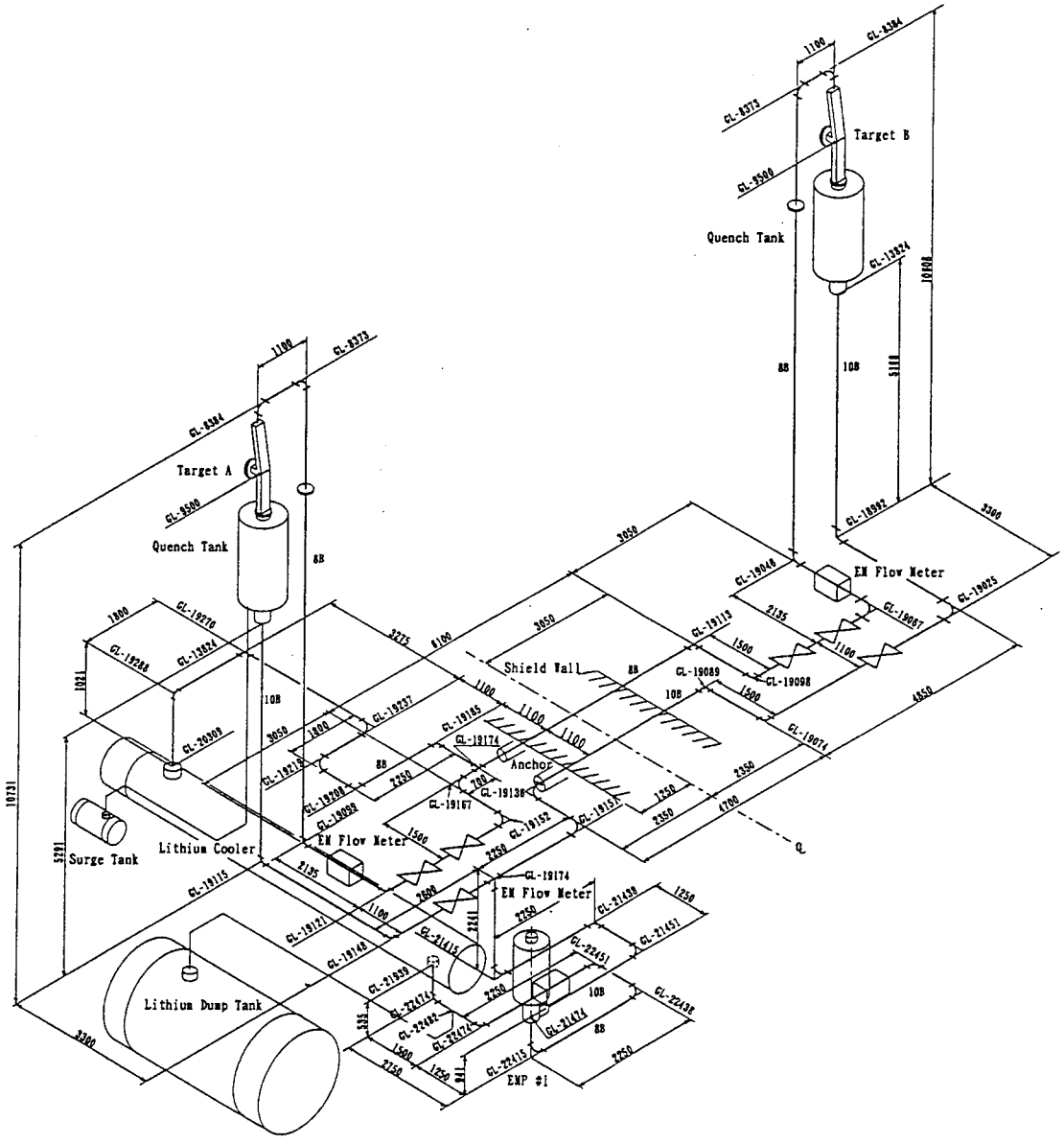

Fig. 3.2.1A-1 Optimized layout of primary lithium loop

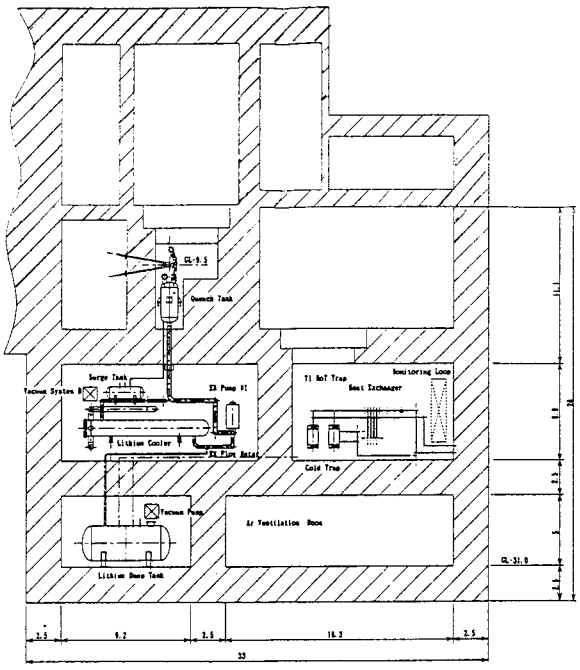

Cross sectional view (A-A)

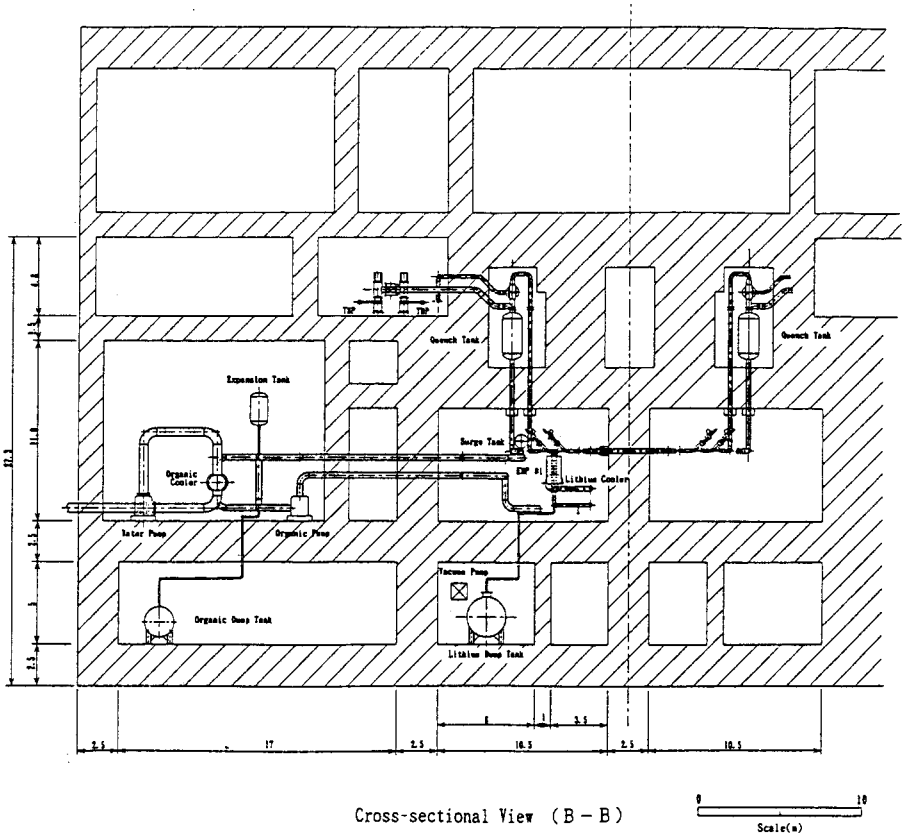

Fig. 3.2.1A-2: Layout of the lithium cell and target system

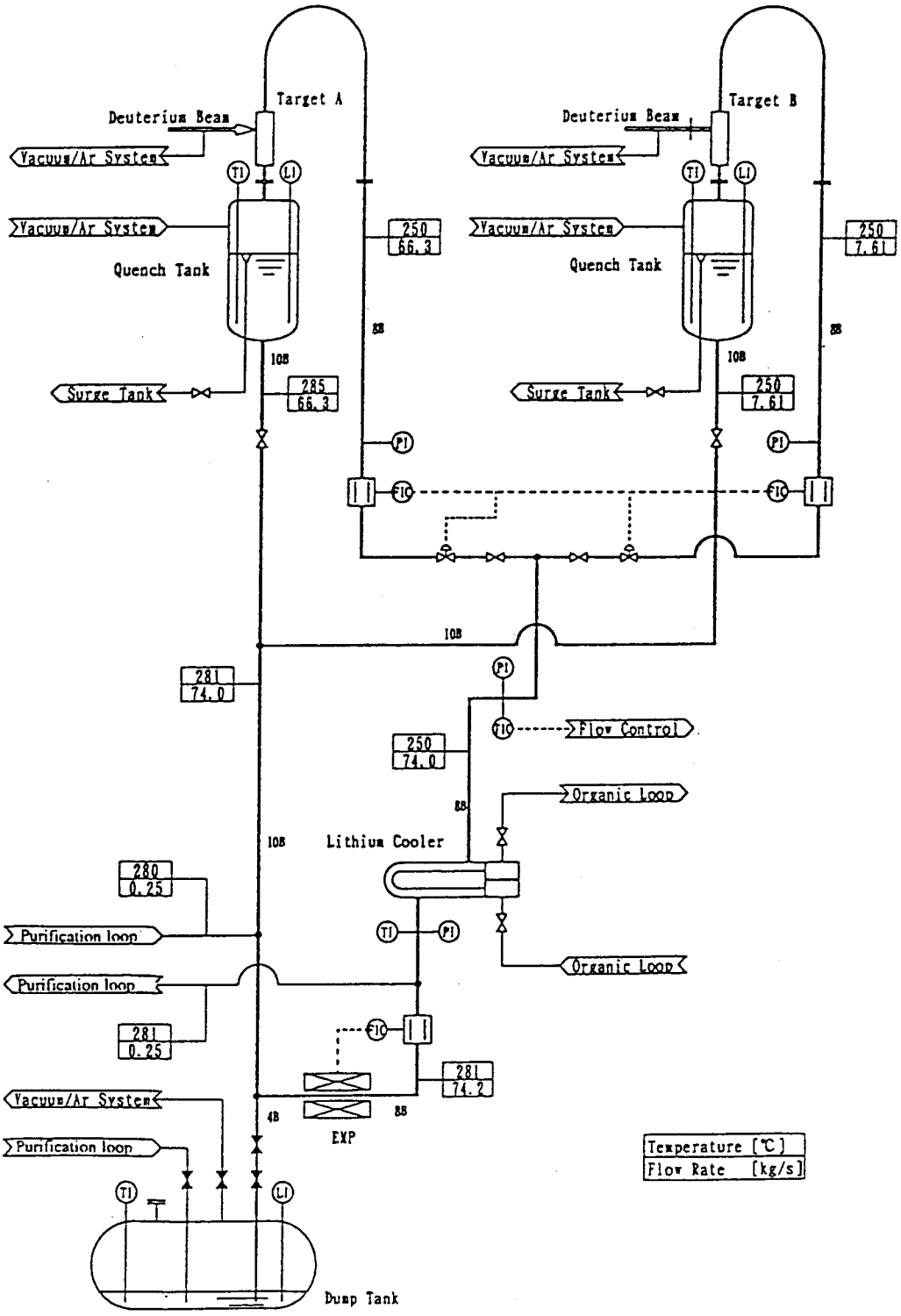

Fig. 3.2.1A-3 Heat and flow balance on the primary lithium loop

3.2.1B Target Assembly

For the target assembly design, especially for the structure of the replaceable backwall, some basic designs were proposed in CDA. The main problems were the method of lithium-tight sealing and the feasibility of the mechanism of backwall exchange. A conventional cramp and lip-weld type backwall was designed with the remote handling device in JAERI. In ENEA an improved version of the bayonet and metal O-ring seal type backwall was developed, allowing for the displacement of the junction inside the nozzle. A further ENEA effort was devoted to the development of a design for the coupling the bayonet scheme with the LIP welded system.

Description and justification:

For the target assembly design, especially for the structure of the replaceable backwall, some basic designs were proposed in CDA. The main problems were the method of lithium-tight sealing and the feasibility of the mechanism of backwall exchange. A conventional cramp and lip-weld type backwall was designed with the remote handling device in JAERI and a bayonet and metal O-ring seal type backwall was improved in ENEA.

Contributors*:*

Organization	Principal Investigator	
JAPAN	JAERI:	Y. Kato, M. Ida, H. Nakamura, H. Takeuchi, H. Katsuta
	IHI:	H. Kakui
EC	ENEA:	S. Cevolani, D. Giusti, R. Stefanelli, D. Tirelli
USA	ANL	T. Hua, D. Smith

Main responsibility : JAERI

Milestones:

1) Validation of CDA design	Dec. 1997
2) Target assembly design with remote handling devices	Apr. 1998
3) Design of remote handling device	Aug. 1998
4) Documentation	Nov. 1998

3.2.1B.1 Impact on CDA

The practical target assembly and the remote handling device were designed on the base of the CDA design. The test cell volume needs to be changed in accordance with the evaluation of the operation space of a remote handling device for the target assembly.

3.2.1B.2 Results & Conclusions

One of the options of an improved target assembly is shown in Fig. 3.2.1B-1. In this design, a symmetrical nozzle at the outlet of the straightener and a replaceable backwall are adopted. For the backup of the seal tight structure of the replaceable backwall, a YAG laser device for lip welding will be introduced. This device has been developed for the ITER project in JAERI. After the backwall is welded, a cramp is set to fix and hold it on the base of the assembly. The YAG laser device also has a function to cut out the backwall during replacement. The remote handling device has another function to shape up the cutting edge for the welding. The structure of the

replaceable backwall is shown in Fig. 3.2.1B-2. The other option for the replaceable backwall, the bayonet type, has been improved in ENEA and the basic structure is shown in Fig. 3.2.1B-3.

The target assembly is planned to be exchanged in the IFMIF operation schedule using the remote operation machine. When the target assembly is exchanged, three lip-welded seal flanges have to be separated at two joints of the primary loop and at the end of accelerator beamline (HEBT). One of these lip seal flanges of the target assembly with the YAG laser welding and cutting machine is shown in Fig. 3.2.1B-4.

Furthermore, the coupling of the bayonet scheme with the lip-weld system was studied. This solution appears to be feasible. However, these designs do not have the advantages of the reference bayonet scheme (i.e. the one without lip-weld) which seems to be more suitable for the IFMIF purposes.

3.2.1B.3 Future Directions

After focusing on the promising model, more detailed design of the remote handling device should be made and a prototype should be for its performance with a water loop and then with a lithium loop. Information regarding the heavy irradiation effect on the candidate backwall materials should be obtained to evaluate the deformation and the life time of the backwall. Ideas to solve the following two technical problems should be proposed in the next phase and the practical method should be developed:

1. Before the backwall or flanges are set up, the attached lithium on the surface of a used flange should be removed by a remote handling device.
2. The activated metal powder will be produced at the lip cutting by laser. Contamination in the test cell should be prevented.

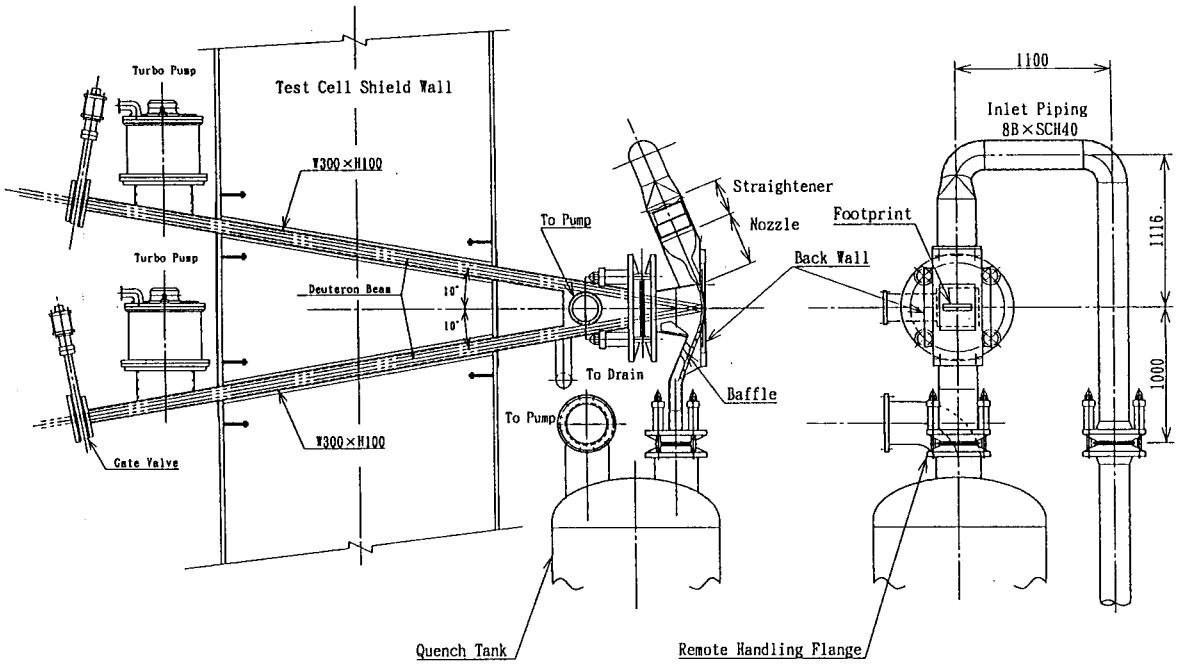

Fig. 3.2.1B-1 Improved target assembly

Fig. 3.2.1B-2: Assembly of the replaceable backwall

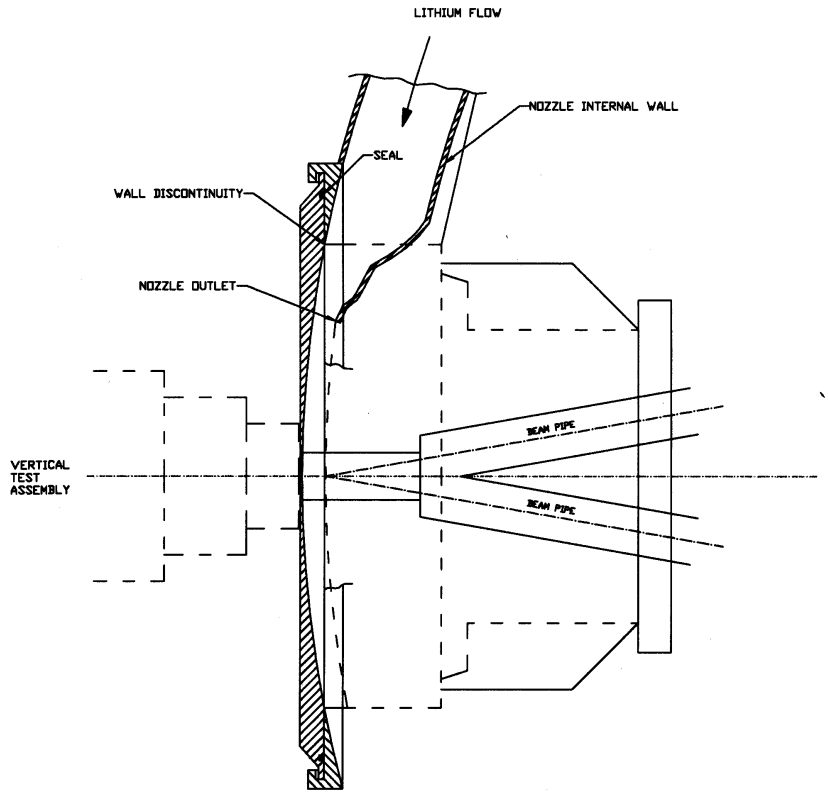

Fig. 3.2.1B-3 Replaceable backwall structure of improved bayonet type

Fig. 3.2.1B-4 Structure of YAG laser welding and cutting machine

3.2.2A Thermal and fluid dynamics of Li target flow

Description and justification:

In IFMIF, the two D^+ beams will be focused onto a rectangular region (50 mm-high x 200 mm-wide) of the Li target. Most (> 95%) of the kinetic energy of the D^+ beam power (=10 MW) is deposited and turned into heat within the Li target flow. The liquid Li target should remove the generated heat to keep the stability and the integrity of the target flow itself. Furthermore, the Li target flows in high vacuum should be better than 10^{-3} Pa to ensure the D^+ beam stability. The temperature increase in the Li target should thus be well suppressed to avoid both the voiding in the target and the significant vaporization at the free surface. To meet these conditions, the Li target flows at high speed 10-20 m/s along a concave wall. Depth-wise static pressure distribution due to the centrifugal force results in a significant increase in the saturation temperature along with the depth. In the IFMIF-CDA, a contraction nozzle to provide the Li jet flow was requested to be located at a distance of ~150 mm from the upper edge of the D^+ beams

to minimize the deformation due to the neutron irradiation. The Li jet with a free surface is required to be stable along the whole length of about 350 mm and whole width of 260 mm. The characteristics of the IFMIF target flows have been studied experimentally [1] and analytically [2],[3],[4],[5]. To clarify the thermo and hydraulic stability of the Li target flow, the analyses of the jet flows have been performed using a multi-dimensional thermo-hydraulic computer code FLOW-3D [3]. The FLOW-3D code was employed because the code can deal with flows with a free surface using the VOF (volume of fluid) model.

The CDA design calculations performed by means of the RIGEL code [4,8] were compared with the first velocity profiles obtained by the JAERI water experiment; these analyses confirmed the validity of the RIGEL methodology [7].

The hydraulic stability of the target primary loop was also investigated from the point of view of cavitation. The effect of such phenomenon both on the IFMIF jet and on the JAERI water experiment were studied [9].

Contributors*:*

Organization	Principal Investigator
JAERI	M. Ida, H. Nakamura, Y. Kato
ENEA	D. Tirelli, S. Cevolani

Main responsibility **:** JAERI

Milestones:

1) Analysis of hydraulic stability	Aug.	1997
2) Analysis of thermal stability	Feb.	1998
3) Documentation	Dec.	1998

3.2.2A.1 Impact on CDA

Regarding the thermal and hydraulic stability of the Li target flow, the analyses of the jet flows have been performed. Feasibility is shown for the CDA target with a nozzle, curved backwall and long free surface.

3.2.2A.2 Results & Conclusions

3.2.2A.2.1 Jet Behavior around Nozzle Exit

A two-dimensional fluid dynamics numerical analysis was performed for IFMIF plane jet target flows on a concave wall to clarify the mechanisms yielding a free-vortex-like depth-wise velocity distribution ($u \cdot r$ = constant, where u is the local velocity at the radial location r) in the target flow below the exit of a straight contraction nozzle designed to form the jet flow with a uniform velocity profile (see Fig. 3.2.2A-1). The results obtained are summarized as follows.

1) As shown in Fig. 3.2.2A-1, static pressure distribution in the jet on the concave wall due to centrifugal force was found to penetrate into the upstream straight region of the nozzle. According to the pressure distribution, the flow is accelerated along the front wall, while the flow is decelerated along the backwall. As shown in Figs. 3.2.2A-2 and 3.2.2A-3, the pressure and velocity distributions change rapidly around the location (0 mm) where the wall curvature changes from straight to arc. The decrease and increase in the static pressure along the walls results in the specific depth-wise velocity distribution in the jet, following the Bernoulli's theorem. As shown in Fig.3.2.2A-4, the calculated velocity agreed with the measured one well, except near the boundary layers.

2) As shown in Fig. 3.2.2A-5, the distance between the nozzle exit and the inlet of the concave backwall was found to control the jet thickness such that a short straight section causes an increase in the jet thickness. However, the increase was smaller than 0.4 mm.

3.2.2A.2.2 Three dimensional convection

The effects of an onset of convection on the temperature profile of the target Li flow were analyzed. The convection appears near around the side edge of a beam footprint. In the steady state of the target flow, it is clarified that the temperature profiles at time t in the specific horizontal target section which moves with the average flow velocity v agrees well with the temperature profile at the location r = v t , where r is the distance from the lower edge of the beam footprint and t is the time from the instant that the specific section passes through the lower edge of the beam footprint. This is the practical method to obtain approximate 3-dimensional temperature profiles by 2-dimensional calculation at each time t in order to save significant computation time [2]. According to the initial condition of the 2-dimensional calculation, the temperature profile at t = 0 was obtained in a first step.

- Deuteron beam energy: 40 MeV with energy dispersion 0.5 MeV
- Total beam current: 250 mA,
- Beam footprint: 20 cm(w) x 5 cm(h)
- Backwall radius: 250 mm

The range of the target flow velocity evaluated in IFMIF-CDA was 10 to 20 m/s. To show the effect of convection more clearly, the calculation was made along the extremely long range backwall (2 m) which has a constant radius (250 mm). The results of the calculation for the flow velocities of 10 and 20 m/s are shown in Fig. 3.2.2A-7 and Fig. 3.2.2A-8, respectively. The results are summarized as follows.

1) From Fig. 3.2.2A-7, it is clear that even at the location of r = 2000 mm , a part of the maximum surface temperature (~590 K) does not exceed the boiling point (617 K) at the vacuum pressure of 10^{-3} Pa. Under practical conditions with a shorter backwall and larger radius, the temperature increment should be much smaller than evaluated. In Fig. 3.2.2A-8, the same patterns of the effect of convection as in Fig. 3.2.2A-7 is shown. However, it appears earlier in time t but longer in distance r. Therefore, there is no demerit to rise up the flow velocity as far as the effect of convection.
2) As shown in Figs. 3.2.2A-7 and 3.2.2A-8, the heat conduction was found effective for the temperature transient around the center (X = 0 mm) of the target flow, while the convection was effective around the edge (X = 100 mm) of the high-temperature region. The peak temperature in the jet greatly decreases because of these two heat migration mechanisms. The decrease in the peak temperature allows to use a large-radius backwall near the quench tank.

3.2.2A.2.3 Comparison between the RIGEL code and the water experiment results

The design calculations performed by means of the RIGEL code within the framework of the IFMIF-CDA demonstrated the capability of the reference jet design to fit the design constraints. This RIGEL analysis was based on a velocity profile inside the jet computed by the code itself: the first jet velocity profiles measured in the frame of the JAERI Water Experiment [1] allow for their insertion into the RIGEL code. The influence of the measured profiles, here shown in Fig. 3.2.2A-9, on the main design parameters, was investigated. The design of the subsystem does not result concerned by this novel value of the input velocity profiles to be assumed. As an example, in Fig. 3.2.2A-10 the jet boiling margin as resulting from these last calculations is presented.

3.2.2A.2.4 Cavitation effect on the hydraulic stability.

The theoretical analyses of the cavitation risk in the jet indicate the opportunity to extend the cavitataion study to other target loop components, i.e. pump, flow straightener and nozzle. With respect to the pump, the present NPSH value is about twice the requested one, a fairly good safety margin; an experimental investigation of this parameter is envisaged anyway. This situation is illustrated in Fig. 3.2.2A-11. A flow straightener design solution also basing on cavitation criteria was developed by means of the code DIAFR, see Fig. 3.2.2A-12. This going to the nozzle, the minimum cavitation number, i.e. the maximum cavitation risk, was found to lie on the jet region near to the nozzle exit and opposite to the curved wall. Further analyses suggest the displacement of the attachment between the removeable backwall and the permanent target structure upstream of the nozzle internal region. The investigation of cavitation phenomena in the JAERI Water Experiment is suggested; some indications concerning with the dynamic similarity and noise detection technique (CASBA device) were also given.

3.2.2A.3 Future Directions

We should examine the thermal and/or hydraulic behaviors in the upstream reducer nozzle and the downstream quench tank. After the experimental and analytical examination with the water and Li target flows, we should design a nearly optimum target assembly.

References

[1] H. Nakamura et al., Proc. of NURETH-8 (1997) 1268.

[2] M. Ida et al., JAERI-Research 98-022 (1997).

[3] M. Ida et al., “Thermal and Fluid Analysis for the IFMIF Lithium Target Jet Flow,” Proc. of NURETH-*8*, Sept. 30-Oct. 4, 1997, p. 1276, Atomic Energy Society of Japan, (1997).

[4] S. Cevolani, “Thermal Hydraulics of Liquid Metal Jets”, Proc. of NURETH-8, Sept. 30-Oct. 4, NURETH-*8*, Sept. 30-Oct. 4, 1997, p. 1276, Atomic Energy Society of Japan, (1997). 1997, p.1284.

[5] M. Ida, et al., “Fluid Stability Analysis for IFMIF Target”, Proc. of AccApp-98, Sept.20-23, American Nuclear Society, [1998], to be published.

[6] FLOW-3D User’s Manual Ver.7.1, Flow Science Inc. (1997).

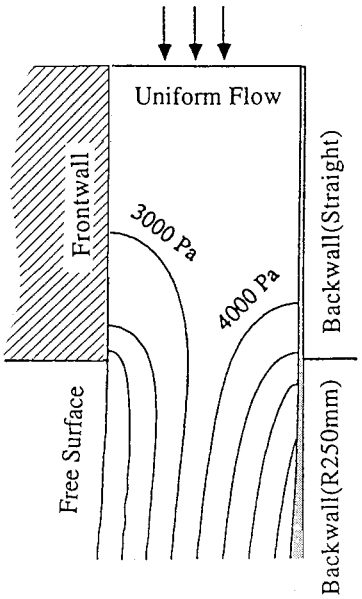

Fig. 3.2.2A-1: pressure distribution inside the Li-jet

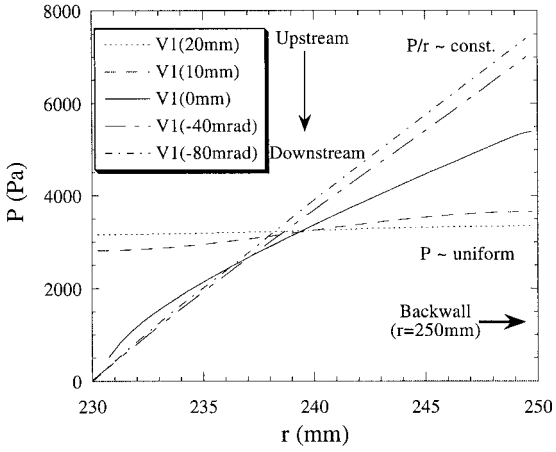

Fig. 3.2.2.A-2: Pressure transition

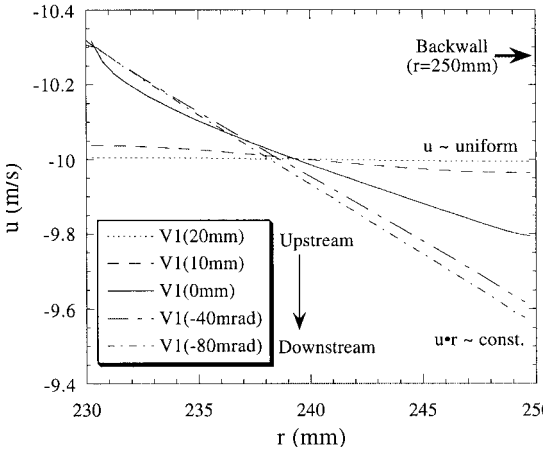

Fig. 3.2.2.A-3: Velocity transition

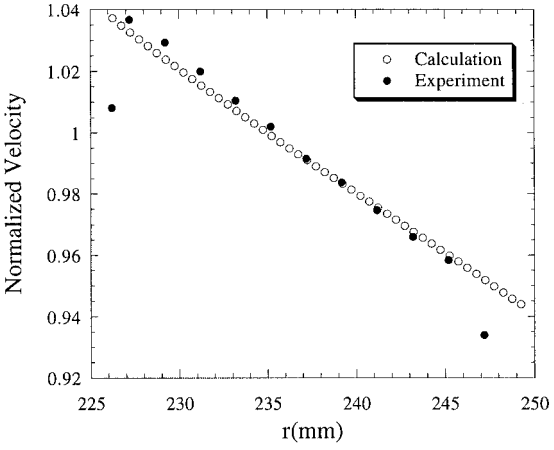

Fig. 3.2.2.A-4: Velocities at 49 mm below nozzle exit

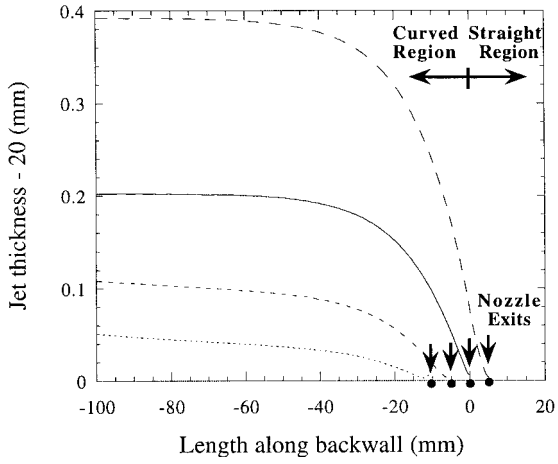

Fig. 3.2.2.A-5: Jet thickness

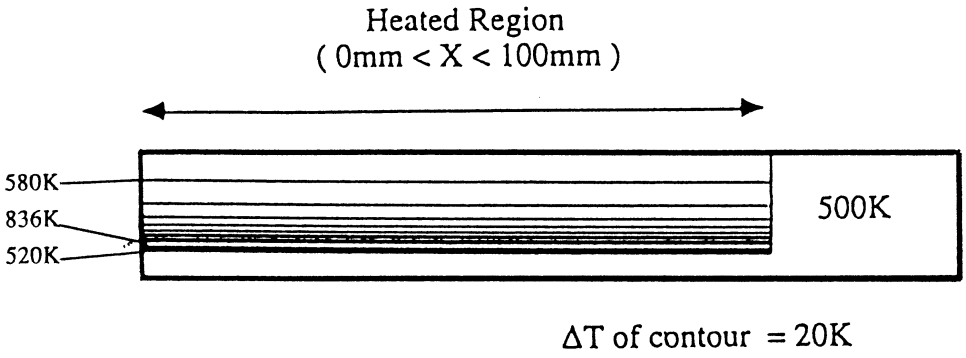

Fig. 3.2.2.A-6: Isotherms after irradiation

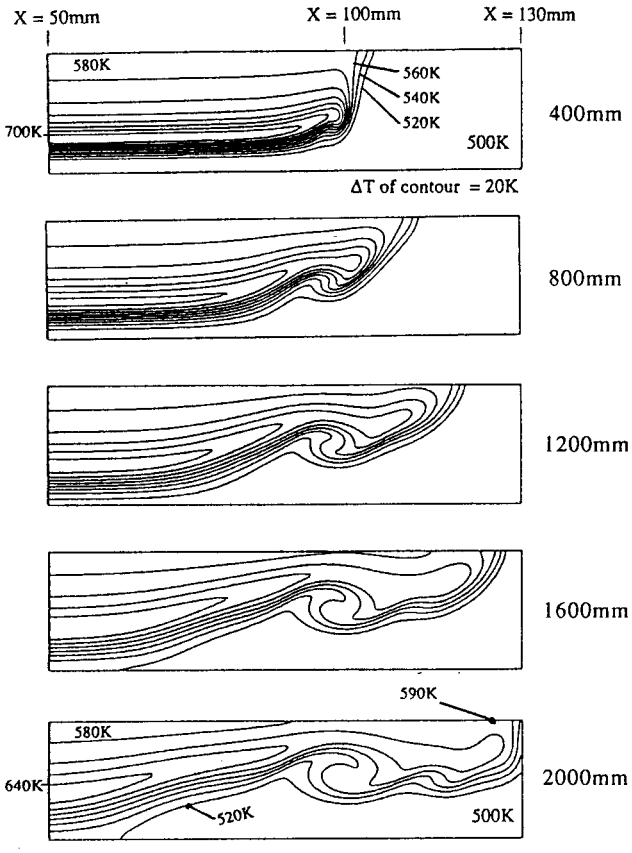

Fig. 3.2.2.A-7: Isotherms downstream (u = 10 m/s)

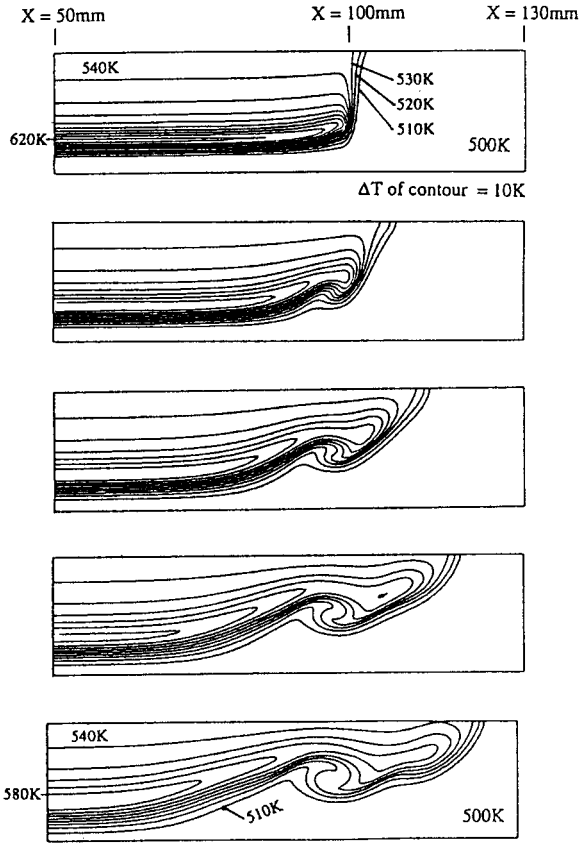

Fig. 3.2.2A-8 Isotherms at downstream (u = 20 m/s)

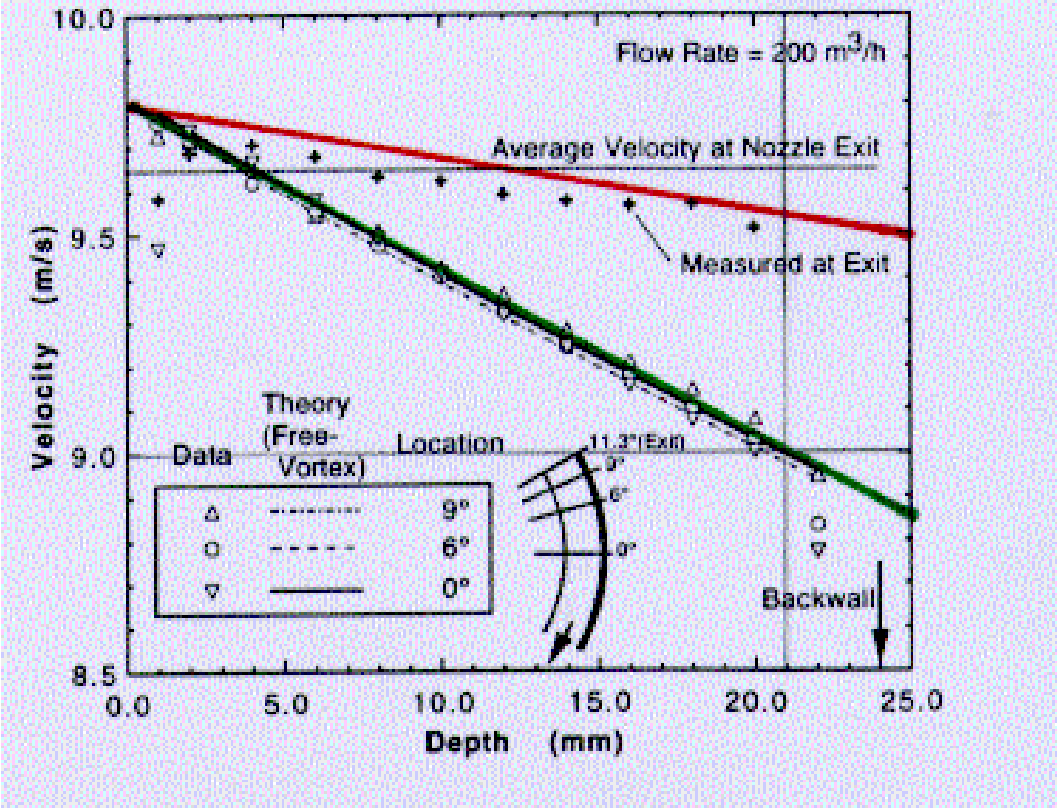

Fig. 3.2.2A-9: Experimental velocity profiles [1]

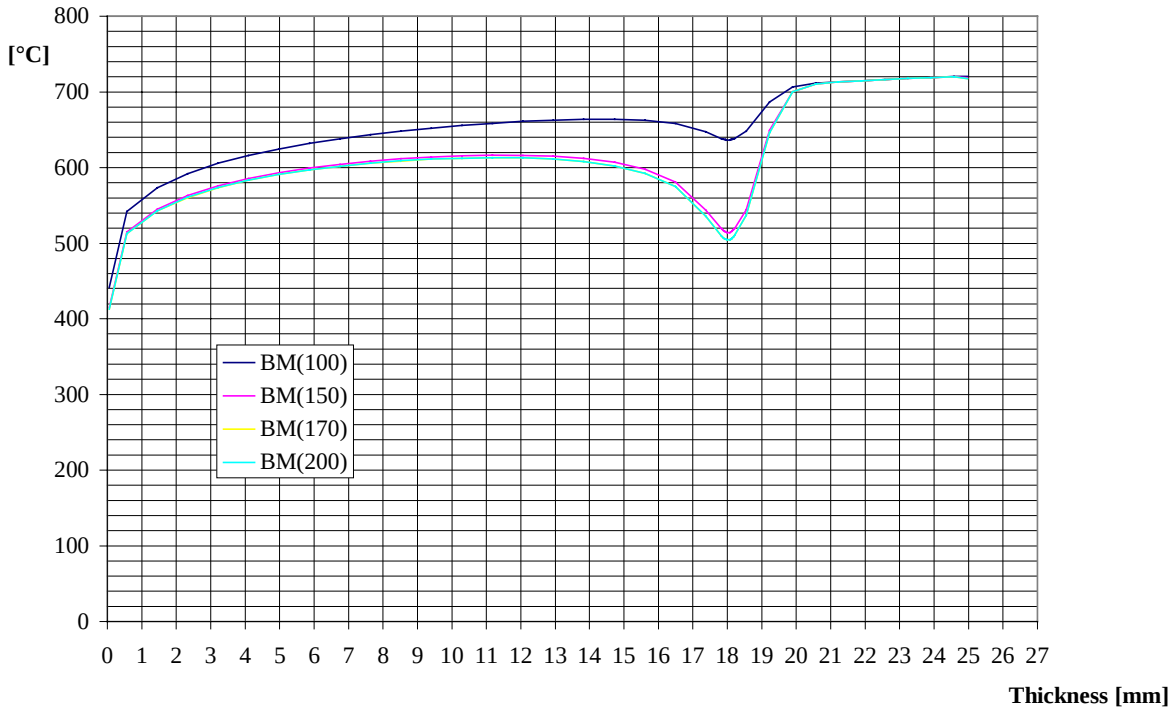

Fig. 3.2.2A-10: Boiling margin in the jet as resulting from the experimental velocity profile

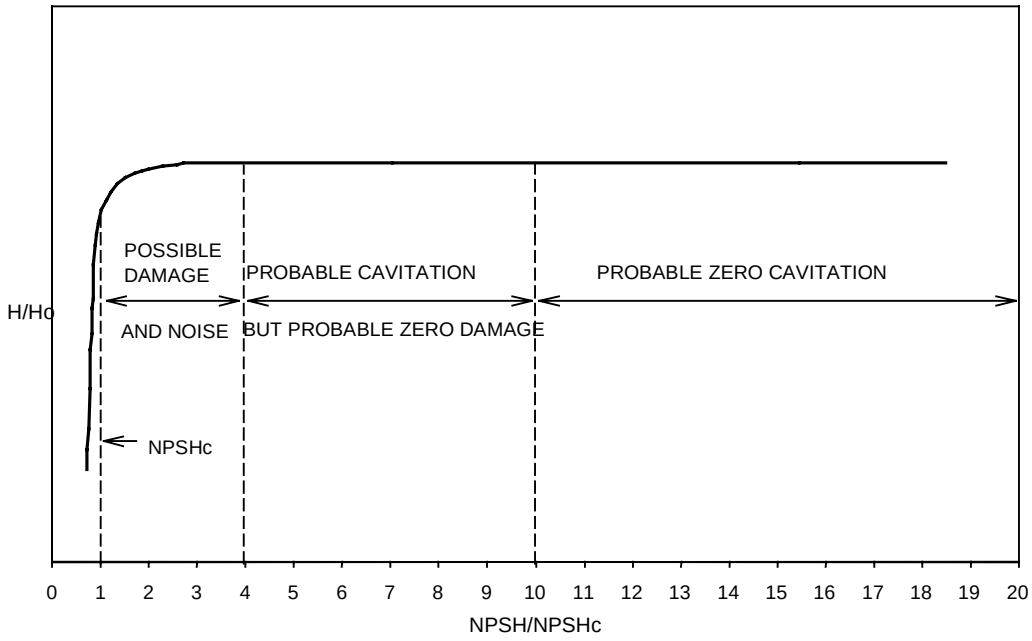

Fig. 3.2.2A-11: Pump normalized head versus NPSH ratio

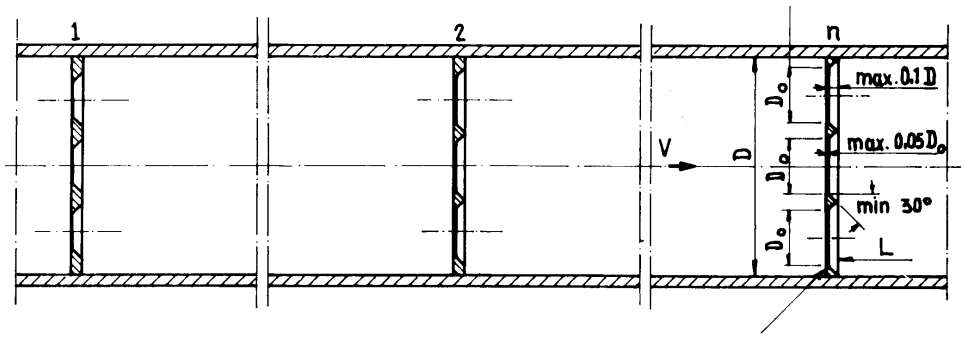

Fig. 3.2.2A-12: DIAFR sharp-edged orifice plates applied to straightener

3.2.2B Water Simulation Experiments

Description and justification

Flow simulation experiments using water have been performed in the IFMIF CDA to support the investigation of characteristics of high-temperature high-speed lithium target flows. In the CDA, a prototype-scale facility was prepared in JAERI by tentatively defining the design of components of the IFMIF target assembly; pipe (size), straightener, egg-crate matrix, reducer nozzle, downstream channel. The cross-sectional size of the water jet flow was 240 mm wide and 24 mm-thick. The FMIT results suggested that the reducer nozzle design is one of the key issues to realise the stable target flows. For the water simulation experiments, therefore, a two-dimensional double-reducer nozzle (Fig. 3.2.2.B-1) was newly proposed and facilitated. The experiments demonstrated that the nozzle successfully provides stable plate-like water jet flows on a concaved backwall with a radius of 250 mm according to the FMIT design. In this experiment, the simulated 130 mm-long target region was also tentatively defined before the definition of the CDA final guideline for the IFMIF target configuration [1].

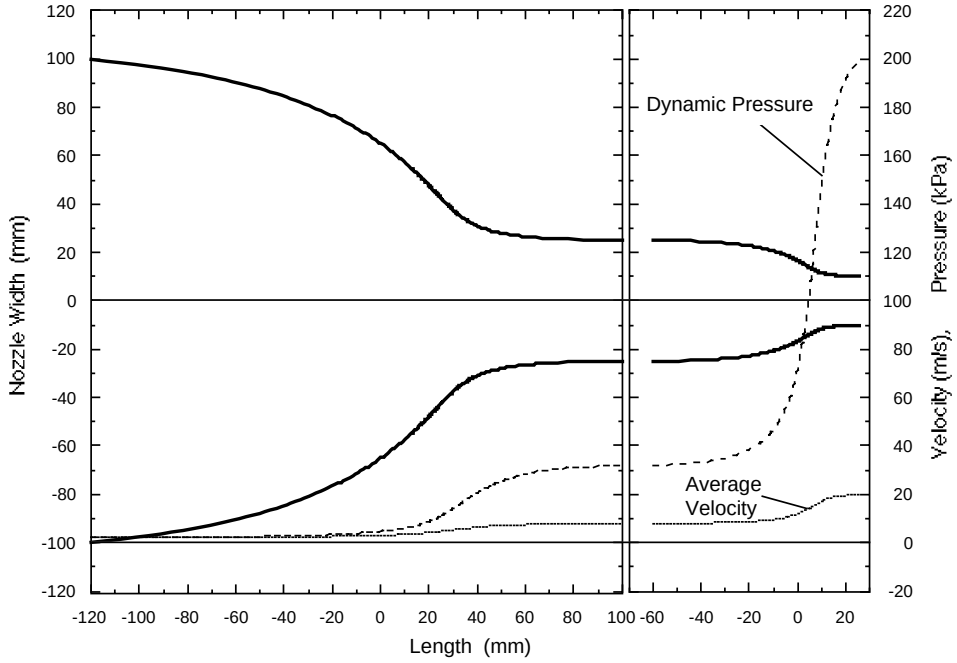

Fig. 2.2.2B-1: Double-reducer nozzle using the Shima converging nozzle equation (arbitrary for distance between reducers)

The experimental investigation coupled with analyses in the CDE attempted to clarify the detailed mechanisms of several phenomena which were observed previously, including the FMIT program and the IFMIF CDA, but were not completely clarified yet. Such phenomena include the depth-wise velocity profile in the target flow on a concave wall, characteristics and generating and growth mechanisms of interfacial waves, thickness change (distribution), practical influences of gas (air) in the water simulation experiments onto the interfacial wave conditions, etc. A new backwall design; the replaceable backwall as proposed in the CDA, posed a necessity to clarify the influence of singularities onto the target flows, which may happen at the connection of backwall plates.

A detailed characterization of the high-speed plate-like flow around the nozzle exit and on a backwall was attempted first by separately performing small-scale water experiments with a horizontal straight backwall. A small-sized double-reducer nozzle was applied to obtain water jet flows (100 mm wide and 10 mm thick). Characteristics of interfacial waves and mechanisms of the generation and growth of the interfacial waves are being investigated. The flow responses at such singularities, such as step and/or gap on the backwall and mechanisms to cause cavitation at such singularities and the nozzle exit end (tip) under low-pressure (vacuum) conditions are investigated further. These are necessary to predict the target lithium flow response in vacuum and to design an optimized replaceable backwall geometry by predicting the flow response in case of the replaced backwall causing such singularities on the backwall etc.

Measurement of parameter such as multi-dimensional velocity profiles is one of advantages of performing the water simulation experiments, because it is difficult to obtain such information from a lithium flow which is opaque to visible light and electrically conductive. The measured data form a database to validate the numerical analyses including multi-dimensional analyses to reveal overall characteristics of the IFMIF lithium target flow under operation (beam irradiation). High-temperature lithium flow experiments, however, are necessary to confirm the predictive results obtained through these water simulation experiments and numerical analyses, to define and validate practical target conditions and a configuration suitable for a long-term operation and to develop a measurement instrumentation specific to the lithium flow monitoring.

Contributors

Organization	Principal Investigator
JAERI	H. Nakamura, Y. Kato
Nagoya University	K. Ito, Y. Kukita

Main responsibility: JAERI

Milestones

1) Construction of small-scale test facility	March 1997
2) Experiments for characterization of interfacial waves	March 1998
3) Experiments for singularities and low-pressure conditions	November 1998
4) Documentation (incl. analyses of experimental results)	December 1998

3.2.2B.1 Impact on CDA

There are no findings which are contradictory to the target (assembly) design approved in the CDA. The obtained results increased the knowledge on the characteristics of target flows and supported the target (assembly) design approved and proposed in the CDA. Note that a two-dimensional double-reducer nozzle proposed in the CDA water simulation experiments (Fig. 1) was dealt with as a proven component in the CDE experiments to provide for stable high-velocity plate-like flows. Detailed measurements in the CDE water simulation experiments newly posed the issue of requesting liquid lithium flow experiments to confirm the interfacial wave conditions of the target flows. No experimental effort has ever been performed to validate the free jet option.

3.2.2B.2 Results and Conclusions

Depth-wise Velocity Profile in Target Flows on Concaved Backwall

In the CDA experiments, detailed velocity distributions around the nozzle exit were measured for the first time through experiments under the FMIT and IFMIF programs. In the CDE, multi-dimensional analyses based on the CDA results revealed the flow structure around the nozzle exit [2]. The concave wall connected to the reducer nozzle was found to provide an non-rotational free-vortex-like velocity distribution in the target flow because of a depth-wise static pressure distribution which is formed by a centrifugal force. Consequently, target flow is accelerated on the free-surface side and decelerated on the backwall side to have a “slanted” velocity profile (Fig. 2) specific to such flow geometry. This velocity profile is preferable to decrease the free-surface temperature and, thus, to improve the vacuum in the target assembly during the operation.

Interfacial Wave Characterization

The interfacial wave characterization experiments using the small-scale facility have been successful in tracing a time variation of the jet thickness, thus wave form, using a newly developed optical method with a fast-response two-dimensional light spot sensor (Fig. 3) [3]. The wave amplitudes were obtained by integration of the slope angle data increased monotonically along the flow axis in the measured range (up to 6 cm from the nozzle exit) as shown in Fig. 4, except for a peak near the nozzle exit, where the wave form was typically two-dimensional. The influence of air on the wave growth in the experiment has not been identified yet, but will be investigated in the “low-pressure” experiments.

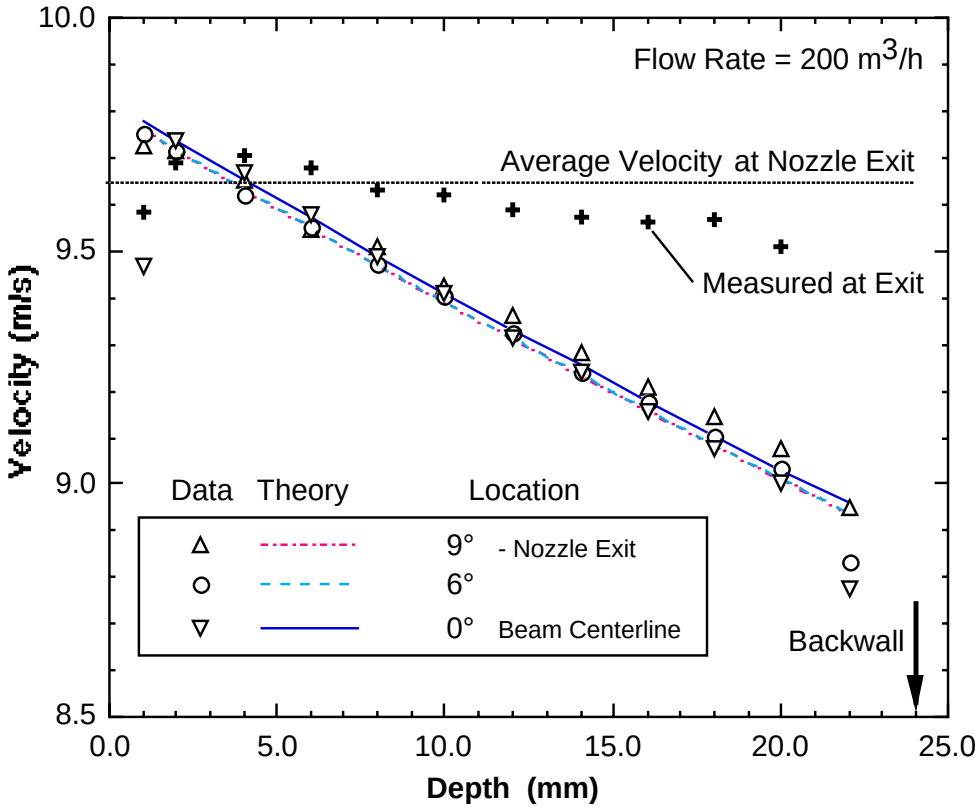

Fig. 3.2.2B-2: Depth-wise velocity distributions in simulated target flow

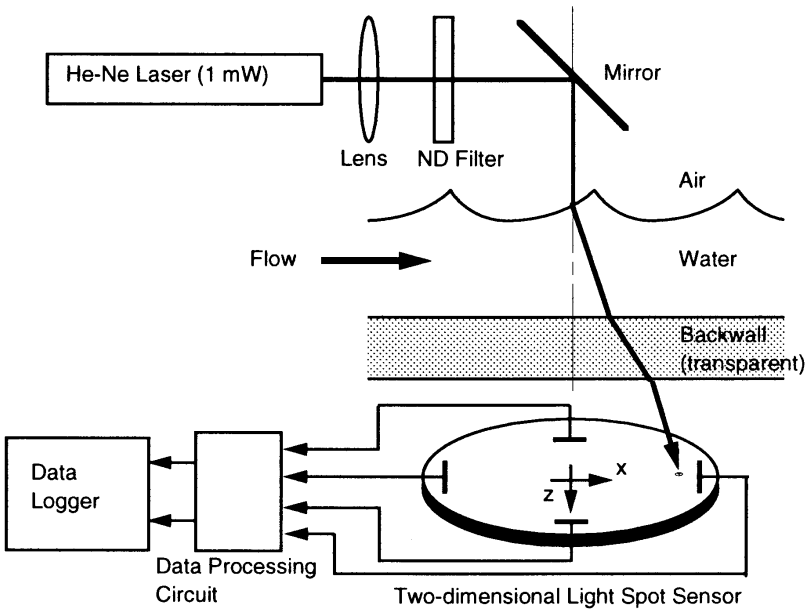

Fig. 3.2.2B-3: Measurement setup of local slope angle of fluctuating free surface

In the same experiments [3], the velocity distribution around the nozzle exit was measured in detail using a laser Doppler velocimeter (LDV) especially on the free-surface side. The measured velocity distribution for the boundary layer indicated that the boundary layer has been relaminarized in the nozzle. However, the characteristic of the velocity distribution was found to change from “laminar” to “turbulent” when the average velocity was increased as shown in Fig. 5. This phenomenon seems to be in accordance with the experimental observation that a smooth

free-surface region between the nozzle end and two- and three-dimensional wave region becomes short and vanishes when the average velocity was increased. If the interfacial wave condition is mainly controlled by such turbulence condition beneath the free surface, the flow simulation for the interfacial wave condition based on the Weber number would collapse. The lithium flow experiment is thus indispensable to clarify such an important question, although the measurement of a detailed velocity profile is difficult.

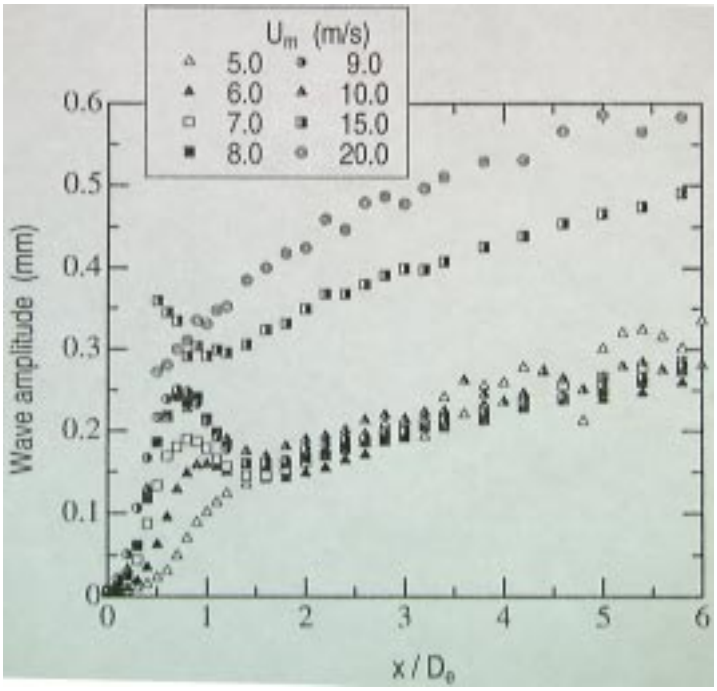

Fig. 3.2.2B-4: R.M.S. wave amplitudes of thickness fluctuation

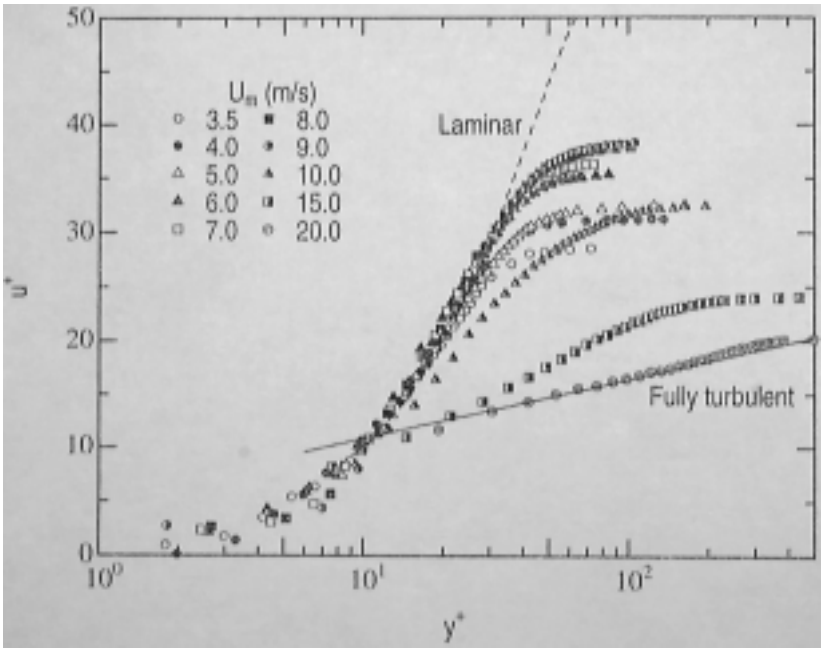

Fig. 3.2.2B-5: Velocity distributions in the boundary layer at the nozzle exit (free-surface side)

3.2.2B.3 Future Directions

Water Simulation Experiments:

1) Perform experiments which have not been finished completely by the end of the CDE, especially for the "low-pressure" and "singularity" experiments.
2) Investigate influences of a long and thus large-radius backwall in the CDA design on the flow stability.
3) Investigate downstream channel (drain slope) flow response especially around the liquid level in the quench tank. Splashing and disintegration of the jet flow should be avoided because such phenomena may lead to uncovery of high-temperature core in the target flow to vacuum.
4) Investigate issues found during the multi-dimensional analyses and Li experiments.

Lithium Flow Experiments

There are many issues to clarify and develop, such as,

1) Erosion of target assembly components by flowing Li, such as internal structure of flow straightener, reducer nozzle, backwall and downstream channel.
2) Interfacial structure (ripples etc.) of target flow free-surface.
3) Development of measurement instruments for such parameters such as jet thickness distribution, interfacial roughness and velocity, and distortion of target assembly.
4) Influence of interfacial roughness on Li evaporation rate.

Experience should be gained through the various kinds of Li flow experiments for the above issues.

References

[1] H. Nakamura, K. Ito, Y. Kukita, M. Ida, Y. Kato and H. Maekawa, "Water Experiment of High-Speed, Free-Surface, Plane Jet Along Concave Wall," Proc. of NURETH-8, vol. 3 (1997) 1268-1275.

[2] H. Nakamura, K. Ito, Y. Kukita, M. Ida, Y. Kato, H. Maekawa and H. Katsuta, "Experimental and Analytical Studies on High-Sped Plane Jet along Concave Wall simulating IFMIF Li Target," Proc. of ICFRM-8 (1997) 256, to be printed in J. of Nucl. Materials.

[3] K. Ito, Y. Tsuji, H. Nakamura, Y. Kukita, "Free Surface Waves on High Speed Water jet Simulating Liquid Metal Target," Fusion Technology (submitted, 1998).

3.2.2C Transient Thermal Analysis of the Target Lithium Loop

Description and justification:

The IFMIF target loop consists of the primary Li-loop, of secondary organic oil and tertiary water loops. Every loop, especially the Li loop, should be controlled to keep the temperature constant. Especially in the primary lithium loop, temperature changes may cause instability of flow. A source of potential instabilities are D^+ beam fluctuations. To clarify the thermal response of the Li loop after beam(s) failure, the thermal transient analysis has been performed using a modified RETRAN[1], which is originally a reactor transient computer code dealing with water.

Contributors*:*

Organization	Principal Investigator
JAERI	M. Ida, H. Nakamura, Y. Kato

Main responsibility : JAERI

Milestones:

1) Analysis of the thermal response for the primary loop	Jul.	1998
2) Analysis of thermal response for the secondary and tertiary loops	Nov.	1998
3) Documentation	Dec.	1998

3.2.2C.1 Impact on CDA

Analysis of thermal response for the target loops has been performed with a modified computer code to handle Li, organic oil and water. It will contribute to the control procedure of the loops.

3.2.2C.2 Results & Conclusions

The code RETRAN was modified to deal with the ical properties of Li. With the modified code, one-dimensional transient thermal analysis was performed for the primary loop of the F target shown in Fig. 3.2.2C-1. The failures of one and two beam(s) were supposed. No change in the temperature of second loop was also supposed. The results obtained can be summarized as follows.

As shown in Figs. 3.2.2C-2, Li temperatures would become uniform near the temperature corresponding to that of secondary loop 220 °C within several minutes after two beams failure. As shown in Fig. 3.2.2C-3, the hotter and colder Li temperatures would become about 252 °C and 235 °C respectively, also within several minutes after one beam failure.

3.2.2C.3 Future Directions

The thermal response of the secondary and tertiary loops should be examined. After the examination, we should design a shutdown or control procedure of those loops in case of long and short-period of beam(s) failure.

References

[1] RETRAN-02 Manuals, EPRI.

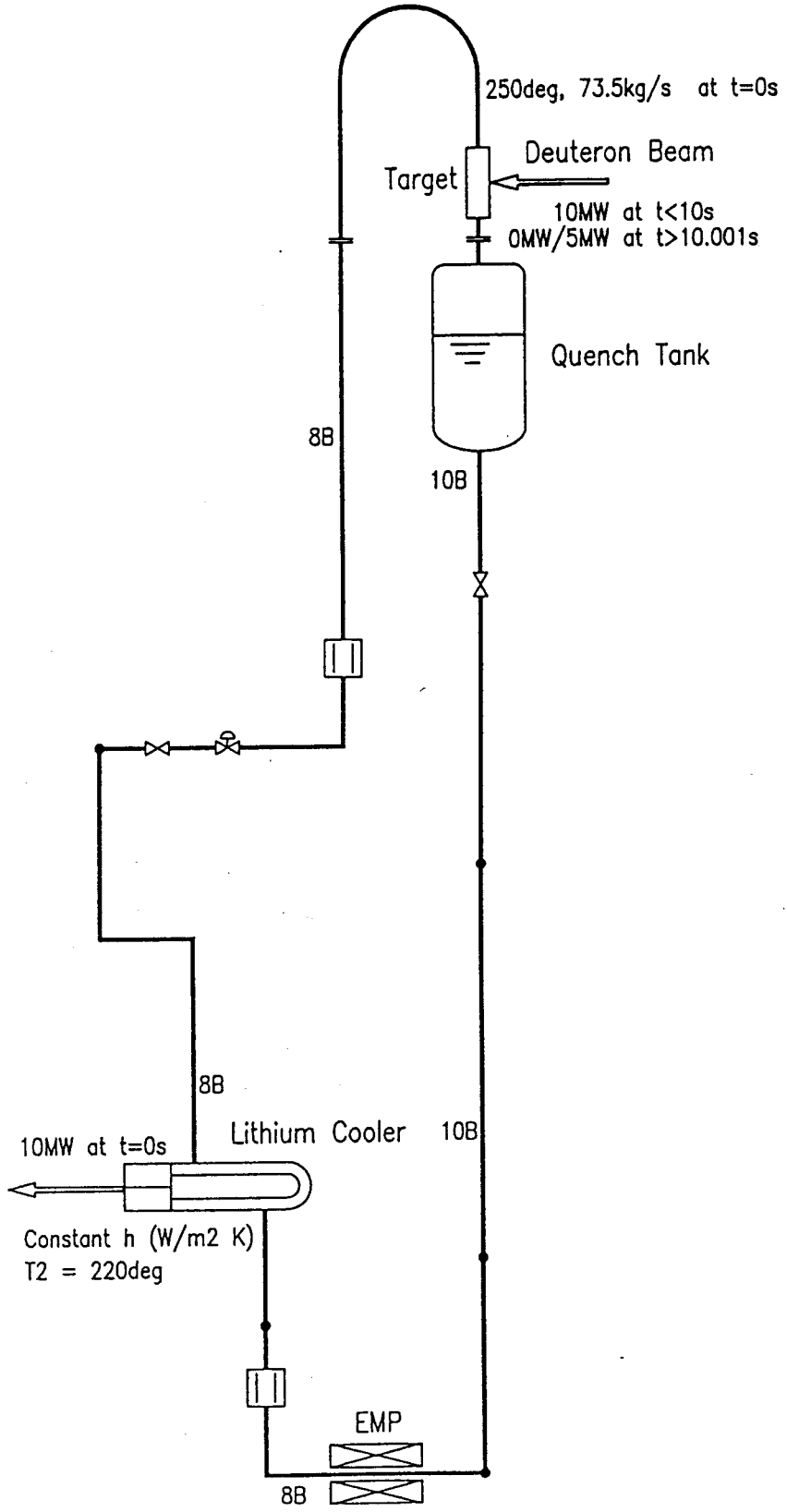

Fig. 3.2.2C-1 Calculation model

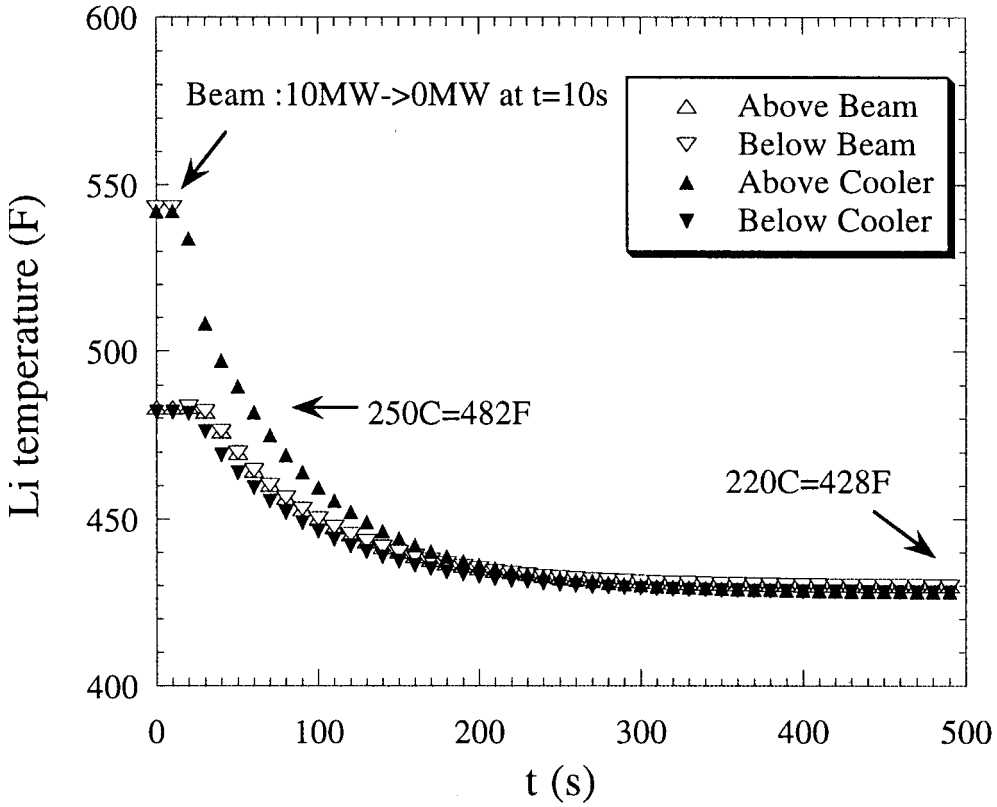

Fig. 3.2.2C-2: Temperature transition (two beams failure simultaneously)

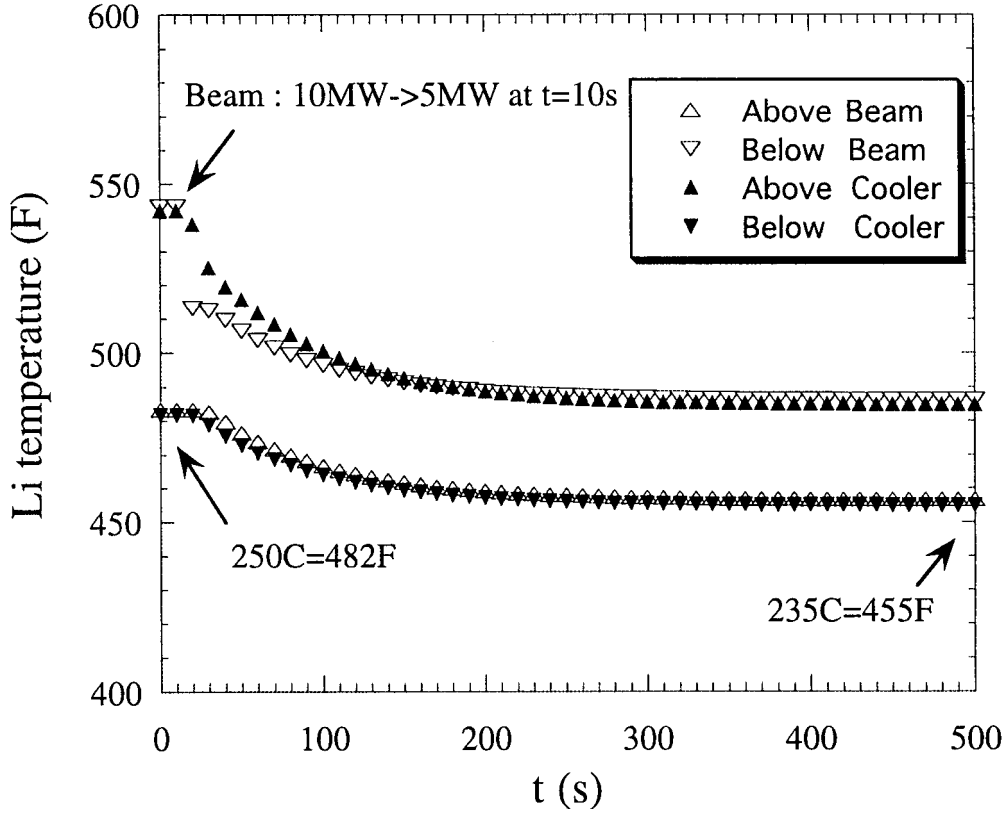

Fig. 3.2.2C-3: Temperature transition (one beams failure)

3.2.3 LITHIUM SAFETY

Description and justification:

An "integrated" safety analysis methodology has been developed in order to identify and quantify the specific events that could occur during the lithium loop operation and could cause environmental hazards. This methodology includes:

- Safety analysis of lithium target system and its support systems: this analysis has already been carried out with FMEA (Failure Mode and Effect Analysis) to identify the relevant target related hazards and the major initiating events of accident sequences;
- Dependent failure analysis, which has been finalized to investigate all failures that could increase the unavailability of a function;
- Accident sequence analysis, which has been fulfilled to identify and quantify the accident sequences that could occur during normal plant operation: this activity has been carried out by typical methods of the Probabilistic Risk Assessment (PRA) used for nuclear power plants.

The analysis has been carried out based on the detailed conceptual design of the target assembly and loop systems reported in ref.[1].

Contributors:

Organization	Principal Investigator
ENEA Bologna	F. Bianchi, L. Burgazzi
JAERI	M. Konishi, H. Takeuchi

Main responsibility: ENEA

Milestones:

1) Validation of CDA Analysis	April 1997
2) Dependent Failure Analysis	Sept. 1997
3) Accident Sequence Analysis	May 1998
4) Documentation	Dec. 1998

3.2.3.1 Impact on CDA

The foregoing detailed safety analysis confirms what was pointed out in the CDA phase: potential target related hazards due to tritium production and lithium operation are very low because IFMIF target facilities have been designed both to reduce the accident probability and, at the same time, to eliminate any subsequent release to the environment.

3.2.3.2 Results and Conclusions

3.2.3.2.1 Safety Analysis

The evaluation of possible hazards has been performed at component level for the target facilities and related areas using the Failure Mode and Effect Analysis (FMEA). This technique, which allows to detail systematically all possible failure modes of each subsystem and to identify

their resulting effects on the system, has been considered the most suitable to provide the safety-related information and consideration in the conceptual design phase because it can be extended to a more detailed analysis in the later phases of the project. The hazard analysis, oriented towards detailing on a component-by-component basis all possible failure modes of components and identifying their effects on the lithium target system, has been performed referring to a detailed flow diagram shown in Figure 3.2.3-2 and is reported in ref.[2]. As outcome of the foregoing analysis, the following potential environment, safety and health hazards associated with the IFMIF target lithium system operation are identified together with the relative engineered safeguards aimed at preventing the onset of accidents and mitigating the consequences.

Lithium Loop Hazard

The IFMIF lithium system contains approximately 21,000 litres of liquid lithium. Lithium is an alkali metal and the lightest and least reactive of the alkali metal family. The melting point is 180.6°C. Solid Li does not burn spontaneously in air, but liquid Li is (very) reactive with air, water, concrete, carbon dioxide and nitrogen. Lithium fire is also accompanied by the release of tritium and Be-7 in the forms of lithium aerosols.

Therefore lithium leaks, resulting in a possible lithium fire through lithium/air reactions, must be assumed during the loop lifetime because of possible environmental hazards, although design, construction, material and operation requirements make this event very unlikely.
Due to radiation concerns, personal access to the lithium cells is prohibited during operation, therefore manual fire extinguishing may not be timely and effective for preventing the propagation following an initial fire. Consequently the IFMIF policy requires the lithium loop system to be designed to guarantee no combustion of lithium in the event of a lithium leak. At present this is achieved by the use of a multiple confinement of lithium carrying components combined with an oxygen monitored and controlled argon atmosphere. The primary confinement is the lithium carrying components, such as pipes, tanks, heat exchanger, hot and cold traps. A simple sheet metal structure, referred to as a guard vessel, surrounding the primary confinement constitutes the secondary confinement and the space between the primary and secondary confinement is filled with an argon gas which is circulated at a low flow rate for impurity monitoring and control; besides in the guard vessel a contact type leak detector is installed so that the Li leakage can be detected early. The tertiary confinement is the lithium cell which is air-tight and maintained under an argon atmosphere at a slight positive pressure. It is equipped with oxygen meters to monitor the oxygen concentration. The floor and the walls are covered with a steel liner to prevent lithium concrete reactions. Finally, the atmosphere in the annulus portion outside the argon boundary is dry air at a lower pressure. Any lithium spill that fails to be contained within the secondary confinement will immediately freeze and never ignite. The multiple confinement concept is illustrated in Fig. 3.2.3-1.

Radioactive Materials

The two most radioactive materials related to the target system are tritium and beryllium-7. IFMIF will produce approximately 10 grams/year of tritium. Under normal operating conditions, a few grams (3-5 grams) of this tritium are confined in the loop components and the remainder of the tritium is being accumulated in the cold or hot trap. It is anticipated that cold trapping would reduce the circulating concentration of Be-7 by two orders of magnitude so that under normal operating conditions the cold trap would contain most of the inventory of Be-7.

Although radioactive materials are a potential hazard for the environment in case of an accident, IFMIF facilities have been designed both to reduce the accident probability and, at the same time, to eliminate any subsequent release to the environment.

Radioactive Wastes

The radioactive waste generated by the target facilities consists of solid, liquid and gaseous waste. Solid waste includes: (1) the replaceable backwall which is designed for annual

replacement; (2) the target assembly which is replaced once every 10 years and (3) the cold trap replaced annually. Liquid wastes are composed of the liquid solvents utilised for the backwall replacement operation. Gaseous wastes consist of the small amount of tritium present in vacuum exhaust of the target chamber. The amount of waste of the target system is summarised in ref.[1].

3.2.3.2.2 Dependent Failure Analysis

The types of dependencies to be examined are the following:

- Sequence Functional Dependencies, which consider the effects of the status of one system or safety function on the success or failure of another. These dependencies are explicitly accounted for in the event tree analysis.
- Inter-System Dependencies, which include the effects of support systems and other systems on the front line systems. In this phase of the IFMIF conceptual design, these dependencies are not modelled in the system fault trees. Also Inter-System Dependencies due to common cause failures are not included in the system fault trees.
- Inter-Component Dependencies, also called common cause failures, due to shared root causes of failures. Only common cause failure relative to valves and circuit breakers have been assumed and these dependencies have been explicitly accounted for in the fault trees analysis.

Moreover a qualitative screening analysis within each system and among different redundant systems performing the same function is performed in order to identify group of components that are considered to have some potential for failure due to the same cause. The components identified for a detailed common-cause failure analysis are:

- Instrumentation and control components;
- Valves;
- Electrical components (circuit breakers, etc) and mechanical components (blower, etc.)
- Dependencies due to human actions, such as incorrect calibration of sensors or instruments, or a diagnostic error which might affect the manual actuation of redundant systems. These dependencies are not explicitly modelled as separate events in the fault trees.

3.2.3.2.2 Accident Sequence Analysis

A preliminary analysis, from the probabilistic point of view, of some accident sequences concerning the target facilities and the support/interfacing systems has been performed in order to assess the probability or the frequency of those major accidents that can lead to the damage of the target facilities and the IFMIF plant and, as an extreme consequence, can cause environmental hazard. The analysis is developed on the basis of the flow diagram of the lithium loop system (Fig. 3.2.3-2) and other plant information included in ref.[1].

Methodology and calculation tool

The methodology and the calculation tool adopted are the fault tree and event tree technique, widely utilised in the PRA (Probabilistic Risk Assessment) studies, and theb RISK SPECTRUM code, a PC software package for system risk and reliability analysis. Fault tree analysis and event tree analysis are two of the most versatile methods in assessing the system safety and are of great help in reducing the risk, improving the reliability or increasing the availability in systems and processes. In RISK SPECTRUM code (ref.[3]) the fault trees and event trees are built with the component reliability model, the component reliability data are assigned and the final risk assessment is quantified through the analysis of combinations of fault trees and event trees.

The accident sequence scenarios are modelled through the event trees: a certain initiating event can initiate different chains of events with many alternative consequences. The initiating events of the accident sequences are chosen from the results of the FMEA analysis, which, because of their accident evolution, can affect the target facility and consequently the whole

experimental plant: they concern either the arget facility cooling loops only or the conventional facilities, e.g. the electrical power distribution system and the vacuum system.

In the typical accident scenarios there are safety systems that must operate if an accident occurs . If the first system could fail there are usually other systems that can prevent a serious accident: each scenario corresponds to a certain combination of failed or functioning systems. The safety systems that have the function of stopping the accident sequence evolution and mitigating the consequences are the fast beam interrupt system and the fast beam isolation system for the beam-target interface and the emergency equipment, like diesel generators and backup batteries, for the electrical power.

Each sequence in an event tree represents a certain combination of events; in some cases each event can be represented by an individual event, while in many other cases the events correspond to failures of complex systems, i.e. to the top event of a fault tree. The initiating events considered in this study are limited to internal initiators, that could occur during normal operation of the target system. The following event initiators are analysed (ref.[4]):

- Loss of electrical power
- Loos of vacuum
- Loss of lithium flow
- Loss of secondary cooling loop
- Loss of water cooling loop
- Loss of cold trap cooling loop
- Loss of electrical power to the target

Results

The results (ref. [4]) indicate that the probabilities of occurrence of the accident sequences leading to the backwall rupture as most severe consequence are very low.

The backwall rupture frequencies of different initiators are presented in Table 3.2.3-1 together with the total failure frequency, 3.0E-9/year which is a negligible value; Table 3.2.3-1 shows that the major contribution to the backwall rupture is due to the loss of lithium flow accident.

Table 3.2.3-1: Overall backwall rupture results

INITIATOR	INITIATOR PROBABILITY	BACKWALL RUPTURE FREQUENCY (1/year)	%
Loss of lithium flow	2.8E-2	2.8E-9	93
Loss of secondary cooling loop	9.7E-4	9.7E-11	3
Loss of water cooling loop	9.7E-4	9.7E-11	3
Loss of electrical power to the Target	3.7E-3	1.4E-11	1
	TOTAL	3.0E-9	

3.2.3.3 Future Directions

As two major hazards relevant to the target system the FMEA identifies the tritium accumulation in the lithium loop and the risk related to the liquid lithium loop operation. These results are reflected in the design and operation procedures: as regards the former safety issue, majority of the tritium is removed by trapping, while for the latter one the lithium loop is contained in a multiple enclosure with inert atmosphere in order to eliminate lithium fire risk.

The preliminary dependent failure analysis stresses that with the present design of the electrical power distribution system a failure of electrical power supply of the target system can defeat the redundancy or diversity.

With relation to the probabilistic evaluation of the accident sequences concerning the target facilities and the support/interfacing systems, the sequences of each event tree that can harm the plant with a potential hazard to the environment are analysed and quantified with the methods of the fault trees and event trees.[5]

The results obtained from the probabilistic evaluation indicate that the frequencies/probabilities of occurrence of the most dangerous accident sequences, i.e. involving the backwall rupture, are negligible.

Due to the uncertainties in the definition of the systems at this stage of the design the results must be considered to be of preliminary nature: thus, a more detailed design level is recommended for a subsequent analysis review (this is particularly relevant as far as the dependent failure analysis and the accident sequence analysis are concerned).

References

[1] IFMIF CDA TEAM, International Fusion Materials Irradiation Facility Conceptual Design Activity, RT/ERG/FUS/96/11.

[2] F. Bianchi et al. “Safety Analysis of IFMIF Target Facility System: Updating of FMEA”, doc. ENEA-CT-FBB-00005, December 1996.

[3] U. Berg, L. Sardh, “RISK SPECTRUM User’s Manual Version 2.12”, Relcon Teknik, April 1994.

[4] F. Bianchi et al. “Safety Analysis of IFMIF Target Facility System: System analysis”, doc. ENEA-CT-FBB-00006, March 1997

[5] L. Burgazzi , et al., “IFMIF Target Safety Concepts and Analysis”, Proc. of AccApp-98, Sept.20-23, American Nuclear Society, [1998], to be published.

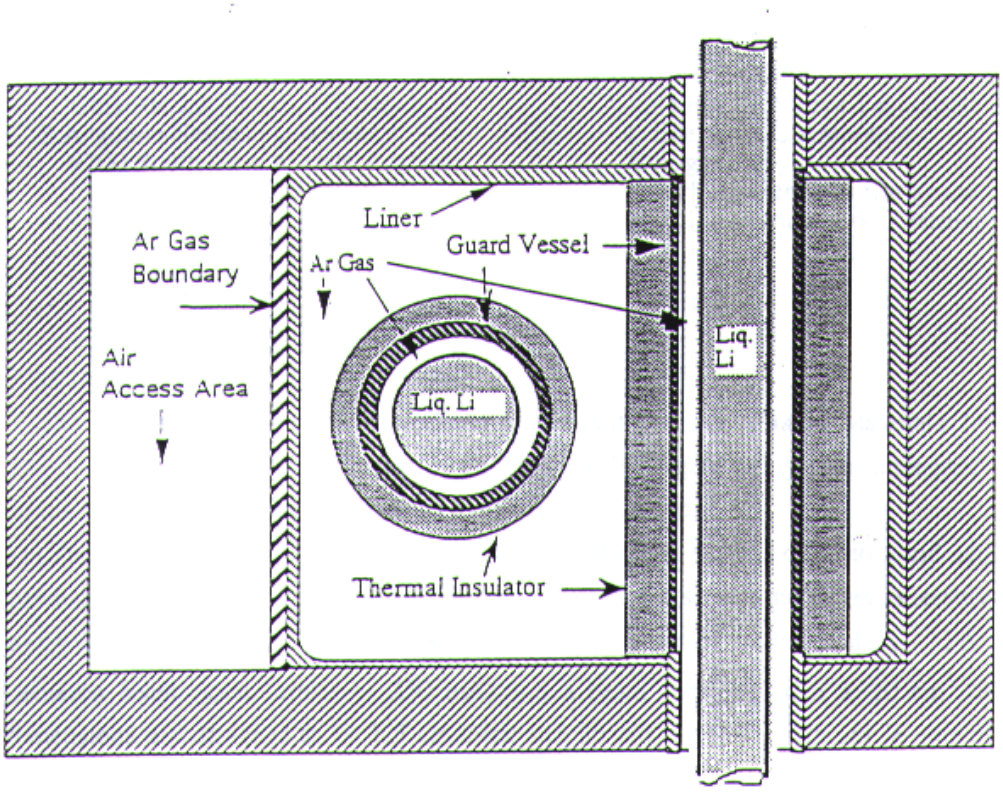

Fig. 3.2.3-1: Multiple confinement concept

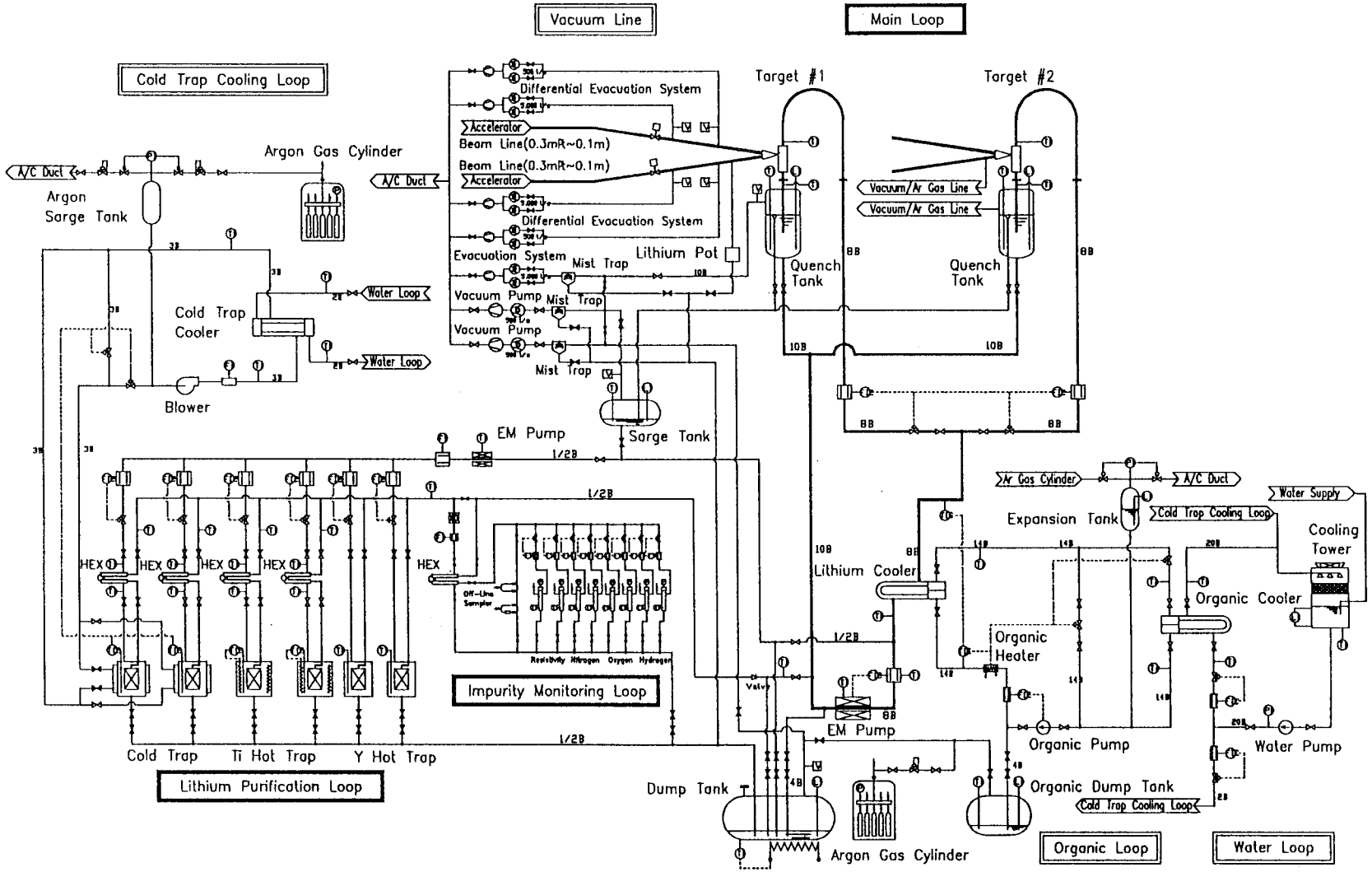

Fig. 3.2.3-2: Flow Diagram of Lithium Loop Facility

3.2.4 Lithium Purification and On-line Monitor

3.2.1.1 Description and justification:

The major impurity product expected, in terms of quantity, is the deuterium deposited in the lithium jet by the beam. Among the deuteron-lithium nuclear reaction products, tritium and beryllium (Be-7) are the most noteworthy elements for radiological safety. These elements as well as oxygen and carbon, are removed from the main lithium loop by the cold trap. As an option for the system, a hot trap with an yttrium getter is also considered for tritium removal.

Nitrogen and some corrosion products in lithium are removed by a hot trap with a titanium getter. A high nitrogen concentration has a potential to increase the corrosion rate on the construction materials and may build up from air contamination during repair or exchange of the components and adhesion to component surfaces. Carbon can build up from

HX tube leakage. The design process for the cold trap is similar to the case for sodium and the technology has been well established. It appears to be more practical to remove tritium by the swamping method of cold trapping than with a hot trap which has not yet been put into practice of hydrogen isotopes. A basic evaluation for the swamping method used to control the tritium level with a cold trap is provided.

Contributors

Organization	Principal Investigator	
Japan	Y. Kato, S. Konishi, H. Katsuta	(JAERI)
	Y. Kukita, et.al.	(IHI)
US	T. Hua	(ANL)
	L. Green	(Westinghouse)

Main responsibility: JAERI

Milestones:

1) Validation of CDA design	Aug. 1997
2) Analysis of the swamping method	Oct. 1997
3) Documentation	Dec. 1998

3.2.4.1 Impact on CDA

A promising result is obtained for the removal of tritium from the primary lithium loop by an analysis of the swamping method.

It was recognized in the CDA that the item "Lithium Purification and On-line Monitor" should have a high priority to make lithium loop the future R&D.

The evaluation of this item again drew attention to the fabrication of the impurity-test lithium loop.

3.2.4.2 Results and Conclusions

By the hydrogen swamping method, the tritium inventory in the IFMIF primary lithium loop can be kept at about 3g . Other impurities will also be controlled within about 20ppm by a cold trap and a hot trap.

In the IFMIF target facility, the control of the concentration of tritium and beryllium is especially important for the safety. Considerable design experience has been gained from the use of this equipment in sodium and lithium facilities but the experiments for hydrogen isotopes with swamping and beryllium trapping are very few. Hence, it is important to obtain these experimental data with a basic lithium loop. Most of the impurity monitoring devices require

more basic study and developing efforts.

Production rate of the main impurity elements

Tritium is produced by direct reactions of the beam with the lithium, as well as by the capture of low energy backscattered neutrons by Li-6. Total tritium production rate is estimated to be about 10 g/y. The tritium inventory has to be minimized in the system, since this could be the dominant source term in the event of a radiological release. Tritium is removed by the cold trap with protium sparging, the so called swamping method, or, as an option, by a hot trap with an yttrium getter. Using one of these methods, the total tritium inventory in the circulating lithium in the loop will be kept to about 3 grams.

The most highly radioactive impurity is expected to be Be-7, (half-life: 53-d, decay γ: 0.48 MeV) produced from (d, n) and (d, 2n) reactions with lithium. If not removed, this product will build up to a saturated activity of about 4.5×10^{15} Bq. The Be will exist as a chemical form Be_3N_2 in the lithium and the solubility of Be_3N_2 is about 0.5 appb at 500K. The cold trap will remove the ^7Be, and its equilibrium concentration in the loop will be kept at 1 appb. However, some of Be-7 is expected to deposit around the loop, and is very likely to limit the remote handling operations.

At the initial lithium charge, about 0.84 kg of oxygen impurity is expected to come from the surface contamination of the loop components. During maintenance (4 times per year), about 1.2 kg/y (=0.3 kg/y x 4) will be absorbed by the lithium.

Also during maintenance, about 4 kg /y (=1 kg/y x 4) of nitrogen will be absorbed by the lithium.

The effect of different hydrogen isotopes on the cold trap performance is neglected. The solubility of hydrogen in lithium at 473 K, the operation temperature of the cold trap in the IFMIF target system, is about 440 appm (= 63 wppm). In the initial operation of the target lithium system, the impurity level of hydrogen is estimated to be about 105 appm (= 15 wppm) or so, if the system is constructed under good management conditions. When the beam is turned on, the hydrogen isotope will increase to 440 appm from 105 appm with no effect of the cold trap. The production rate for all hydrogen isotope by the d-Li reaction is about 0.159 appm/day as shown in Table 3.2.4-1.

Table 3.2.4-1 Production rate of hydrogen isotopes

	Type of isotope		Weight	Concentration
	/deuteron	(atom/s)	(g/day)	(appm/day)
H	0.06	9.36×10^{6}	1.34×10^{-2}	8.76×10^{-3}
D	1	1.56×10^{18}	4.47×10^{-1}	1.46×10^{-1}
T	0.03	4.68×10^{16}	2.03×10^{-2}	4.42×10^{-3}
Total		1.70×10^{18}	4.81×10^{-1}	1.59×10^{-1}

Swamping method

The swamping method is expected to decrease the tritium in the lithium system. Before the beam on target operation, hydrogen is injected into the lithium until its concentration reaches 440 appm. The results of the analysis for the hydrogen isotopes concentration C(t) and tritium concentration CT(t) are shown in Fig. 3.2.4-1 and Fig. 3.2.4-2.[1]

From Fig.3.4.1, it is clear that even for the case of M =5 appm, where M is the hydrogen injection (swamping) rate, C(t) is lower than the saturation solubility (=1365 appm) for hydrogen at 523 K which is the minimum operating temperature of the lithium main loop. All the curves are saturated within about 10 days after cold trap operation. Also from Fig. 3.4.2, it

requires about 3 appm / day for M to restrict tritium to about 3 g (= 0.65 appm) in the main lithium loop.

Impurity monitoring system

The following impurity detectors are planned to be set up in the IFMIF impurity monitoring sub-system. Most of them are required to make R&D by real lithium loop experiments in the next CDA phase.

1. Hydrogen meter

The concentration of hydrogen isotopes in lithium is detected by measuring their partial gas pressure which comes through a Niobium (Nb) or Nb-Zr membrane. To distinguish the isotopes from the other, a quadruple mass spectrometer will be installed.

2. Oxygen meter

The detector of an yttrium doped solid electrolyte cell of ThO2 has been developed for a sodium system. The corresponding detector of this type will be developed for the lithium system. The compatibility with the liquid lithium remains to be confirmed.

3. Nitrogen meter

This is the electrochemical device applying a molten-salt electrolyte cell. As a molten salt, the LiCl-LiF-Li_3N system will be promising, but further study will be required for development.

4. Electroresistivity meter

Electrical conductivity measurement of lithium will be available to detect the high level nitrogen concentration in lithium. R&D is required to determine the feasibility.

5. Off-line sampling system

This is a lithium sampling system to analyze impurity elements in the off-line analytical chemistry system. A practical remote-operation system should be developed.

3.2.4.3 Future Directions

A lithium loop of appropriate scale should be constructed and the basic studies for impurities control by the cold trap and the hot trap should be made. Also the impurity monitoring device or system should be developed for this loop.

Reference

[1] Y. Kato et al., "Impurity Control in Liquid Lithium Loop for IFMIF Target Facility", *J. of Nucl. Mater.*, to be published.

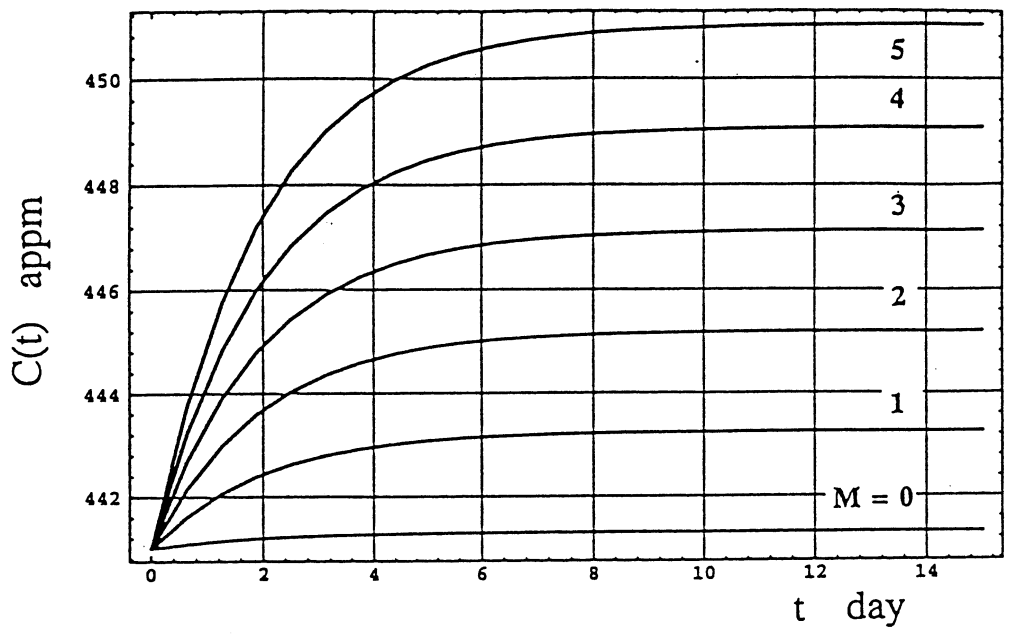

Fig. 3.4-1: Concentration of hydrogen isotopes, C(t).

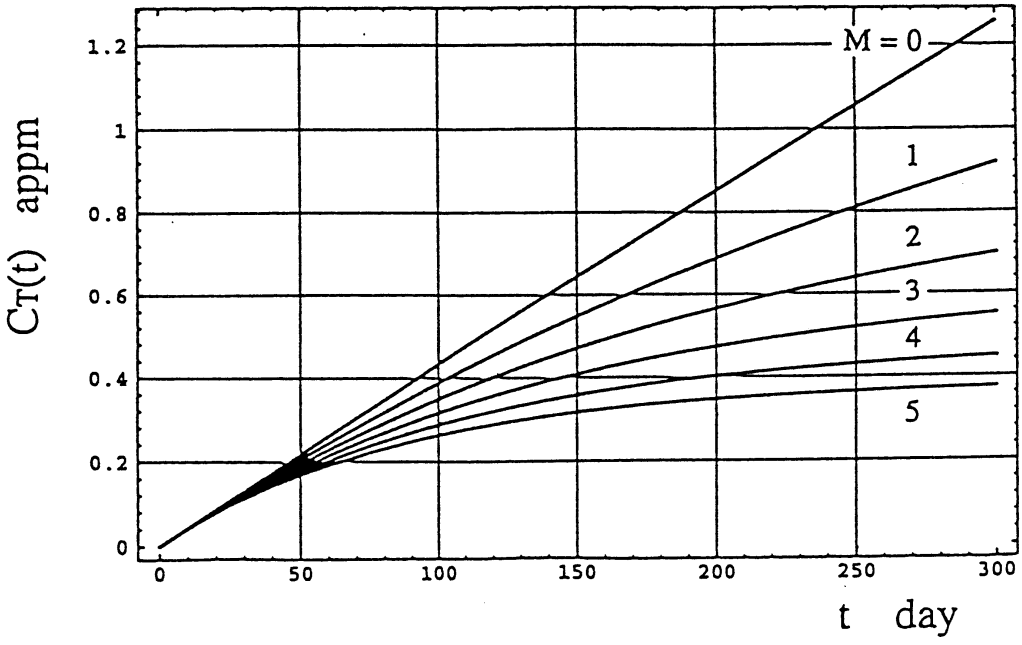

Fig. 3.2.4-2 Tritium Concentration, $C_T(t)$.

4. ACCELERATOR FACILITIES

4.1 INTRODUCTION

The International Fusion Materials Irradiation Facility (IFMIF) requires generation, by a linear accelerator (linac), of 250 mA continuous current of deuterons at a nominal energy of 35 MeV, with provision for operation at 30 MeV and 40 MeV. Our basic approach is to provide two linac modules, each delivering 125 mA to a common target. This approach has availability and operational flexibility advantages. The deuterons are stripped in a molten lithium target, producing a neutron energy spectrum representative of a fusion device. The deuteron current and energy requirements involve 10 MW of continuous beam power. An additional several megawatts is involved in rf efficiency of the amplifiers and accelerating cavities. The rf system is a major part of the accelerator.

In 1978~1985, a Fusion Materials Irradiation Test (FMIT) facility was carried to final design, with a requirement for 100 mA at 40 MeV, or 4 MW of beam power. On this project, prototyping was completed to 2 MeV and about 50 mA. The Los Alamos Meson Physics Facility proton linac has operated for many years at 1 mA average current to 800 MeV. Other projects now in progress include Accelerator Production of Tritium, for which a 100 mA cw proton linac prototype to ~10 MeV is under construction. The technology base for making the required extension to an IFMIF is well in hand, but it is clear that the engineering must be done very carefully, especially in view of a further requirement ñ to insure a plant availability factor of 70% over the projected operating life of this materials R&D factory.

The accelerators begin with a deuteron ion source and a low-energy beam transport to a radiofrequency quadrupole (RFQ) buncher and preaccelerator up to ~8 MeV. For the main accelerating structure from ~8ñ40 MeV, two different technologies are under consideration; normal-conducting accelerating structures made from copper, or super-conducting niobium structures. Determining which is the better approach is a complex question involving physics, engineering, cost, and availability aspects. A high-energy beam transport from the accelerator to the lithium target must perform a variety of functions, complicated by the presence of strong space-charge forces within the beam. Very low beam losses along the accelerator and transport lines is required in order that maintenance can be performed without requiring remote manipulators.

Conceptual design activities during the CDA/CDE phases placed primary emphasis on identifying and defining all interface issues between the accelerator facility and the target, test cell and conventional facilities. Conceptual design work internal to the accelerator facilities emphasized system choices for the basic technology selections, for example the ongoing development of appropriate ion source, low-energy beam transport, extended RFQ preaccelerator, normal-conducting vs. superconducting technology for the drift-tube-linac, and a high-energy beam transport system with beam density distribution tailoring. Fundamental study on the mechanisms and design implications for very low beam loss was accomplished.

4.2 CDE TASKS

4.2.1 RF System Development and Test

Description and Justification:

Development and testing of a 1 MW rf system is identified as the highest impact development item in terms of both cost and RAM. Existing operating experience with amplifiers appropriate to the IFMIF frequency of 175 Mhz is with pulses of a few seconds to order a minute of cw operation, at frequencies generally lower (easier) than the IFMIF frequency. A frequencies a factor of two or more higher, klystrons are used to achieve high duty-factor and cw operation. A gap has existed in commercial tube availability for the IFMIF frequency range. Detailed costs to design, construct, and test the first rf station are available in the extensive costing information developed for the Tokai CDA meeting, so a reliable cost estimate for this task is in hand. A test stand capable of 1 MW tests to 100-1000 hours may be available in France or Russia.

The rf amplifier power level baseline of 1 MW and the defined CDE program have important advantages. The 1 MW power level insures that a competitive bid could be obtained from two manufacturers. Accomplishing a full-scale test of the first system would allow the remaining large procurement to be on a fixed-price basis. The involvement of two manufacturers would help insure a tube supply over the facility lifetime.

A major subtask of this activity is the development and test of the 175 MHz coaxial rf window. A lifetime test of 100 hours at full 1 MW cw power into a resistive load with availability of 95% or better is defined as the design confirmation goal.

Further details are available in JAERI-memo 08-173, August 1996.

Contributors:

This activity should proceed on a contractual basis with the two tube manufacturers and with the test stand facility, assuming one is available. Task supervision would be provided by the IFMIF Accelerator Team, probably with participation by each of the member parties, because of the high importance and interest in this activity.

Organization	Principal Investigator
US; task leader	R. Jameson, US Industry Team
Russia, test stand	V. Teplyakov
France, test stand	J-M. Lagniel with Thomson Tubes

4.2.1.1 Impact on CDA

The CDA design assumes that a 1 MW rf system is available commercially. As the cost of accelerator system is strongly dependent of the rf system cost, the continuous development of the rf system is necessary to keep a design margin and cut down the total cost.

4.2.1.2 Results and Conclusions:

No resources were available for this task. However, very good news has been received from Thomson Tubes, who have reported 1 MW cw operation of a 200 MHz diacrode amplifier for one hour. This scales to an even better result at 175 MHz (frequency to 5/2 power). Acceptance tests for LANL (200†MHz), including a 24†hours ìheat run testî, have demonstrated the compliance of this TH628 diacrode with LANL specification. During the 24†hours test, the diacrode has been succesfully operated with 600†kW mean power (pulsed operation with 20% duty cycle, 3.0†MW peak power, 2.27†ms ñ 88†Hz). Therefore, our first priority task has almost been demonstrated. Our specification was a cw test at 1 MW for 100 hours. Thomson could make the 100 hour test for us and have provided a cost estimate.

Future Directions:

- Thomson could make the 100 hour test for us and have provided a cost estimate.
- RF window development and design/test of rf field control for the RFQ and room-temperature and superconducting drift-tube-linacs are high priority tasks.

4.2.2 Injector System Development and Test

Description and Justification:

The injector system has the second highest impact in terms of reaching the required performance and RAM goals for IFMIF. Two technical approaches (the ECR and volume type ion sources) are to be developed, because present status precludes a decision between them, and because substantial ongoing efforts mainly supported by other programs can, with IFMIF augmentation, be expected to progress to a decision point.

Contributors:

Organization		Principal Investigator
EU	CEA Saclay	J.M. Lagniel
	IAPUniv.Frankfurt	H. Klein
JAERI		M. Sugimoto
US		US Industry Team

4.2.2.1 Impact on CDA

Verification of the required basic performance of ion source is critical for assessment of the conceptual design.

4.2.2.2 Results and Conclusions:

Reported progress includes IFMIF relevant work supported by other projects: In the EU and US, IFMIF funding was not available for experimental work during the CDE. Some relevant experimental results were obtained from other projects, including:

(i) The IAP Frankfurt volume type source was experimentally studied using a deuteron beam. A maximum current density of 210 mA/cm^2 has been achieved, and so far 80 mA deuteron current has been measured using an extraction hole with a diameter of 8 mm. A 200 mA cw 94% proton beam (corresponds by scaling to 140 mA deuterons) was extracted in July 1998 from the IAP Frankfurt AMFIS source in cw operation. The extracted current density is 390 mA/cm^2 and the noise level is less than 1%. In parallel, tests of an ion aource with an rf antenna plasma drive are in progress.

(ii) In December 1997, a 126 mA cw proton beam was extracted from the SILHI ECR source at CEA-Saclay through a 10 mm diameter extraction aperture. With the appropriate

conditions,a plasma density J = 213 mA/cm^2 can be achieved, which is close to the requirement for the IFMIF source. LEBT performance was also shown to be well suited to IFMIF. The CEA-Saclay SILHI source has been operated for 100†hours with 96% availability (99% after a conditioning period of 20 hours).

(iii) The LANL ECR proton ion source was operated at ~100 mA for 170 hours with 96% availability.

(iv) In Japan, proton ion source tests are being conducted, concentrating on LaB_6 filaments in comparison to tungsten filaments. The volume source with a long-life filament, LaB6 cathode assembly model, developed at KEK, is under development at JAERI. A performance test using a proton beam was carried out in 1997 at the ion source test stand of the JAERI proton linac laboratory and the result was excellent in comparison with the conventional tungsten filament [1]. The arc efficiency was about 30mA/kW and higher than the case in which the tungsten filament was used. The normalized 90 % emittance was 0.6 π mm mrad and was equivalent to the case of the tungsten. Continuous mode operation was not achieved due to the over-current of arc discharge. The heat spot in the cathode was observed after the test, and it is suspected that the cathode assembly size was too big compared with the plasma volume. An arc discharge test using deuteron gas with the optimized size of cathode assembly is scheduled in the first quarter of 1998, using the Fusion Neutron Source ion source [2].

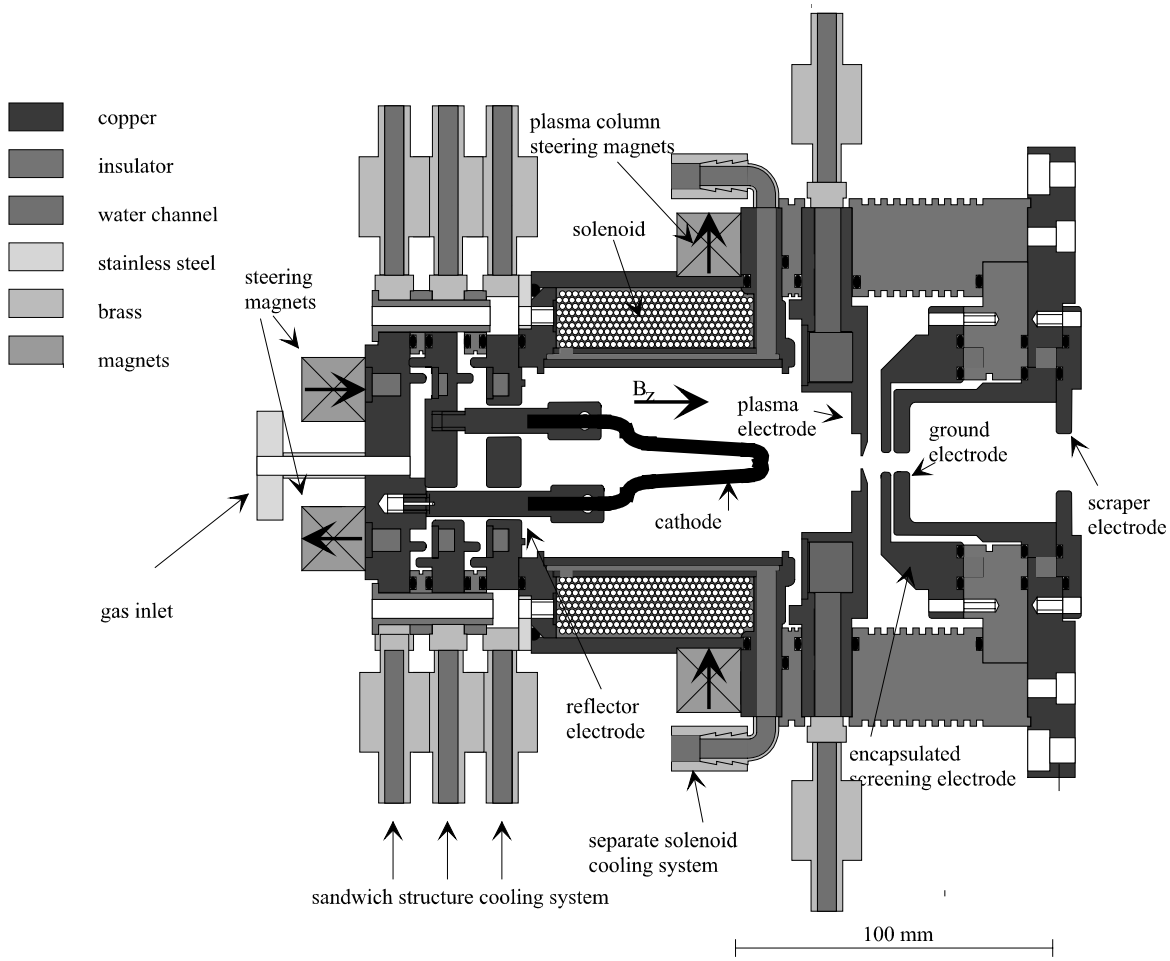

Fig. 4.2.2.1 The Frankfurt volume ion source.

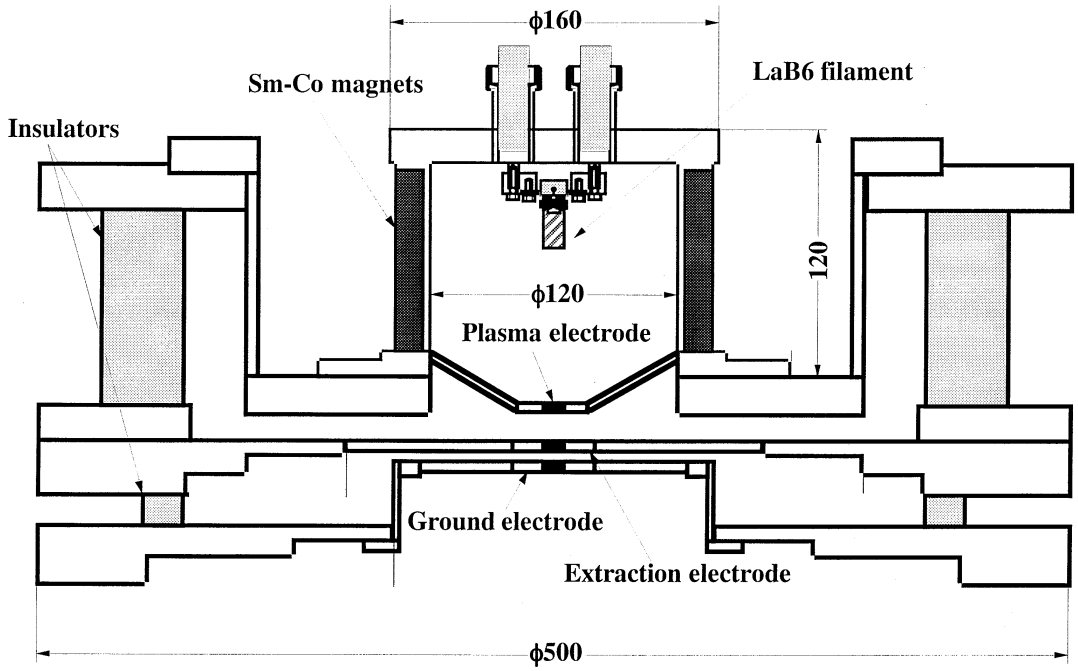

Fig. 4.2.2.2: Schematic of JAERI Fast Neutron Source deuteron volume source assembled with LaB6 filament.

(i) In order to compare different methods of plasma generation, theoretical considerations on an rf-drive were carried out. These will be used when direct comparisons between rf- and arc-discharge operated sources are made on parameters such as lifetime, noise, emittance, etc.
(ii) Neutron production in the ion source and RFQ area was investigated theoretically. At present, the theoretical estimations of neutron and gamma radiation do not correspond with the measurements carried out on the prototype test stand.
(iii) Electrostatic LEBT calculations and experiments show good results for perveances up to 60% of the design value; further work is aimed at understanding the potential of this type of LEBT at the full space charge of the IFMIF design.
(iv) Further calculations, simulations and measurement have been accomplished on aspects of neutralization phenomena in the magnetically-focused LEBT [3-6]. This kind of LEBT seems to be favorable.
(v) Preparations for improved shielding and licensing of the IAP deuteron test stand continued.

4.2.2.3 Future Directions:

The full IFMIF task still requires a full operational test producing a deuteron beam from at least one of the ion source candidates, coupled to the low-energy-beam-transport. The initial goal is full cw operation meeting all the technical and RAM specifications for a period of 100 hours. The second goal would be operation for 1000 hours.

For the volume source, high-duty mode operation using the LaB6 cathode should be established under the condition of the deuteron plasma similar to that obtained by the tungsten filament. Deuteron beam extraction tests will be made to prove that the beam quality is preserved during the lifetime of the cathode. Further improvement of the fraction of desired species is necessary to meet the requirement.

Table 4.2.2.1 Status of ion source development for Neutron Science Research Program

Ion Source Type	Volume; LaB6 cathode-driven
Institute	JAERI
Date of Test	Dec. 1996 (emittance) ; Jun. 1997 (lifetime)
Test data:	
Ion	Proton
Extracted beam voltage	100 kV
Measured beam current	140 mA (at min. emittance)
Current measurement method	HVPS current
Calibration method	HVPS - external register
Beam Noise, %	not measured
Duty Factor, %	10 % (1 ms, 100 Hz)
Duration of Test	hours
Breakdown Frequency	2/h
Cause of breakdown	HV column instability
Fraction of desired species	80 %
Method of species fraction measurement	Doppler shift spectroscopy & dipole magnet
Measured emittance,normalized, rms	0.15 π mm mrad
Idem, 90 %	0.7 π mm mrad
Emittance measurement method	Double slit scan
Location of measurement	1 m downstream from source
Extraction aperture:	
# of apertures	1
Aperture radius, mm	5
Arc current	100 A
Arc voltage	60 V
Rf frequency, MHz	n/a
Rf drive power, W	n/a
Cathode power, W	
Gas pressure, mT	0.75
Gas flow, sccm	4
Solenoid: # of	1 (between source and emittance measurement device), 1 (before RFQ)
Other	adjustable intermediate electrode; High-duty operation is prohibited due to arc over current (cathode size is too large)

4.2.3 All Other Conceptual Design Activity

Description and Justification:

There are many other tasks necessary to reach a stage where productive preliminary design activity can start. An overall category for these detailed design tasks is maintaining beam loss and activation low enough that remote handling is not necessary. The tasks involve detailed design of the accelerator beam transport from ion source to target, fundamental investigations to gain understanding of the loss mechanisms, coordination with neutronics calculations and shielding design, engineering design of the accelerator, and so on.

Fundamental work in beam dynamics and beam halo studies are required in concert with detailed computer simulations. Mechanical engineering support will be required throughout. Improved RAM analysis and cost estimates of the more detailed design will be required, and technical coordination of these closely-coupled activities is essential.

Contributors:

Organization	Principal Investigator
US	R. Jameson, US Industry Team
EU	H. Klein, J.M. Lagniel
Japan	M. Sugimoto
Russia	V. Teplyakov, B. Bondarev
JAERI	M. Sugimoto

4.2.3.1 Impact on CDA

The full accelerator design, from injector to HEBT will be refined to verify that the stringent design requirement on the beam loss will be met. This effort is strongly supported by fundamental studies of beam matching methods, beam halo development and the effects of beam loading. The detailed transport simulations with a high precision using on the order of 10^6 macro-particles should be followed. A current-independent match between the RFQ and DTL or SCL will be sought to remove one cause of beam halo. Beam loading and RF transient effects will be assessed for the RFQ and DTL or SCL.

4.2.3.2 Results and Conclusions:

CDE work is reported below. IFMIF benefited substantially from work being done on other projects; some of this work is also included in the outline.

The 1997 CDE IFMIF Accelerator Team Meeting was held 26-30 May 1997, in Paris under the sponsorship of Saclay. The proceedings have been published as CEA Saclay Report No. CEA-DSM-GECA 97/54. In addition to the principal IFMIF partner institutes, participants from KEK, Japan and POSTECH, South Korea were invited to join the discussions of RFQ simulation. Numerous questions and team communications related to these codes had resulted in the decision to devote a large part of the meeting to this subject. Intense discussion was held on all aspects of the RFQ particle dynamics, on the simple fast code versions well-suited to optimization problems, and on source code details of the commercial MRTI RFQ codes (LIDOS.RFQ). The meeting and subsequent work have resolved the questions satisfactorily, and more detailed design studies are in progress.

After this meeting, the IFMIF Executive Committee was asked about the possibility for recognizing future collaborative effort with the South Korean group. This was warmly answered in the affirmative. South Korea will soon become a member of the IEA, and then could become full members of the IFMIF team as well. Pending this, they are welcomed as participants in the IFMIF endeavor.

Work in the US included:

(i) A technical report covering issues of RFQ simulation was completed [7]. Work continued on various detailed aspects of the RFQ design, including the role of equipartitioning and possible ways to use the RFQ to prepare an optimal beam for injection into the DTL.

(ii) An Operations and Reliability Development Activity was performed [8]. This preliminary report describes the interim results of a review of operations and reliability of existing accelerator facilities. During the International Fusion Materials Irradiation Facility (IFMIF) Conceptual Development Activity performed in 1995-1996, it was found that although accelerators have been in use for over 50 years, reliability data for accelerator components such as ion sources, focusing magnets and their power supplies, rf windows, circulators, drift tubes, etc., has not been collected. Thus, even though it is possible to develop models for analysis of accelerator reliability and maintainability using the standard reliability tools, the necessary supporting failure rate and repair time information is not available. Therefore, this effort was undertaken to collect data, review the literature, identify and visit a number of accelerator facilities to review their experience and accumulated information.

The Los Alamos Neutron Science Center (LANSCE) is an accelerator facility with enough operating history to supply meaningful reliability data. A companion paper [9] describes the data collection and analysis effort of the LANSCE accelerator operational data which was initiated to supply the accelerator reliability models with credible input data. A preliminary database of beam trips was assembled using operational data records, Central Control Room Logbook, and Operations Shift Supervisors Summary Reports covering 1996-97. The events were classified according to the underlying cause into categories corresponding to typical accelerator subsystems. Mean Time Between Failures (MTBF) and Mean Down Time (MDT) estimates were obtained for magnets, RF stations, power supplies, etc. For the components considered, both MTBF and MDT were found shorter than expected. The results are useful for identifying development issues in high power accelerators.

Continuous and highly reliable operation has been established as a basic design criterion for IFMIF. Specifically, the overall requirement for IFMIF calls for an average 70% on-line availability performance, corresponding to 6132 hours in a calendar year of 8760 hours. To assist in achieving this goal, a comprehensive RAMI model for all the subsystems of the IFMIF facility, including the twin accelerators, test cell, target, conventional facilities, and central instrumentation and control has been developed. This model generates an allocation of the availability requirements to all the major components of the subsystems. The modeling approach, major assumptions, and the principal results are described in a second companion paper [10].

Work continued on various detailed aspects of the RFQ design, including the role of equi-partitioning and possible ways to use the RFQ to prepare an optimal beam for injection into the DTL.

Work in Japan included:

(i) Estimates of deuteron beam induced radiation and activity in the accelerator and transport channels were surveyed, and the analysis of the measured thick target neutron yield has been reworked.

(ii) In a study of beam loading effects in the RFQ and DTL or SCL [11,12], , the fundamental behavior of the electromagnetic field inside the cavity under heavy transient beam loading has been investigated to establish the optimal method for RF system control. Fig. 4.2.3.1 shows the implementation of selective directional coupling devices into the IFMIF RFQ linac. Three hybrid rings surrounding the RFQ structure are used to distribute the input power to four RF ports that excite each quadrant of RFQ to satisfy the geometrical symmetry. It provides the information about the reflected waves at each port and the reflection will be absorbed at the dummy load. The principle to compensate the beam loading effect is schematically shown in Fig. 4.2.3.2 using the frequency domain representation. The corrective rf signal is constructed to keep the fundamental cavity mode stable within the predefined frequency bandwidth around the resonant frequency. The beam loading effect can be represented using the summation of the time derivative of the particle energy, so that the corrective signal can be derived from its Fourier transform. As the result of minimization of the rf power for the compensation, the control signal may have a error function-like form for step function-like beam injection. It also indicates the optimal form of acceleration gradient along the linac to optimize the rf control signal. The results can be generally extended to the non-step function-like beam injection and the optimal control is less dependent of the beam current.

The effectiveness of the developed method depends on the bandwidth of the feedback control and a short time delay of signal processing is preferable. In the typical case of 30 m feeder line length and 1 ms processor time, the required stability of the injection beam is estimated to be less than 3 %.

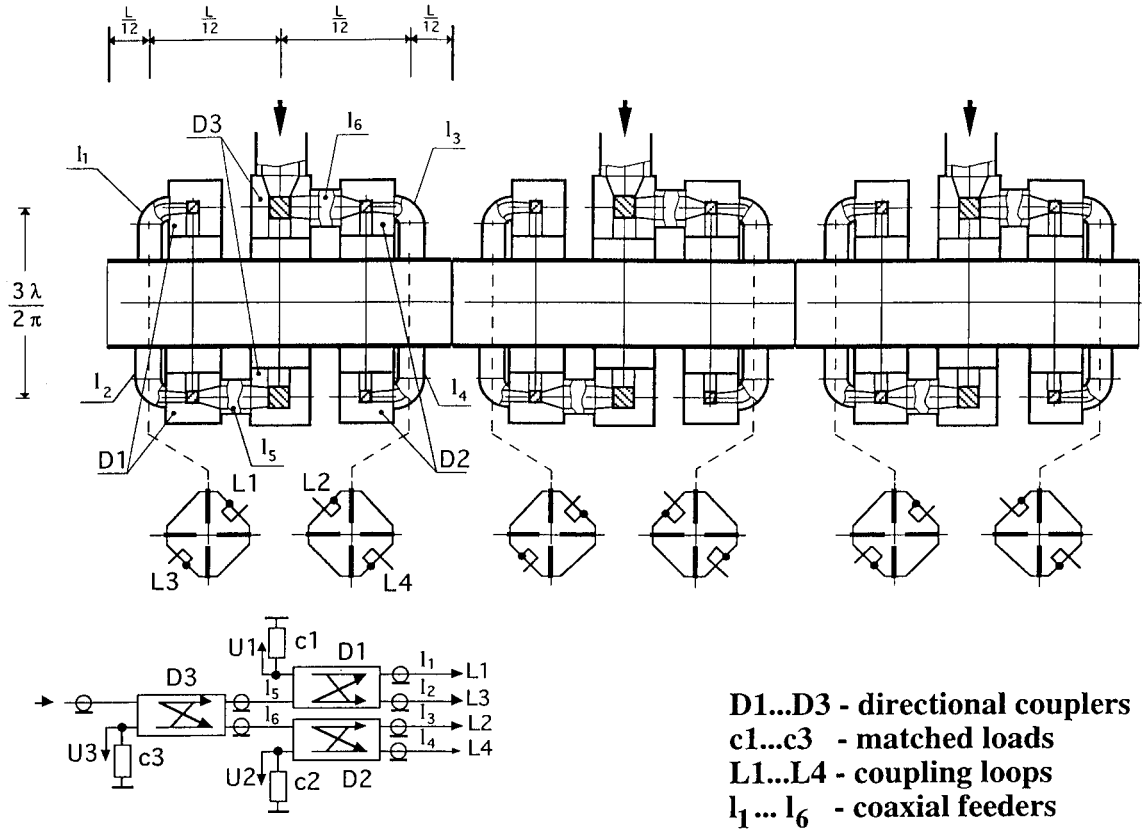

Fig. 4.2.3.1 Alternative design of IFMIF-RFQ RF feed system using the selective directional coupling device.

(iii) Beam transport and loss simulations of the DTL or SCL were expanded [13,14]. The conceptual design of superconducting linac (SCL) option has been updated from the CDA report and the major features of SCL option are given in Fig. 4.2.3.3. Another SCL design using a quarter-wave resonator has also been carried out to reduce the volume of the cryo module, as shown in Fig. 4.2.3.4 and Table 4.2.3.1.

Beam transport calculations have been done for the SCL using the PARMILA code. The case of null injection beam current was simulated and compared.

(iv) A beam dynamics simulation code based on a PIC method has been developed to follow the internal field of the intense beam as accurately as possible. The calculation was carried out for a simplified model of IFMIF RFQ to check the validity of the algorithm[15,16].

(v) An assessment of the cost of the IFMIF facility if built in Japan was presented[17].

Work in EU included:

(i) A technical document [18] groups together the reports published by the CEA team during the period June 96-June 97. All these detailed technical reports summarize the high intensity linear accelerators studies done during this period, including the calculations and conceptual design relevant to IFMIF.

(ii) The mechanism of space-charge neutralization has been investigated both experimentally and theoretically. The aim of these studies was to gain knowledge of the beam behavior in Low Energy Beam Transport lines in order to be able to match the beam to the accelerator as perfectly as possible (beam mismatches are a main source of halo formation). The results allow the space-charge neutralization for various LEBT conditions to be known precisely, thus allowing accurate calculation to match the IFMIF beam to the RFQ.

(iii) An important point concerning the beam loss problem is the ability designers have to predict them at extremely low levels. An effort of several years between CERN, CEA-Saclay and Los Alamos National Laboratory has resulted in a new powerful simulation code (DYNAC), with improved accuracy for RF field modeling and for space-charge calculation; the code is now ready for detailed simulations of the IFMIF DTL.

(iv) Beam loss studies continue, including further investigations on halo formation in the longitudinal plane (accelerated beams) Experimental results will be obtained for unbunched beams in continuous or periodic focusing channels.

Work in Russia included:

(i) A 130 mA, 0.1-1.8 MeV RFQ was commissioned this year. Multipactoring was studied. Future studies will include operation under ultra-high vacuum conditions (10^{-10} Torr goal).

(ii) A 3-dimensional model based on Poisson's equation and macroparticle motion equations solution was developed for the high level code LIDOS.RFQ.

(iii) LIDOS.RFQ code testing was done on the IFMIF RFQ. The first level was used to find an optimal version, and higher level codes are used for real field calculations and beam losses estimation. It now includes poweful tools to simulate vane displacement and rf field transients between coupled sections of the RFQ.

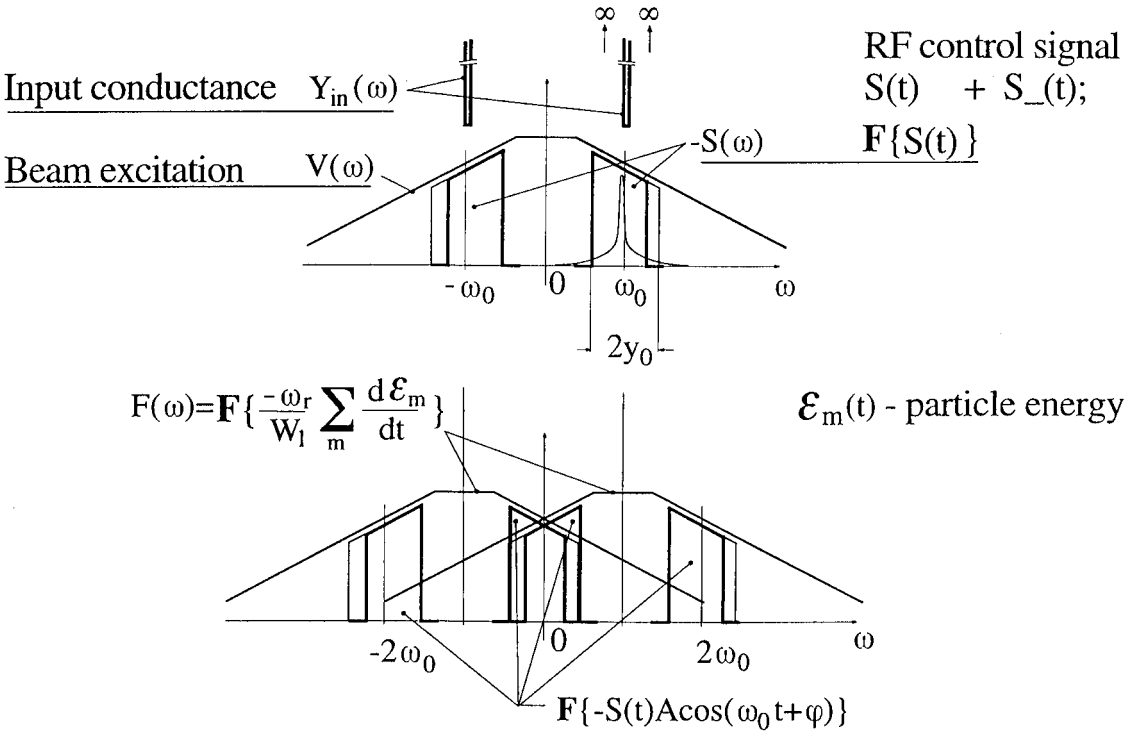

Fig. 4.2.3.2: Principle of the beam loading compensation using the rf control signal in the frequency domain and applying the directional coupling device.

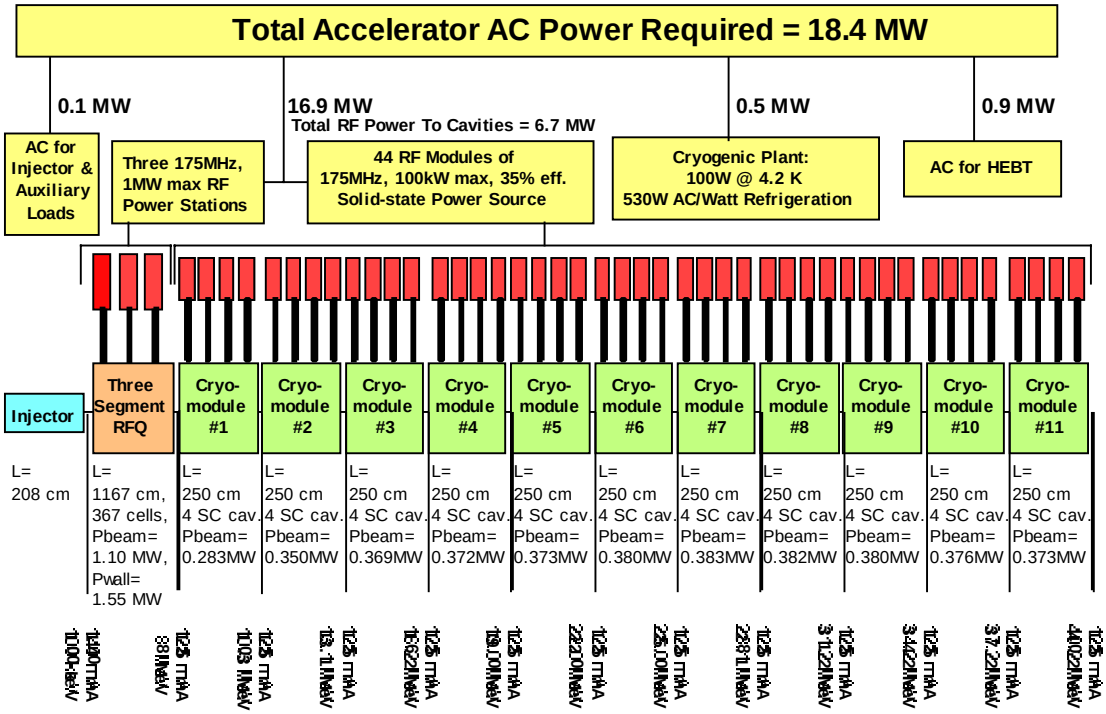

Fig. 4.2.3.3: Major features of superconducting linac option for IFMIF accelerator system.

Table 4.2.3.1 Specifications of quarter-wave resonator for IFMIF SCL.

Material	Nb
Frequency	175 MHz
Thickness of inner conductor	60 mm
Gap length	60 mm
Outer conductor:	
Width	180 mm
Length	340 mm
Q value	1.5×10^{9} (surface resistance of Nb~50nW)
	(7.5×10^{8}*)
Emax/Eacc	9.6
	(4.0*)
Bmax/Eacc	2.3×10^{-2} T/(MV/m)
	(1.2×10^{-2}*)
<Ey>/Eacc	~0.01 **
Height	530 mm

* values of the l/2cavity.

** y component of average electric field per half cell

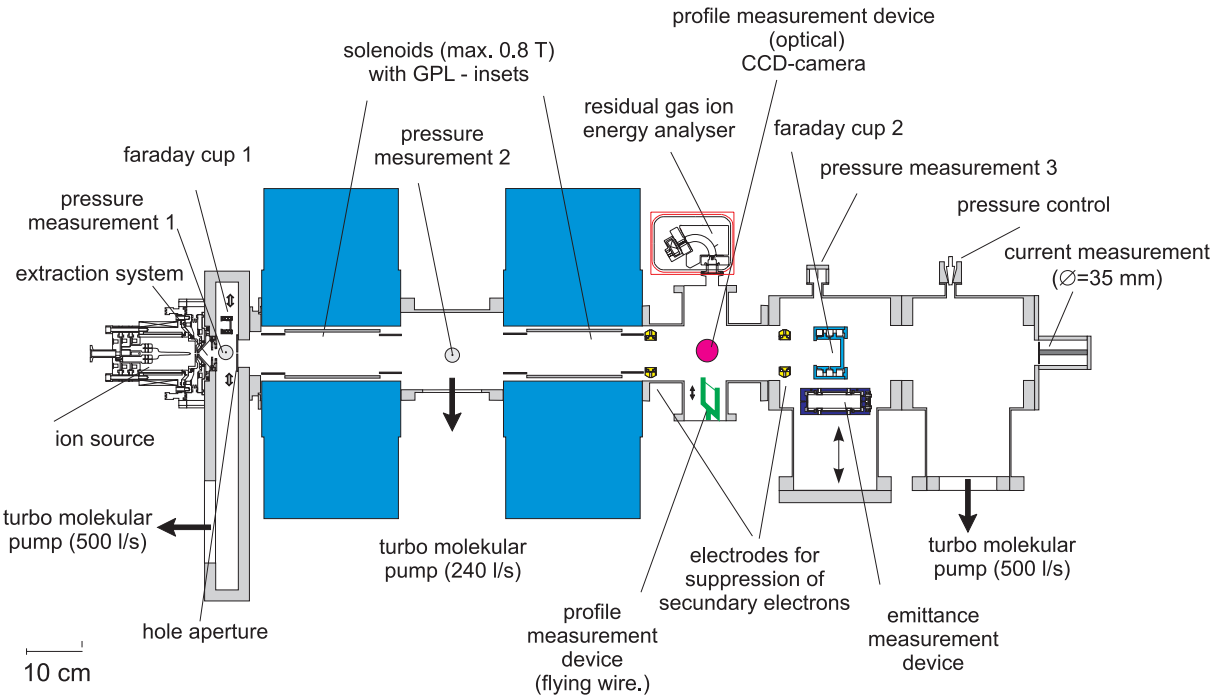

Fig. 4.2.3.4: Low-energy-beam-transport (LEBT) test stand in Frankfurt.

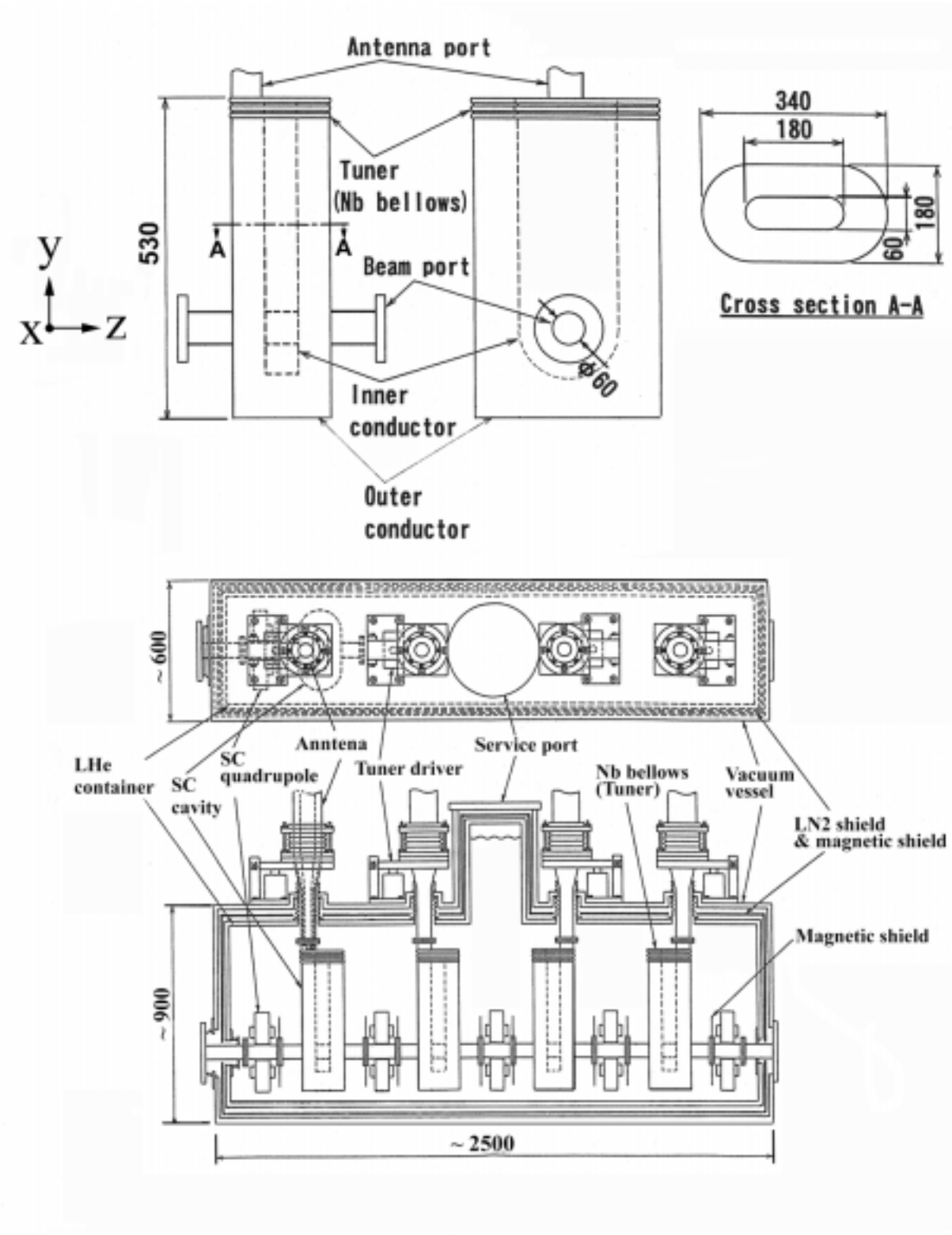

Fig. 4.2.3.5: Quarter-wave resonator for IFMIF accelerator system (top), and representative cryo module schematic using quarter-wave resonators (bottom).

4.2.3.3 Future Directions:

The IFMIF CDA/CDE was very effective in its definition and evaluation of system interface and integration issues, and in addressing a subset of the most critical accelerator technology issues relevant to extending the required accelerator physics and engineering base to high-beam-intensity facilities such as IFMIF that are intended for factory-type operation with very high availability over extended periods. Future work includes testing and selection of ion source and low-energy-beam transport, and verification of a viable rf amplifier. Detailed design work must begin on the entire system. Continuing study on the fundamental design requirement for very low beam loss will continue.

Beam dynamics simulations using different precise particle tracking codes must be performed and compared through the whole system from ion source to end of HEBT. The results must be applied to estimation of the exact beam loss during the acceleration and transport, and the resulting activation. It should be low enough to allow hands-on maintenance during the lifetime of the facility.

The advanced rf system control method should be evaluated for the realistic rf system using a system response simulator.

Precise beam simulations for the SCL option using more realistic models should be carried out to confirm the merits of the SCL option. The cost of the solid state rf source is a critical issue to employ the SCL design and continuous efforts to improve the efficiency are necessary.

The conceptual design should be refined to reduce the technical risks and insure the operational ability to meet the RAM requirement by taking into account design simplification and cost reduction.

References

[1] H. Oguri, M. Kinsho, N. Ouchi and Y. Touchi, Present Status of 2 MeV Beam Test with a Positive Ion Source and an RFQ Linac, JAERI-Review 97-011, 255 (1997).

[2] M. Seki, Y. Okumura, H. Oguri, N. Miyamoto, C. Kutsukake, S. Tanaka, Y. Abe, T. Ono and H. Watanabe, Development of a New High Current Ion Source for FNS, JAERI-Review 97-011, 292 (1997).

[3] A. Sauer, Diplomarbeit, “Untersuchung zum Einfluss von Strahlanpassung und S-Transport auf die Teilchendynamik am Beispiel des alten HERA-RFQ Injektors IAR”, Feb. 1998.

[4] K. Reidelbach, Diplomarbeit, “Hochzeitaufgel¸ste Messungen mit einem Restgasionenenergie-spektrometer an hochperveanten teilkompensierten Ionstrallen”, 1998.

[5] J. Pozimski, Promotion, “Untersuchengen zum Transport raumladungs kompensiertes niederenergetisches und intensives Ionenstrahlen mit einer Gabor-Plasma-Linse”, 1997.

[6] R. Ferdinand, J. Sherman, R. R. Stevens Jr., and T. Zaugg, “Space-charge neutralization measurement of a 75-kev, 130-mA hydrogen-ion beam”, PAC 97, Vancouver Canada.

[7] R.A. Jameson, “A Discussion of RFQ Linac Simulation”, Los Alamos Report LA-CP-97-54, September 1997.

[8] C. Piaszczyk and M. Rennich, “Analysis of the Operations and Reliability of Existing Accelerator Based Facilities-Interim Report”, ORNL document ORNL/M-6227.

[9] M. Eriksson & C. Piaszczyk, "Reliabiity Assessment of the LANSCE Accelerator System", Proc. of 2nd Int. Topical Mtg. on Nuclear Applications of Accelerator Technology (AccApp'98), Gatlinburg, September 20-23, 1998.

[10] C. Piaszczyk & M. Rennich, "Reliability Analysis of the IFMIF", Proc. of 2nd Int. Topical Mtg. on Nuclear Applications of Accelerator Technology (AccApp'98), Gatlinburg, September 20-23, 1998.

[11] M.A. Chernogubovsky and M. Sugimoto, JAERI Research 98-041, 1998.

[12] M.A. Chernogubovsky and M. Sugimoto, "Optimal RF Control at Transient Beamloading", Proc. of 2nd Int. Topical Mtg. on Nuclear Applications of Accelerator Technology (AccApp'98), Gatlinburg, September 20-23, 1998.

[13] Yoshio Tanabe, Nobukazu Kakutani, Tomoko Ota, Akiko Yamaguchi, Osamu Takeda, Yoshihiro Wachi, Choji Yamazaki, and Yasutsugu Morii, "Preliminary design study and problem definition for intense CW superconducting deuteron ion linac for fusion material study", Fusion Eng. and Design, 36 (1997) 179-189.

[14] N. Kakutani, K. Nakayama, Y. Tanabe and O. Takeda, Proc. of 6th European Particle Accelerator Conf. (EPAC 98), Stockholm, July 1998.

[15] M. Sugimoto, M. Kinsho, M.A. Chernogubovsky, JAERI; Y. Hojo, Hitachi Ltd., "Impact of the Beam Dynamics for the Concept of IFMIF Accelerator", 1st Asian Particle Accelerator Conference, 23-27 March 1998, Tsukuba, Japan.

[16] M. Sugimoto, "Precise Beam Simulation of High Current Linac for IFMIF". Proc. 2nd Intl. Topical Mtg. on Nuclear Applications of Accelerator Technology (AccApp'98), Gatlinburg, Tennessee, US, Sept 20-23, 1998.

[17] IFMIF International Fusion Materials Irradiation Facility Conceptual Design Activity Cost Estimate in Japan, ed. M. Sugimoto, JAERI-memo 09-103, March 1997.

[18] "IFMIF Accelerator Studies (96-97)", CEA-DSM-GECA 97/42, June 12, 1997.

5. Design Integration (Conventional Facilities)

5.1 Introduction

5.1.1 RAM

An overall facility availability goal of 70% is a primary IFMIF specification. This requirement constitutes a new major design factor. Existing accelerator-driven facilities typically operate with much reduced yearly operating hours than intended for IFMIF, and therefore more time for maintenance, but these facilities do represent the available experience base with relevant components. However, none of the information from major existing facilities had ever been systematically collected and analyzed. Intending to put the RAM aspect, along with physics, engineering and cost aspects, on a systematic and inter-correlated basis, during the CDA the IFMIF team conceived and developed the powerful Accelerator System Model (ASM), and used it to guide conceptual design choices and the development of a credible RAM model.

During the CDE, the subsystem and component RAM database was systematically developed by obtaining voluminous data from a number of operating accelerator facilities, and by beginning the task of translating the information into a consistent format and performing the required analyses.

Already at the stage achieved by the CDE, important and new insight into the reliability requirement has resulted. The initial objectives were to study the operating procedures employed in these facilities to achieve the recorded availability, and to collect performance data. It was found that the organization of operations across the facilities is remarkably similar, with differences mainly reflecting more or less formality depending on the facility size. A preferred database format for future data capture has been proposed and endorsed by a number of facilities.

At this time, the state of the art in the area of reliability of repairable systems leaves a lot of uncovered ground even outside the field of accelerators. Continued development of this methodology is thus necessary to achieve the IFMIF system design with the required availability characteristics. There are three major directions recommended at this time for future activities: continued data collection, continued statistical inference analysis, and development of modeling approaches for accelerators as repairable systems (in the form of stochastic process simulations).

5.1.2 Safety

An activity aimed at the safety assessment of the entire IFMIF plant and its subsystems (Test Cell, Target, Accelerator and Conventional Facilities) has been carried out using the PRA (Probabilistic Risk Assessment) methodology. Although the available results show that the IFMIF plant is quite safe and presents no significant hazard to the environment, they must be considered as preliminary because the level of detail for the conceptual design is not sufficient to reach a final assessment.

5.1.3 Central Control System

Two instruments have been evaluated by JAERI that are important for the interface between the accelerator, target and test cell. The first one is a neutron monitor based on compact multi-channels calibrated by an activation wire detector. The second one is an infrared camera to measure the beam position and temperature distribution on the target.

5.2 CDE Tasks

5.2.1 Reliability Availability Maintainability

Accelerator Reliability Database

Description and justification:

During the International Fusion Materials Irradiation Facility (IFMIF) Conceptual Development Activity performed in 1995-1996 [1,2], it was found that although a significant history of accelerator operation has been accumulated over the past 50 or so years, no formal reliability database for accelerator components has ever been assembled. Thus, even though one can attempt to use the standard reliability analysis tools to build accelerator reliability models [3,4], the required input data for these models in the form of failure rate and repair time information are not readily available. It was therefore proposed [5] that a survey of the operating facilities was to be performed to collect the required data.

Contributors:

Organization	Principal Investigator
Northrop Grumman	C. Piaszczyk

Main responsibility: Northrop Grumman

Milestones:

1) Data Collection	July 1997
2) Data Analysis	March 1998
3) Documentation	September 1998

5.2.1.1 Impact on CDA

Much effort in reliability theory is devoted to the study of repairable systems. Accelerators are an example of such a system. It is well known that in a repairable system, the effectiveness of a working system depends not only on the characteristics built into it during design and production, but also on the quality of its operation, maintenance, repair, etc. Thus, system reliability analysis is an integral part of optimal preventive maintenance planning and its execution. It also has a significant impact on both performance and cost. Quantification of system reliability characteristics can only be carried out on the basis of data. Because of the high costs associated with obtaining such data, the statistical database the reliability engineer is dealing with is usually, if not always, incomplete. It is therefore important to use the experience from existing operating facilities to the maximum extent possible.

5.2.1.2 Results and Conclusions

During 1997, several operating accelerator facilities were surveyed with two preliminary objectives. The first objective was to study the operating procedures employed in these facilities to achieve the recorded availability and the second objective was to collect performance and equipment failure data for use in reliability models. A significant amount of information was collected [6,7]. Some of the collected data have been analyzed and yielded estimates of failure and repair rates for major accelerator components [8]. Another approach, attempting to characterize the accelerator reliability as a combination of failures and repairs as two alternating

stochastic processes has also been considered [9]. This latter approach could serve as a basis for the development of novel simulation modeling methods in the future. Initial findings of the effort at this stage can be summarized briefly as follows:

(i) The organization of operations across the facilities is remarkably similar. The differences stem primarily from the size of the individual facility. A smaller facility tends to operate more informally with the individuals covering larger territories and the larger facilities maintain a more formally organized personnel structure.

(ii) All facilities maintain a record of downtimes and their causes (insofar as these are actually understood). In some cases, the most recent data are available in electronic form. Usually, the organization of these records does not lend itself to automatic extraction of failure rates for individual components but requires significant additional effort. Recommen-dations have been made to the accelerator operators both individually and as a group concerning the type of data and the preferred database format to be followed for maximum utility for future reliability analyses [10]. Essentially, they were asked for more emphasis in the description of the details characterizing each fault condition.

(iii) Existing accelerator facilities were found to operate with availabilities between 80-90% over the scheduled operation time. However, the scheduled times are typically between 30-50% of the calendar year, thus allowing for a substantial amount of maintenance and up-grade work. Extension of the operating availability by reducing the length of the shut-down could limit the availability of future machines due to the inability to perform critical repairs. In addition, the surveyed facilities schedule between 5% and 30% of beam time for studies to analyze and further improvement of accelerator operation and performance. It is to be noted here that the accelerators surveyed are typically large accelerator facilities used primarily as scientific instruments for high energy physics experiments. Small accelerators built for medical or industrial uses operate practically 100% of the time and have an excellent reliability record.

5.2.1.3 Future Directions

At this time, the state of the art in the area of reliability of repairable systems leaves a lot of uncovered ground even outside of the field of accelerators [11]. Continued development of this methodology is thus necessary to achieve the IFMIF system design with characteristics satisfying the desired requirements. There are three major directions recommended at this time for future activities: continued data collection, continued statistical inference analyses, and development of modeling approaches for accelerators as repairable systems (in the form of stochastic process simulations).

References

[1] “IFMIF, International Fusion Materials Irradiation Facility Conceptual Design Activity, Final Report”, M. Martone, ed., January 1997

[2] “Reliability Analysis of the IFMIF”, C. Piaszczyk, M. Rennich, American Nuclear Society Accelerator Applications Conference, Gatlinburg, TN, September 1998

[3] “Accelerator Reliability, Availability, and Maintainability”, C. Piaszczyk, Maintainability and Reliability Conference, Knoxville, TN, May 1997

[4] “Accelerator Systems Model (ASM) - a Powerful Tool for Parametric Studies of Emerging High Power Accelerator Applications”, C. Piaszczyk, et al., American Nuclear Society Winter Conference, Albuquerque, NM, November 1997

[5] “IFMIF RAMI Proposal”, C. Piaszczyk, March 1997

[6] “Reliability Survey of Accelerator Facilities”, C. Piaszczyk, M. Rennich, Maintainability and Reliability Conference, Knoxville, TN, May 1998

[7] “Operational Experiences at Existing Accelerator Facilities”, C. Piaszczyk, NEA Workshop on Utilization and Reliability of High Power Accelerators, Mito, Japan, October 1998

8] “Reliability Assessment of the LANSCE Accelerator System”, M. Eriksson, C. Piaszczyk, American Nuclear Society Accelerator Applications Conference, Gatlinburg, TN, September 1998

[9] “Understanding Accelerator Reliability”, C. Piaszczyk, LINAC ‘98, Chicago, IL, August 1998

[10] “Developing a Reliability Database Using Records from Existing Accelerator Facilities”, C. Piaszczyk, Workshop for Accelerator Operators, Vancouver, BC, May 1998

[11] H. Asher and H. Feingold, “Repairable Systems Reliability”, Marcel Dekker, Inc. 1984.

5.2.2 Safety Assessment of the IFMIF facility

Description and justification:

Only preliminary safety requirements were made on the entire facility in the past two years of the CDA. Dependencies among supporting systems and the front-line systems and other dependencies have not been studied in a quantitative manner. However, extensive and quantitative analysis will be required for the safety assessment, and a safety database for a more detailed design. For this purpose, it is required to further study some of the safety issues, and perform a safety analysis of the IFMIF facility as a whole. The result will facilitate the improvement of the conceptual design.

Quantitative safety analysis on the entire facility and the subsystems of the IFMIF will be performed by the safety analysis specialists. Fault tree, probabilistic estimates, risk and accident analysis will be the major methods to be applied. The analysis will be conducted on the latest version of the design with specific requirements for the possible sites in virtual nuclear institutes. Some major potential hazards of the IFMIF facility that could lead to a dangerous situation for the plant and environment will be studied extensively. The environmental impact will also be one of the important topics. The results should be reviewed by a group of specialists outside of the IFMIF project, and also used for the preparation of the documents required for the approval process.

Contributors

Due to the nature of this task, personnel from all the facility groups design integration, accelerator, target, test cell will be involved.

Organization	Principal Investigator
ENEA	Bianchi, Burgazzi, Martone
Univ. Tennessee, ORNL	Shannon
JAERI	H. Maekawa

Main responsibility: ENEA

Milestones:

- Task planning and assignment	97 June
- Preliminary review reported	97 Nov
- Interim report of safety analysis and accident sequences	97 Dec.
- Additional tasks planned	98 March
- Event accident sequence analysis	98 May
- 80% review, environmental impact review	98 Sep.
- Final report	98 Dec.

5.2.2.1 Impact on CDA

The foregoing detailed probabilistic safety analysis confirms what was pointed out in the CDA phase: test cell facilities do not have significant potential hazards during operation; potential target related hazards due to tritium production and lithium operation are negligible; also conventional facilities related hazards are very low; the critical subsystem of the IFMIF plant is identified to be the accelerator (and especially main components as ion source and RF stations): therefore the desired level of safety of this system shall be achieved by first performing

an extensive design verification through testing and analysis of the critical hardware and software.

5.2.2.2 Results and Conclusions

5.2.2.2.1 Introduction and Methodology

A safety analysis, from the probabilistic point of view, of some accident sequences concerning the test cell facilities, accelerator facilities, target facilities and the conventional facilities of the IFMIF experimental plant has been performed in order to assess the frequency of those major accident sequences potentially leading to damage of the IFMIF plant and, as extreme consequence, causing environmental hazard. Moreover the probabilistic safety analysis of the plant, as a whole, is carried out by accounting either the failure of the main utility supply systems (e.g. electrical power supply system, vacuum system, heat rejection system) causing serious safety problems in the entire facility or the accidents which could severely affect the operation and equipment of the IFMIF (e.g. accidents occurring in the target area).

The analysis has been developed on the basis of the information about the plant contained in ref. [1] and, where no detailed plant-specific design data are available, by engineering assessment. The methodology and the calculation tool adopted are the fault tree and event tree technique, widely utilized in the PRA (Probabilistic Risk Assessment) studies, and the RISK SPECTRUM code, a PC software package that performs system risk and reliability analysis based on fault tree and event tree methods (ref. [2]). The accident sequence scenarios are modeled through the event trees: a certain initiating event can initiate different chains of events with many alternative consequences, each scenario corresponding to a certain combination of failed or functioning safety systems. The main steps of the activity performed are as follows:

- safety analysis on the basis of the CDA (Conceptual Design Activity) design stage
- identification of initiating events of accident sequences on the basis of safety analysis and FMEA (Failure Mode and Effect Analysis) outcome (ref. [1])
- definition of the accident sequences
- quantification of accident sequences concerning the test cell by means of the RISK SPECTRUM code.

The initiating events of the accident sequences are limited to internal initiators that could occur during normal operation of the plant - therefore neither the area events nor the external events are taken into account - and are individuated on the basis of the preliminary safety analysis performed in ref. [1] and engineering evaluation of the accident evolution that can harm the IFMIF systems and consequently the whole experimental plant. The safety systems having the function of stopping the accident sequence evolution and mitigating the consequences are mainly the fast beam interrupt system and the fast beam isolation system for the beam-target interface and the emergency equipment, like diesel generators and backup batteries, for the electrical power and the inert gas system for the lithium fire prevention system. The values of frequencies and component reliability data are taken mainly from ref. [1], and, if there not available, from refs. [3] and [4] or by engineering judgement. In the RISK SPECTRUM code the fault trees and event trees are built with the component reliability model, the component reliability data are assigned and the final risk assessment is quantified through the analysis of combinations of fault trees and event trees. Due to the uncertainties either in the definition of the systems at this stage of the design or in the availability of the failure and reliability data of the components, conservative assumptions are made and/or any simplifications are introduced in the system model based analysis and therefore the results must be considered to be preliminary.

5.2.2.2.2 Test Cell

The following event initiators related to the test cell are identified and analyzed:

- Loss of test cell cooling
- Loss of test cell vacuum
- Loss of VTA thermal control
- Loss of Coolant Accident (LOCA)

The results obtained from the RISK SPECTRUM code show that the frequencies of occurrence of the accident sequences that can harm the plant and potentially affect the environment are very low. In particular the frequencies of the accident sequences representing a potential risk to the environment, i.e. those sequences implying the loss of test cell cooling, the loss of test cell vacuum and NaK LOCA together with test cell vacuum loss, followed by the safety systems failure, are not higher than 1.0^{-6}/year.

The distributions of frequencies of the accident sequences that can lead to plant contamination and therefore cause possible environment effects are summarized in table 1. The consequences related to the sequences with the test assembly thermal control loss and the He/NaK LOCA in test cell as initiating events, followed by the safety systems failure, can potentially affect only the test assemblies or the test cell and do not represent a hazard to the environment.

5.2.2.2.3 Accelerator System

The IFMIF requirement for 250 mA of deuteron beam current delivered to the target will be met by two 125-mA, 40-MeV accelerator modules operating in parallel. Each IFMIF deuteron accelerator comprises a sequence of acceleration and beam transport stages. The accelerator system consists of the following subsystems (ref. 2):

- Injector (Ion Source and Low-Energy Beam Transport System)
- RFQ (Radio Frequency Quadrupole) Accelerator
- DTL (Drift Tube Linear Accelerator)
- RF (Radio Frequency) Power System
- HEBT (High-Energy Beam Transport System)

The following event initiators related to the accelerator are identified and analysed:

- Loss of beam vacuum
- Cooling water failure
- Accelerator facility failure

Loss of electrical power is not expected to cause a critical hazard since the beam is shut down at that time. Accident scenarios caused by beam failure (e.g. accidental beam loss, abnormal beam spot on the target, failure of beam to shut off, etc.) require special emergency and recovery procedures. The results obtained from the RISK SPECTRUM code show that the frequencies of occurrence of the accident sequences that can harm the plant and potentially affect the environment are rather relevant. The distributions of frequencies of the accident sequences that can lead to plant contamination and, therefore, cause possible environment effect are summarized in table 5.2.2.2. In particular, the annual frequencies of the accident sequences representing a potential risk to the environment and having as an initiating event the loss of coolant and accelerator failure are in the range of 10-2/y to 10-4 /y, that is the category of the sequences not likely to occur during the life of the plant. According to the table, the major contribution to the plant contamination frequency is due to the failure of coolant system and particularly to LOCA (Loss Of Coolant Accident).

As regards the accelerator failure, the most critical components are the ion source, the RF stations and the HEBT system, see table 5.2.2.3 which reports the failure probabilities of the major subsystems as results from the fault tree calculations.

Finally, the contribution of loss of beam vacuum to the plant contamination hazard is negligible.

5.2.2.2.4 Target

The following event initiators concerning the target and its subsystems, like e.g. the lithium loop, are analysed:

- Loss of electrical power
- Loss of beam vacuum
- Loss of lithium flow
- Loss of secondary cooling loop
- Loss of water cooling loop
- Loss of cold trap cooling loop
- Loss of electrical power to the target

The results obtained from RISK SPECTRUM code indicate that the frequencies (event/year) of occurrence of the accident sequences are very low, in particular they are not higher than 1.0E-7. The distribution of the plant contamination frequencies among different initiators is presented in table 5.2.2.4 together with the total failure probability, 4.0E-9; table 5.2.2.4 shows that the major contribution to the hazard associated with the target is due to the loss of lithium flow accident.

The most radioactive material related to the target system is tritium. IFMIF will produce approximately 10 grams/year of tritium. Under normal operating conditions a few grams (3-5 grams) of this tritium is confined in the loop components and the remainder of the tritium is being accumulated in the cold or hot trap. Although radioactive materials are a potential hazard for the environment in case of accident, IFMIF facilities have been designed both to reduce the accident probability and, at the same time, to eliminate any subsequent release to the environment.

5.2.2.2.5 Conventional Facilities and Overall Plant

Conventional facilities must provide the housing and the support systems for the three process facilities (test cell, target and accelerator). The main conventional facilities to be analyzed are:

- Heat Rejection System (HRS)
- Electrical Power Distribution System (EPDS)
- Heating Ventilation Air Conditioning (HVAC)
- Central Vacuum System (CVS)
- Ar ventilation system of lithium systems
- Test cell vacuum system

The accident sequences due to loss of the foregoing systems as initiating events are evaluated here; the Ar ventilation system of the lithium systems and the test cell vacuum systems are not considered as initiating event of an event tree but as safety systems to be accounted for the entire plant analysis. The following event initiators concerning the conventional facilities are identified and analyzed:

- Loss of heat rejection system
- Loss of electrical power distribution system
- Loss of heating ventilation and conditioning system
- Loss of central vacuum system

The event trees to be accounted for the whole plant analysis mainly concern the target and Li loop and its support systems like the test cell vacuum system and Ar ventilation system. The following initiator events are analyzed:

- Li LOCA
- Target backwall rupture
- Loss of beam (followed by loss of test module thermal control)

The distributions of frequencies of accident sequences that can lead to plant contamination possibly causing an environmental hazard among different initiators are summarized in table 5.2.2.5. The results obtained from RISK SPECTRUM code show that the frequencies of occurrence of the accident sequences that can harm the plant and potentially affect the environment are very low (order of magnitude 1.0E-5). It is evident from the table that all but the loss of beam contribute to the total annual frequency and that the predominant contributor to the environmental hazard is the loss of the central vacuum system.

5.2.2.2.6 Conclusions

The results of the probabilistic safety assessment extended to the entire IFMIF facility indicate that the frequencies of occurrence of the accident sequences leading to environmental hazard are negligible as regards the target system and very low as far as the test cell and the conventional facilities are concerned. On the contrary the accelerator facility has been identified as a critical system for the IFMIF plant and a frequency of occurrence of dangerous sequences ranging from 1.0E-2 and 1.0E-6 has been assessed. In Figs. 5.2.2.1 – 5.2.2.6 the most significant event trees representative of the accident sequences concerning the test cell, accelerator, target, conventional facilities and the whole IFMIF plant are reported.

5.2.3 Future Directions

Due to the uncertainties in the definition of the systems at this stage of the design, the results must be considered to be preliminary: thus, a more detailed design level is recommended for a subsequent analysis review. In particular, in order to validate the failure probabilities with respect to the accelerator, an activity aimed at the reliability assessment of the accelerator is recommended, too.

References

[1] “IFMIF Conceptual Design Activity Final Report”, RT-ERG-FUS-96-11

[2] U. Berg, L. Sardh “RISK SPECTRUM User’s Manual Version 2.12”, Relcon Teknik, April 1994

[3] WASH 1400 REPORT, US NUCLEAR REGULATORY COMMISSION, 1975

[4] INEL 1988 FAILURE RATE SCREENING DATA FOR FUSION RELIABILTY AND RISK ANALYSIS

Table 5.2.2.1 Test cell plant contamination frequency results

INITIATOR	INITIATOR PROBABILITY	PLANT CONTAMINATION FREQUENCY (1/year)
Loss of test cell cooling system	7.2E-3	7.2E-10
Loss of test cell vacuum system	1.9E-3	1.9E-10
NaK LOCA followed by loss of test cell vacuum	1.0E-3	1.9E-6
	TOTAL	2.0E-6

Table 5.2.2.2: Accelerator plant contamination frequency results

INITIATOR	INITIATOR PROBABILITY	PLANT CONTAMINATION FREQUENCY (1/year)
Loss of beam vacuum	3.1E-4	3.1E-7
Loss of coolant	1.0E-2	1.0E-2
Accelerator failure	9.0E-1	9.0E-5
	TOTAL	1.0E-2

Table 5.2.2.3: Major accelerator subsystem failure probabilities (as results of fault tree analysis)

SUBSYSTEM	FAILURE PROBABILITY
Ion Source	6.4E-1
LEBT	2.4E-2
RFQ	9.2E-3
DTL	5.5E-2
RFQ RF station	1.8E-1
DTL RF station	5.0E-1
HEBT	3.0E-1

Table 5.2.2.4: Target plant contamination frequency results

INITIATOR	INITIATOR PROBABILITY	PLANT CONTAMINATION FREQUENCY (1/year)
Loss of beam vacuum	1.0E-2	1.0E-9
Loss of cold trap cool. loop	2.1E-3	2.1E-10
Loss of lithium flow	2.8E-2	2.8E-9
Loss of sec cooling loop	9.7E-4	9.7E-11
Loss of water cooling loop	9.7E-4	9.7E-11
Loss of electr. power	3.7E-3	1.4E-11
	TOTAL	4.0E-9

Table 5.2.2.5 Conventional facilities plant contamination frequency results

INITIATOR	INITIATOR PROBABILITY	PLANT CONTAMINATION FREQUENCY (1/year)
Loss of heat rejection system	2.2E-4	2.2E-8
Loss of electrical power distribution system	3.7E-3	8.4E-8
Loss of HVAC system	1.4E-4	1.4E-8
Loss of central vacuum system	1.0E-2	1.0E-5
Li LOCA	1.0E-2	1.0E-10
Backwall rupture	1.0E-4	1.9E-7
	TOTAL	1.0E-5

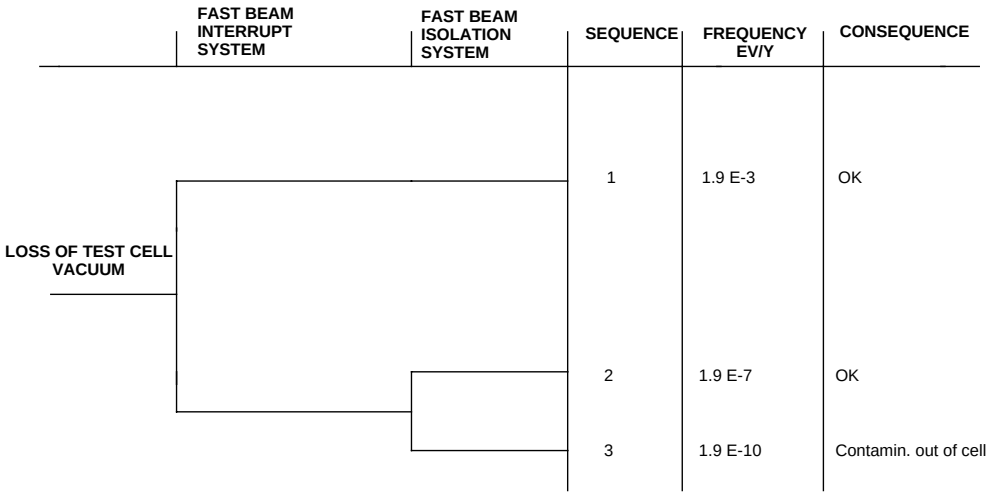

Fig. 5.2.2.1: Loss of test cell vacuum event tree

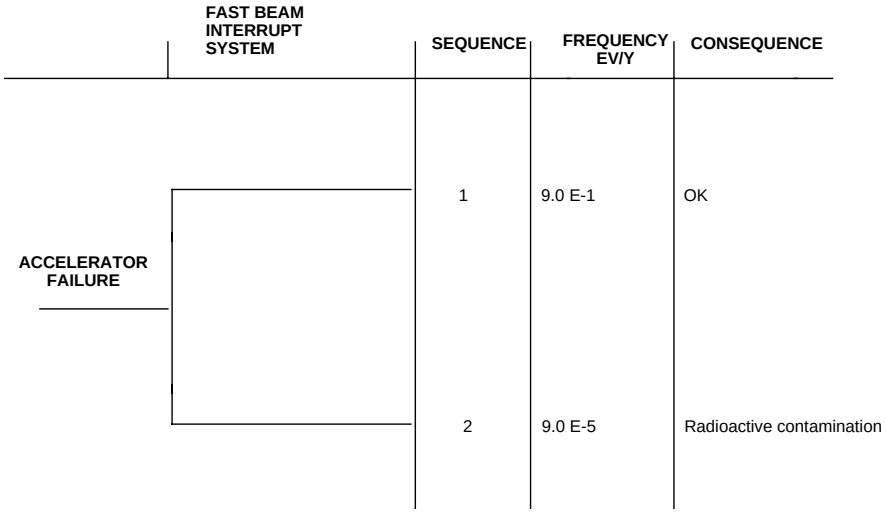

Fig. 5.2.2.2: Accelerator failure event tree

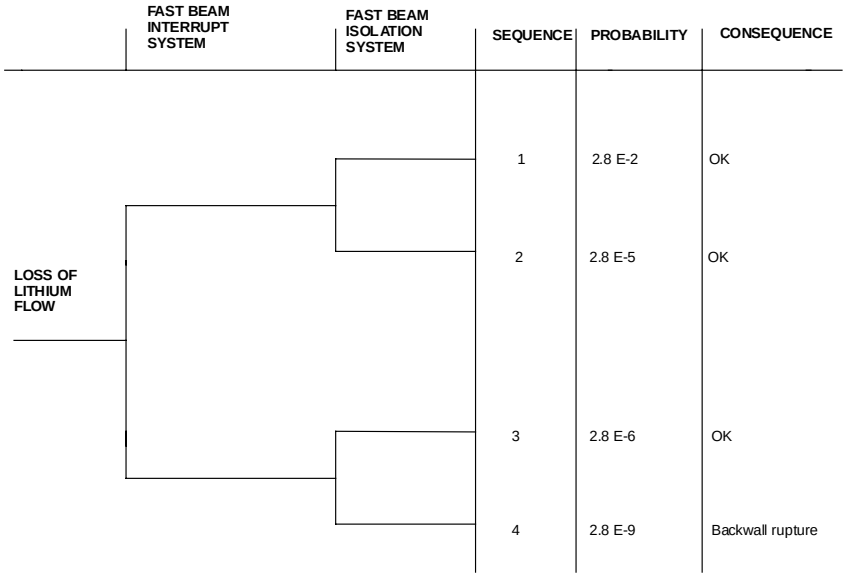

Fig. 5.2.2.3: Loss of lithium flow event tree

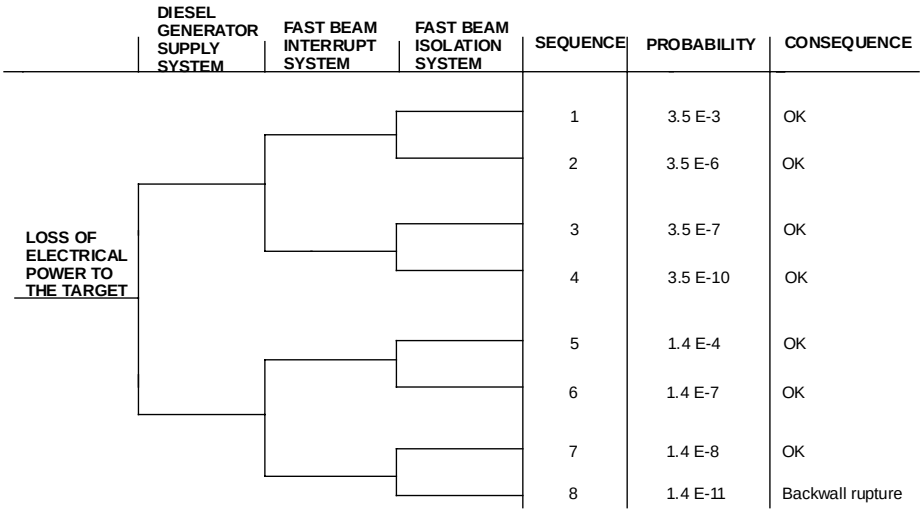

Fig. 5.2.2.4: Loss of electrical power to the target event tree

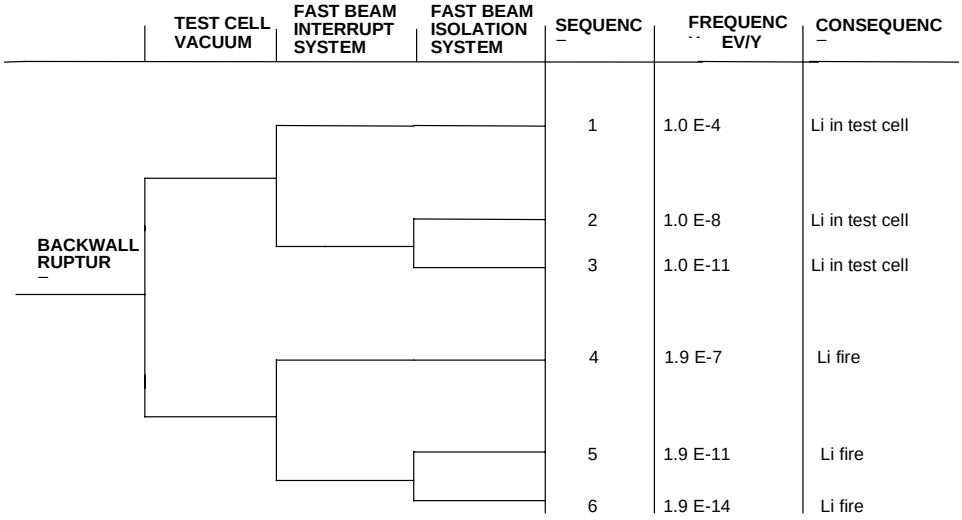

Fig. 5.2.2.5: Backwall rupture event tree

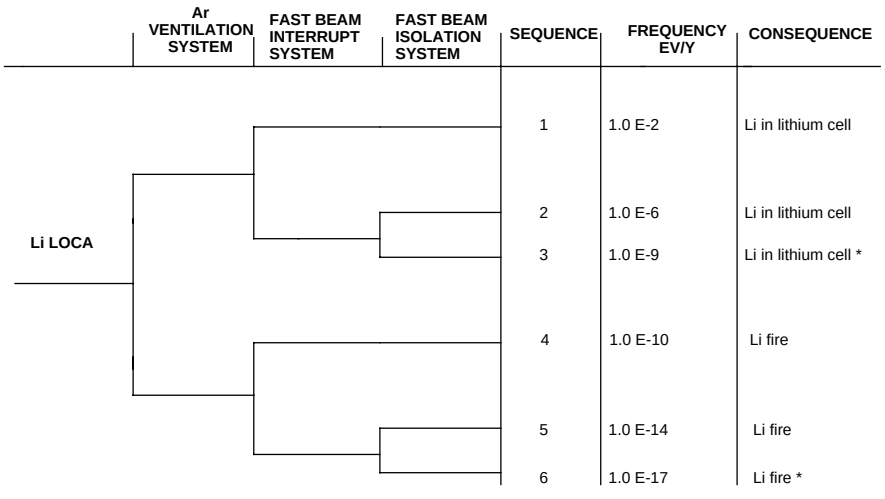

* Risk of Backwall rupture

Fig. 5.2.2.6: Li LOCA event tree

5.2.3 Infrared TV Camera

Description and Justification:

In the IFMIF CDA final report [1], an infrared camera is proposed as beam measurement and monitor instrument on the target for not only footprint but also surface temperature. The measurement of a beam position is important from the points of view of estimating the neutron flux position and checking the state of ion beam operation. The measurement of the surface temperature distribution on a lithium target is significant in order to presume the temperature rise inside a lithium target by using a multi-dimensional thermal-fluid-dynamics numerical analyses code [2]. We studied an infrared camera layout and the possibility to monitor the surface temperature distribution and beam position.

Contributors:

Organization	Principal Investigator
Toshiba Corporation	Yoshio Kita
JAERI	Toshiaki Yutani
	Masayoshi Sugimoto
	Hiroshi Takeuchi

Milestones:

1) Examination of Measurement Principle	May 1998
2) Basic Design of System	August 1998
3) Documentation	September 1998

5.2.3.1 Impact on CDA

On-line lithium target temperature system was designed in order to maintain safety operation of target system and control the beam position on the surface of lithium target position.

5.2.3.2 Results & Conclusions

We designed a layout of an infrared camera system without changing the existing design of the deuteron ion beam and target system. Fig.5.2.3.1 shows the layout of an infrared camera system where the optical path is set through the beam line of the deuteron ion. Since the deuteron ion beams are deflected 10° by the 10° dipole, a metal concave mirror is installed on the extended line of a beam line without interfering with a deuteron ion beam.

Infrared light from a target is reflected 90° by the metal concave mirror and led to the infrared camera through a vacuum sapphire window as shown in Fig.5.2.3.2. The temperature range on the surface of lithium target was assumed to be 250 °C to 350 °C. Fig.5.2.3.3 shows the spectral radiant exitance per wavelength of the black body of 250 °C, 300 °C, and 350 °C. The peak wavelength of each temperature is about 5 μm. As a detector, InSb detector which has the peak wavelength of sensitivity in about 5 μm and an effective wavelength band of about 1μm is used. The radiant exitance per temperature at the wavelength of 5μm is calculated as shown in Fig. 5.5.3.4. The relation between temperature and radiant exitance is almost linear. In the following examination, we assume the lithium surface temperature to be 300 °C. The radiant intensity from the lithium surface is given by following equation.

$$I_0 \times \Delta\lambda \times \varepsilon_\lambda$$

I_0: Spectral radiant exitance of black body at 300°C (= 0.08W/cm^2/μm)

$\Delta\lambda$: detector wave length band (=1μm)

ε_λ: spectral emissivity

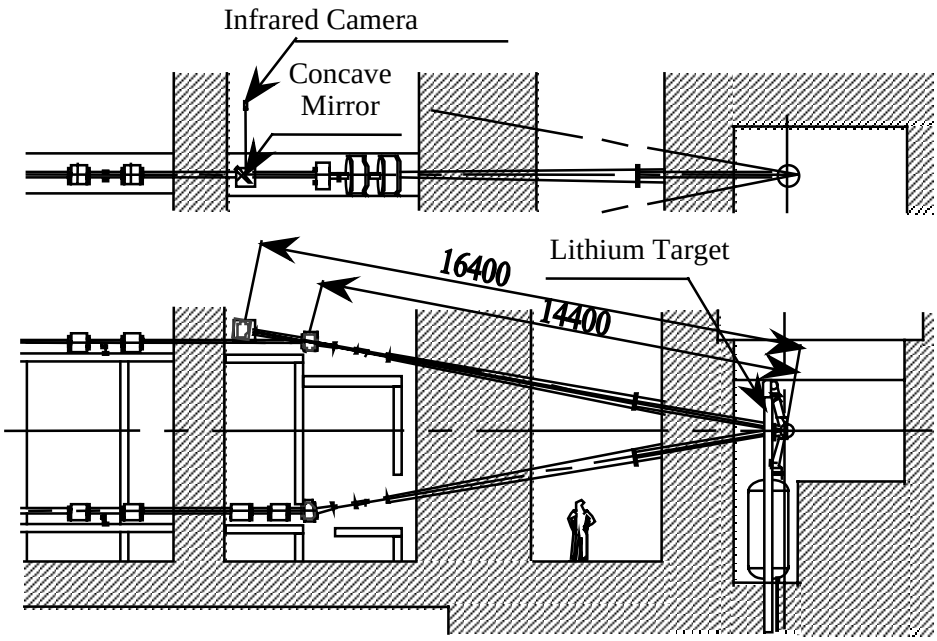

Fig.5.2.3.1 Layout of Infrared Camera

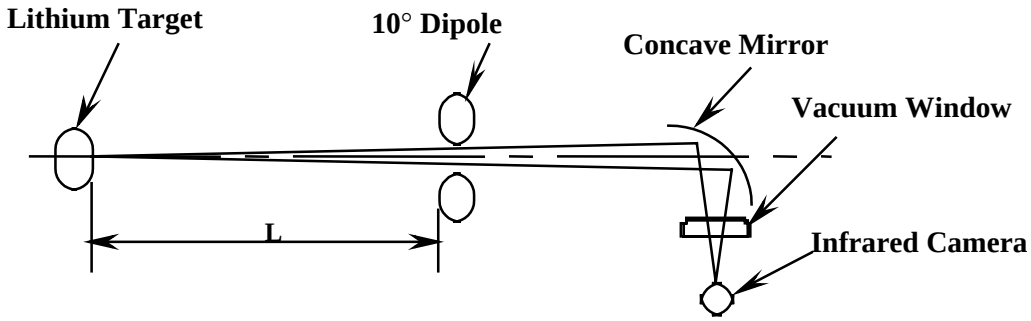

Fig.5.2.3.2 Infrared Camera Optics

Spectral emissivity of a target is given by the following formula in approximation.

$$\varepsilon_\lambda = 36.5\sqrt{\frac{\rho}{\lambda}} = 0.05$$

ρ: resistivity (= 9.4×10^{-6} Ωm)

λ: wave length (=5μm)

As shown in Fig. 5.2.3.2 the view of a camera is restrained by an aperture of 60 mm diameter of the 10° dipole at 14.4 m distance from target, and the quantity of light decreases. The radiant flux emitted from the target (area S_x), which passes through the aperture of 10°

dipole is collected by a metal concave mirror and led to infrared camera. The power P (W/cm^2) on the detector of the camera is given as follows.

$$P = (I_0 \Delta\lambda\varepsilon_\lambda) \times S_X \times \frac{S_1}{2\pi \cdot L^2} \times \frac{1}{A} \times K_1 \times K_2 \times K_3$$

where

S_x: Visual field on target area (diameter ΔX)

S_1: Aperture area of 10° dipole (diameter 60mm)

L: Distance between the target and aperture of 10° dipole

A: Detector sensitive area (diameter 0.6 mm)

K_1: Decay coefficient of air

K_2: Decay coefficient of optics (mirror, window, camera)

K_3: The other coefficient (apparatus characteristics)

The ratio of signal to noise (S/N) is given as follows.

$$\frac{S}{N} = \frac{D^* P\sqrt{A}}{\sqrt{\Delta f}}$$

$$= (I_0 \Delta\lambda\varepsilon_\lambda) \times S_X \times \frac{S_1}{2\pi \cdot L^2} \times \frac{1}{\sqrt{A}} \times K_1 \times K_2 \times K_3 \times D^* \times \frac{1}{\sqrt{\Delta f}}$$

where

D^*: specific detectivity of the sensor

Δf : frequency band width of the circuit

Using the following infrared camera parameters, P is calculated as follows.:

$$P = 5.3 \times 10^3 \frac{S_X}{\sqrt{\Delta f}}$$

where

I_0= 0.08(W/cm^2/μm), Δλ = 1(μm), ε_λ= 0.05, S_1= 28cm^2

A = 2.8x10^{-3}cm^2, k_1= 0.95, k_2= 0.68, k_3= 0.25. D^* = 2x10^{11}(W^{-1}.cm.Hz$^{1/2}$)

As an ion beam uniformity of 10% per cm is required, it is considered that an S/N ratio of 100 is necessary. If Δf is set to be 100 which is an usual value in an infrared camera, space resolution (ΔX) becomes about 5mm and 30 pictures/second are obtained. A temperature distribution is obtained from a distribution of the calculated radiance using the relation of Fig.5.2.3.4. Calibration of temperature is performed by comparing the temperature measured by the thermocouple with the estimated temperature from the amount of radiant at the same upstream position.

The accuracy of the position measurement of a deuteron ion beam is ±1 mm, and the infrared camera also requires the same one. Surface temperature distribution of a liquid lithium target irradiated by a deuteron ion beam is calculated in the report of JAERI-Research 97-030 [2] where a horizontal surface temperature distribution has a comparably clear boundary but a perpendicular (flow direction) surface temperature distribution has no clear boundary. The horizontal surface temperature distribution has a comparably clear distribution since the lithium

target flow velocity is larger than the heat diffusion velocity. The perpendicular (flow direction) temperature gradually increases along the stream and does not have a clear boundary because the downstream side lithium is irradiated for a longer time. Therefore, we need to examine another method to measure the perpendicular beam position. The laser interferometer method of measuring the hollow on the surface of lithium target by the pressure of a deuteron ion beam is one of the ideas. Although the estimated value of 30 μm is the one to be measured by the interferometer, it is smaller than the surface wave amplitude generated on the lithium surface. So, the interferometer method is not promising.

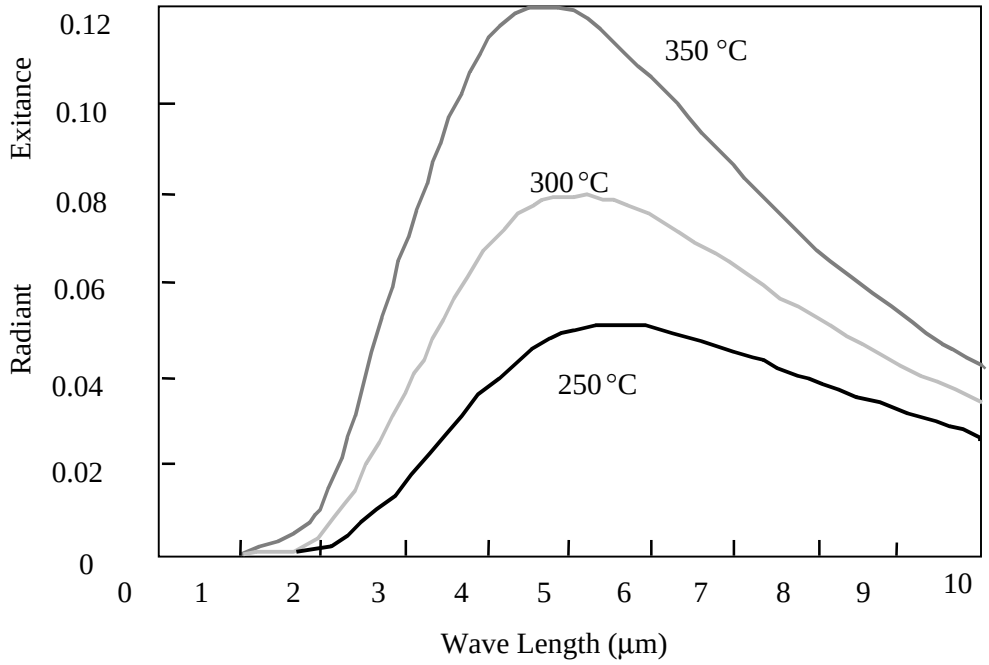

Fig.5.2.3.3 Spectra radiant exitance per wavelength

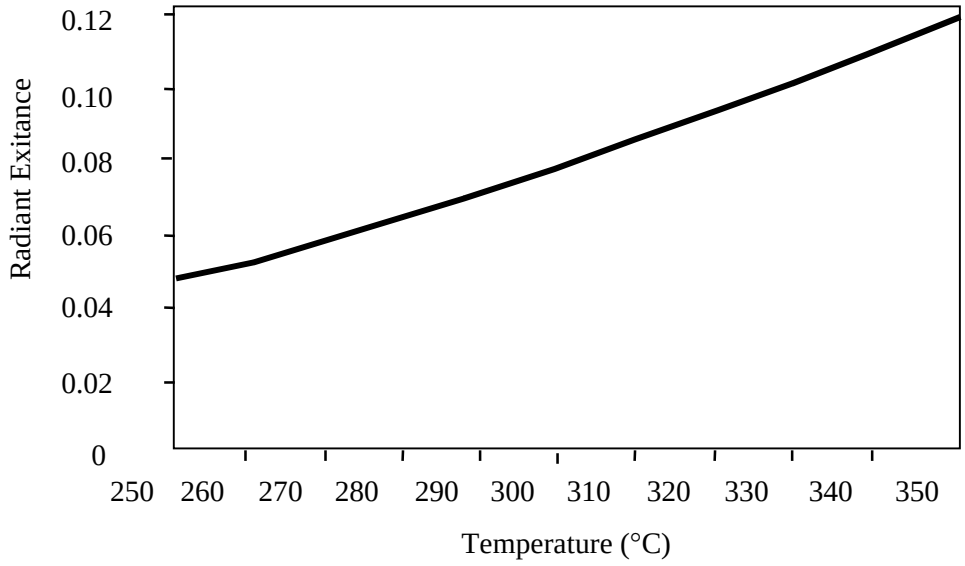

Fig.5.2.3.4 Radiant exitance spectra vs. temperature

5.2.3.3 Future Directions

The infrared camera layout was designed without changing the existing design of the deuteron ion beam line and target vessel. The distribution of surface temperature on target is measured by a space resolution of about 5 mm. But the estimation is based on an assumption that spectral emissivity is given by an approximate equation. Hence actual emissivity should be examined. And in order to realize the space resolution of ±1 mm it is necessary to take in the technique of chopping and data processing. From the above study it is considered that the perpendicular beam position measurement by an infrared camera is hard. Another method to measure the beam profile should be studied.

References

[1] "IFMIF International Fusion materials Irradiation Facility Conceptual Design Activity Final Report", IFMIF CDA TEAM, edited by M. Martone, ENEA RT-ERG-FUS-96-11, Dec. 1996.

[2] M. Ida, Y. Kato, H. Nakamura and H. Maekawa, "Preliminary Analyses of Li Jet Flows for the IFMIF Target", JAERI-Research 97-030 (1997).

5.2.4 Neutron Monitor

Description and justification:

In the previous report [1], passive detectors of multi-foil activation and on-line detectors of miniaturized fission chambers were examined. The activation level of the foil is measured after a few months' irradiation run. The on-line detector of miniaturized fission chambers is sensitive to thermal neutrons. Hence, it cannot directly measure the fast neutron flux profile from the target. In order to measure the neutron flux profile, we examine an on-line compact multi channel neutron detector which is used in a fission reactor as gamma thermometer detector [2]. So as to calibrate the on-line compact multi-channel neutron detector, we examine an activation wire method, by which a measurement is possible without stopping the ion beam operation.

Contributors:

Organization	Principal Investigator
Toshiba Corporation	Yoshio Kita
JAERI	Toshiaki Yutani
	Fujio Mekawa
	Masayoshi Sugimoto
	Hiroshi Takeuchi

Milestones:

1) Examination of Measurement Principle	May 1998
2) Basic Design of System	August 1998
3) Documentation	September 1998

5.2.4.1 Impact on CDA

A basic design of the on-line neutron flux monitor was performed in order to obtain the real time information on the neutron irradiation conditions and the neutron spatial profile of the irradiation region.

5.2.4.2 Results & Conclusions

The gamma thermometer detector is composed of a stainless needle, thermocouple and base copper board (sink) as shown in Fig.5.2.4.1. The heat flux generated in the stainless needle by the nuclear heating of neutron flux is guided to the copper base board (sink), thus a temperature difference (ΔT) is generated between the tip and the sink. The neutron flux is estimated from the temperature difference (ΔT) measured by the thermocouple. In the fission reactor, since ΔT by the gamma ray is larger than by the neutron flux, it is called a gamma thermometer. This on-line compact multi-channel neutron detector is useful for the "target on test" in the period of hot testing because the on-line neutron flux profile measurements make it possible to optimize the accelerator and target system operations.

Since a beam profile uniformity of ±5 %/cm is required for accelerator and target systems, the multi-channel neutron detector must be designed to have a sensor pitch of 10 mm and a measurement accuracy of ±1%. ΔT is calculated using the following equation.

$$\frac{dT(x,t)}{dt} = \frac{q}{C} + \frac{\lambda}{\rho C} \times \frac{dT^2(x,t)}{dx^2}$$

where T is the needle temperature. q is the nuclear heating term, ρ is the specific density, C is the specific heat and λ is the heat conductivity coefficient. Then, ΔT in steady state becomes $(\rho q/2\lambda)\times L^2$. L is the length of the needle. Fig.5.2.4.2 shows the relation between ΔT and L where each parameter is set to q=4.3 (W/g), ρ=7.8 (g/cm^3), C=0.46 (J/g°C), λ=0.16 (W/cm°C). The q value of 4.3 (W/g) is for the14 MeV neutron flux of 10^{15} nv.

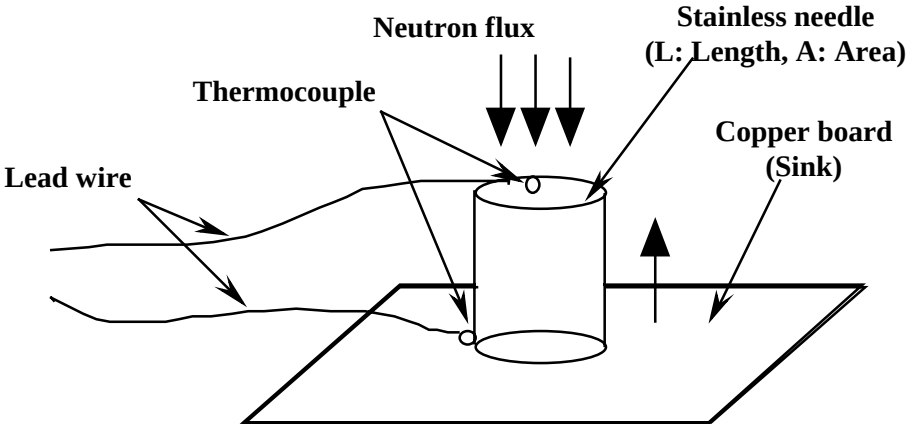

Fig.5.2.4.1: Illustration of gamma thermometer principle

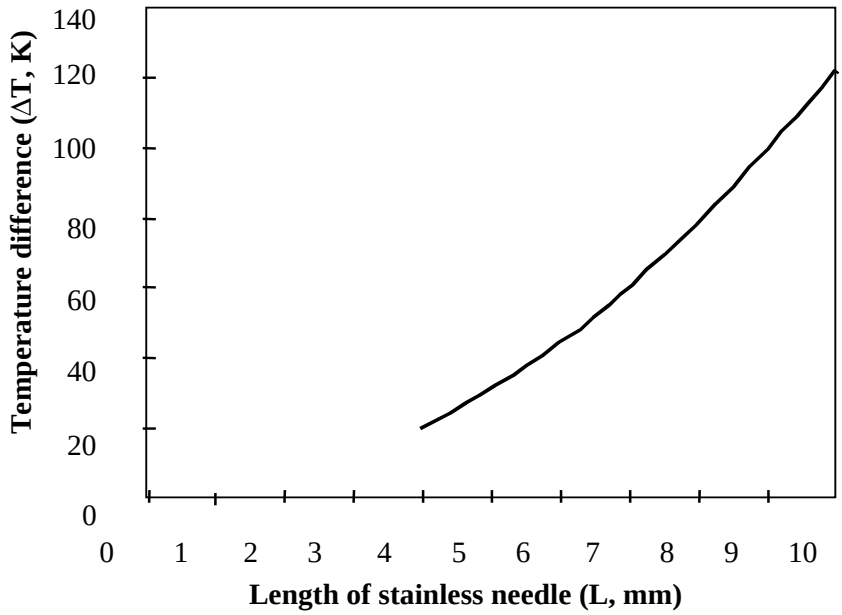

Fig. 5.2.4.2: Temperature difference (ΔT) vs. sensor length

The accuracy of the thermocouple is usually about ±0.7 °C, so the stainless needle length (L) should be set to 7.5 mm in order to realize the S/N ratio of 100 because ΔT of 7.5mm needle is 70 °C. Fig.5.2.4.3 shows the time response in the same case where the 10-90% rise time is about ten seconds.

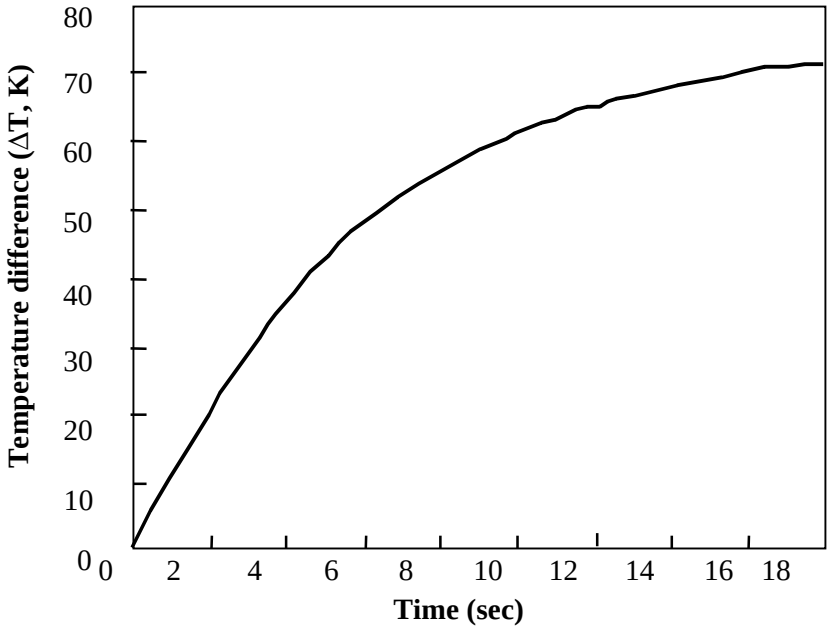

Fig. 5.2.4.3: Time response of sensor

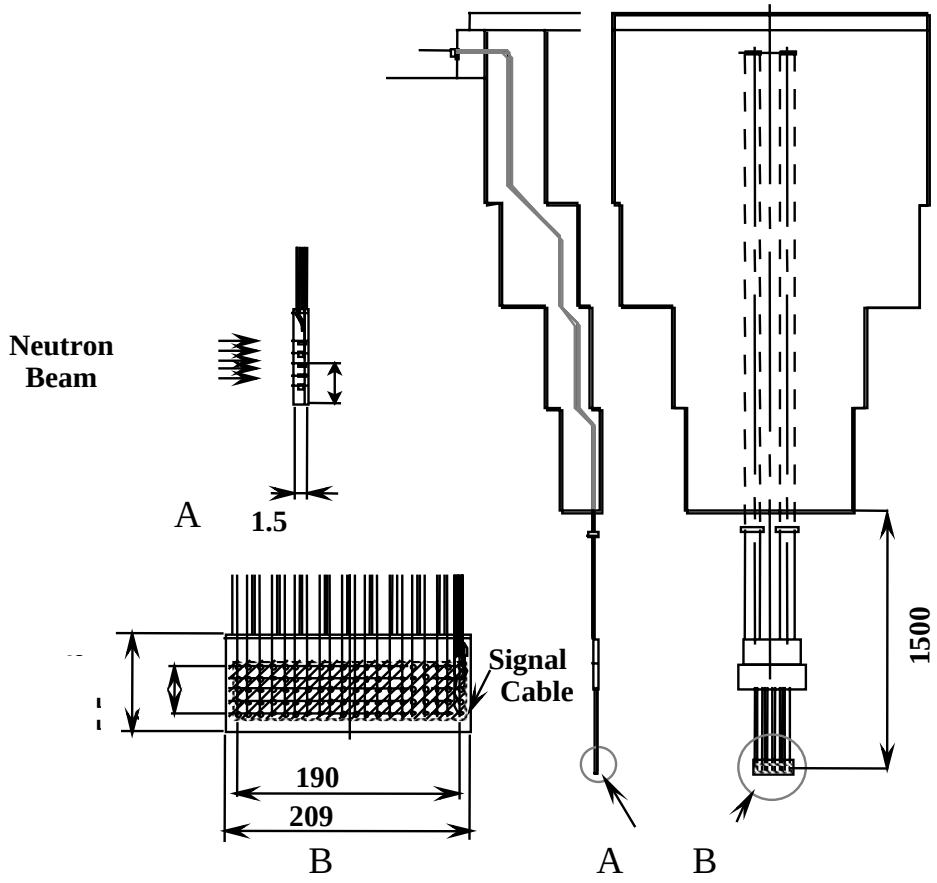

Fig.5.2.4.4: Layout of multi-channel neutron detector

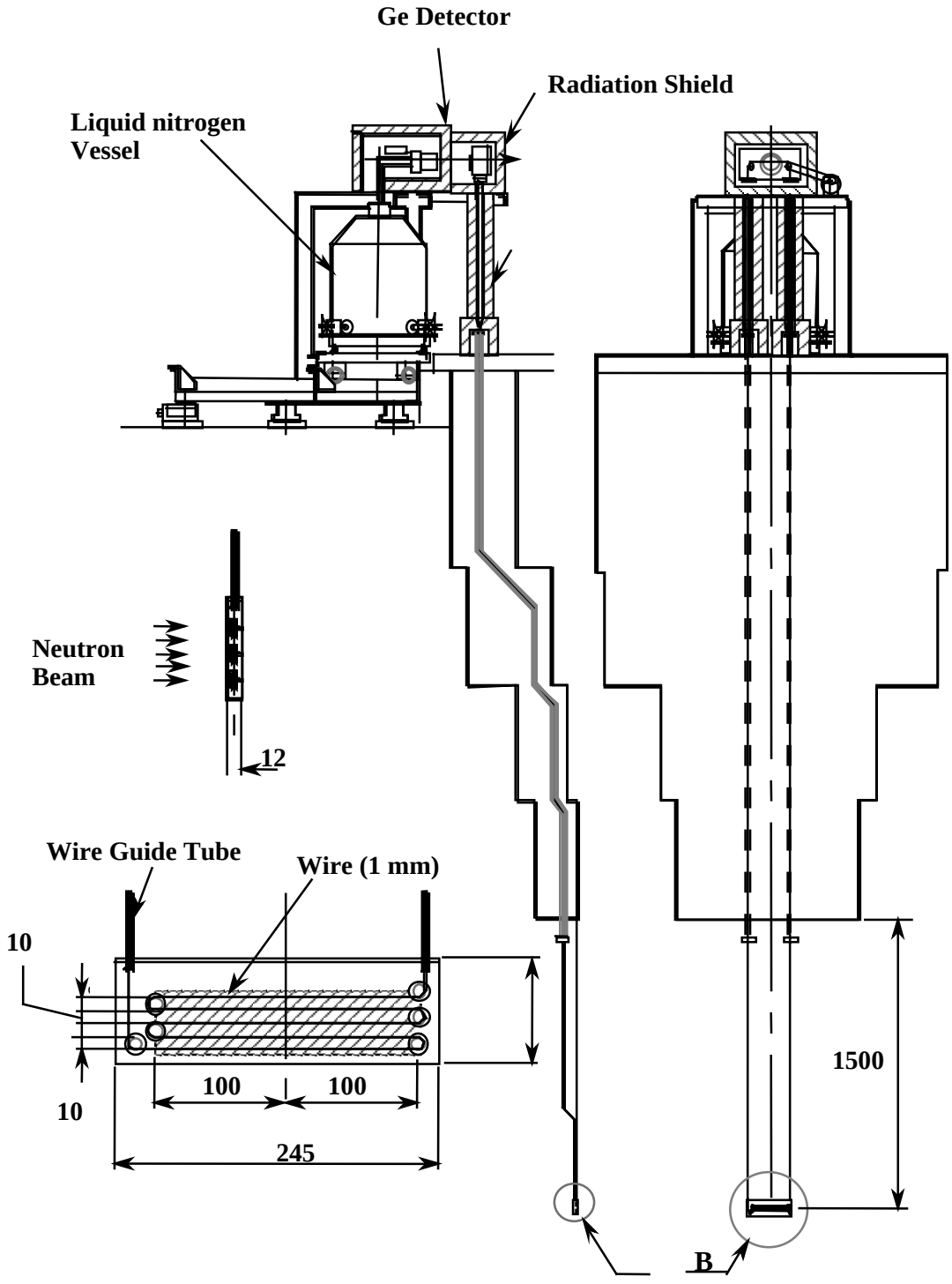

Fig.5.2.4.5 Layout of wire radiation detector

The temperature difference T_0 between the edge and the center of copper base board is approximately resolved as follows.

$$T_0 = \frac{\rho q_0}{16\lambda}\left(A^2 + B^2\right)$$

where A=20 cm, B=5 cm. The center temperature rise T_0 of the base board is about 280 K where the copper nuclear heating q_0 is assumed to be 4.3 (W/g). Copper heat conductivity is set to 3.7 (W/cmK). Since the temperature difference between a tip and base copper board is measured by a thermocouple, the copper base board (sink) temperature is not so important. Although the thermocouple can be used in more than one thousand degrees, too high temperature operation gives a damage to thermocouples. In order to keep the detector in a low-temperature state, the helium gas cooling method examined in the VT1 test cell needs to be applied. Fig.5.2.4.4 shows the layout of the multi-channel neutron detector where the pitch of the stainless needle is 10 mm and size is about 210 mm (wide), 86 mm (high), 15 mm (depth).

Fig.5.2.4.5 shows an activation wire detector where a wire is supported by small pulley and roped off with 10 mm distance and the layout where the wire is automatically wound through the pipe. The gamma ray from the wire is automatically measured by the HP-Ge detector at any time. Since the wire needs to resist the stress by the automatic winch, the strength of the wire is need. Therefore, a stainless wire which is coated by activation materials or passed by beads of the activation material with a hole will be used. By comparing the sensitivity of each individual thermocouple with the data of the wire activation detector, a calibration with good accuracy is realized not only at an early phase of the test but also for a period of ion beam operations.

5.2.4.3 Future Directions

A compact multi-channel (100ch) neutron on-line detector, with a size of about 210 mm (wide), 86 mm (high) and 15mm (depth) is designed to measure neutron flux uniformity of ±5%/cm at the period of "target on test". The detector expected S/N ratio is 100 and the 10-90% rise time is about ten seconds. In order to measure the neutron profile without stopping the machine operation, an activation wire detector is designed with a size of about 245 mm (wide), 80 mm (high) and 12 mm (depth). These detectors are installed in the test cell region because it is necessary that neutron intensity in the test cell is accurately measured. Accordingly, the combination between test cell and these measurement systems should be precisely examined.

References

[1] B.Esposito-Enea Frascati, ”Dosimetry for IFMIF” 1997-7 Karlsruhe, Germany.

[2] J.S. Stutheit, Nucl. Instr. Meth. 63: 300(1968).